THE UNIVERSITY OF ALBERTA

AN INVESTIGATION OF THE LOG PERIODIC ANTENNA AS A LEAKY WAVE DEVICE

by

Frederick T. Halsey

A THESIS

SUBMITTED TO THE FACULTY OF GRADUATE STUDIES

IN PARTIAL FULFILMENT OF THE REQUIREMENTS FOR THE DEGREE

OF MASTER OF SCIENCE

DEPARTMENT OF ELECTRICAL ENGINEERING

EDMONTON, ALBERTA

APRIL, 1963

ABSTRACT

Near field measurements available in the literature show that two waves exist on log periodic antennas. The first, called the transmission line wave originates at the apex, propagates along the antenna and decays in the active region. The second, called the radiation wave originates in the active region, propagates back toward and beyond the apex, and becomes the far field at a suitable distance in front of the antenna.

The hypothesis is made that the effective radiating aperture is located at the front of the active region and is in the plane perpendicular to the antenna structure. The aperture distribution is obtained by considering the radiation wave to behave as a leaky wave in the active region. The far field pattern is found from this aperture distribution using a transform technique. Suitable assumptions are made relating the characteristics of the radiation and transmission line waves in the active region. Thus, the far field pattern can be calculated if the properties of the transmission line wave are known.

The transform used is valid only in the half plane to the front of the antenna. Thus, the theory will predict only the shape of the main lobe since no information is obtained regarding the energy radiated to the rear of the antenna.

The characteristics of the transmission line wave for the log periodic dipole antenna were measured for various parameters of the antenna and these used to calculate the far field patterns.

These calculated patterns were found to show reasonably good agreement with experimentally obtained patterns over the useable range of parameters for this antenna.

ACKNOWLEDGEMENT

The author wishes to thank Professor W. Sinnema for numerous helpful and thought provoking discussions which were held during the course of this investigation.

TABLE OF CONTENTS

TABLE OF CONTENTS

LIST OF FIGURES

LIST OF FIGURES

LIST OF FIGURES

LIST OF FIGURES

LIST OF FIGURES

LIST OF FIGURES

SECTION 1

1. INTRODUCTION

Since the concept of frequency independent antennas was put forward by V. H. Rumsey[1] this class of antennas has received considerable attention in the literature. The logarithmically periodic (or log periodic) class of antennas introduced by R. H. DuHamel was one of the outgrowths of this interest.[2]

In general, the investigation of the properties of log periodic antennas has been carried out experimentally. However, in order to understand their radiation mechanism and thus obtain optimum design principles, a theoretical analysis is clearly required. R. L. Carrel has made an excellent analysis of the log periodic dipole antenna.[3] Briefly, he considered the self and mutual impedances of the elements making up the structure, and with the aid of a computer, was able to predict the behavior of this antenna with a good degree of accuracy. While the theoretical considerations of this approach are straight forward, the numerical solution of the resulting equations is formidable and would be practically impossible to obtain without the use of a computer. P. E. Mayes, G. A. Deschamps and W. T. Patton have explained the operation of unidirectional periodic structures in terms of backward wave radiation.[4] These antennas can be converted to log periodic antennas by tapering the elements. They have shown that the radiation patterns for the two types of structures are similar. It is their intention to consider the log periodic antenna as a slowly varying periodic structure and apply the theory of the

periodic structure to it.

The approach taken in this paper is to determine the far field radiation patterns for log periodic antennas from the near fields existing on the antenna.

Near field measurements available in the literature show that two waves exist on log periodic antennas.[5] The first, called the transmission line wave originates at the apex, propagates along the antenna, and decays in the active region. The second, called the radiation wave originates in the active region, propagates back toward and beyond the apex, and becomes the far field at a suitable distance in front of the antenna.

The hypothesis is made that the effective radiating aperture is located at the front of the active region and is in the plane perpendicular to the antenna structure. The aperture distribution is obtained by considering the radiation wave to behave as a leaky wave in the active region. The far field is found from this aperture distribution using a transform technique. Assumptions relating the characteristics of the radiation and transmission line waves are made by considering the current distribution on the elements in the active region. Thus, the far field radiation patterns can be calculated if the properties of the transmission line field are known.

In this paper, the properties of the transmission line wave for the log periodic dipole antenna are obtained experimentally. A theoretical analysis of these properties is being carried out in

conjunction with the work of Mayes, Deschamps and Patton previously described. A preliminary study of a class of log periodic circuits has been made by R. Mittra.[6]

The presentation of this paper is as follows: The preceding section briefly reviews the theoretical work, known to this investigator, which has been done on these antennas to date. A review of frequency independent antennas briefly describing some of the better known structures and their properties is presented in Section 2. A detailed formulation of the theory is given in Section 3. The measuring techniques used to obtain the characteristics of the transmission line field are outlined in Section 4. The results for measurements made on a log periodic dipole antenna are presented in Section 5. Calculated patterns using the theory developed in Section 3 are compared to radiation patterns obtained experimentally and the results analysed. Section 6 gives a summary of the paper. Two appendices are attatched. The first deals with the solution of an integral obtained in Section 3. The measurements of the transmission line wave along the structure for various parameters of the log periodic dipole antenna are presented graphically in the second appendix. The characteristics of the transmission line wave are obtained from these curves.

conjunction with the work of [illegible], [illegible] and [illegible] previously described. A preliminary study of a class of the periodic [illegible] has been made by [illegible].[6]

The organization of this paper is as follows: The preceding section briefly reviews the theoretical work, [illegible] in this [illegible], which has been done on [illegible]. A review of frequency independent antennas, [illegible] some of the better known structures and their properties is presented in Section 2. A detailed description of the tunnel is given in Section 3. The measuring techniques used to obtain the characteristics of the transmission line [illegible] are outlined in Section 4. The results for measurements made on a log periodic dipole [illegible] are presented in Section 5. [illegible] developed in Section 2 are compared to [illegible] results obtained experimentally and the results analyzed. Section 6 gives a summary of the paper. Two appendices are attached. The first deals with the solution of an integral equation in Section 2. The measurements of the transmission line with [illegible] are [illegible] parameters of the log periodic dipole antenna are presented graphically in the second appendix. The characteristics of the transmission line were [illegible] obtained from [illegible].

SECTION 2

2. A REVIEW OF FREQUENCY INDEPENDENT ANTENNAS

The logarithmically periodic antenna belongs to a general class of antennas usually referred to as "frequency independent antennas". In practice, this class of antennas can be built to give broadband performance over frequency ranges as great as 40:1 or more, provided the structure is carefully modelled in accordance with the basic design principles. Admittedly, these are not the only antennas which can be designed to cover a wide band of frequencies. For example, the discone antenna, the unbalanced conical helix fed against ground, and the Archimedean spiral, can be designed to cover frequency ranges of 4:1, 5:1, and 10:1 respectively.[7] However, the name "frequency independent antennas" is justified since these are the only structures possessing a theoretical independence of frequency. Since their upper and lower frequency limits are determined by independent parameters, the bandwidth of a specific antenna can be increased almost without limit simply by adding more sections to the antenna.

2.1 Basic Formulation

The concept that an antenna specified by angles alone would have characteristics independent of frequency was originally proposed by V. H. Rumsey.[1] The following is a brief résumé of a simplified analysis[8] paralleling Rumsey's earlier work.

Consider an antenna whose terminals are indefinitely close to the origin of a spherical coordinate system, being symmetrically

disposed along the $\theta = 0, \pi$ axis. Let the surface of this antenna be described by

$$r = F(\theta, \phi) \tag{1}$$

For an antenna of finite thickness, several branches of $F(\theta, \phi)$ can be taken, corresponding to the inner and outer surfaces.

Suppose it is desired to scale this antenna to a new frequency which is K times lower than the original frequency. The antenna must be made K times larger, resulting in a surface

$$r' = K F(\theta, \phi) \tag{2}$$

in which K depends neither on θ nor on ϕ.

Imagine that when this is done the new surface is congruent (identical) to the original. This implies that both surfaces are infinite. It can be seen that congruence, if it occurs, can be established through a rotation in ϕ. Translation is barred since both surfaces have their terminals at the same origin and rotation in θ is barred because both pairs of terminals are symmetrically disposed along the $\theta = 0, \pi$ axis. Thus, for congruence,

$$K F(\theta, \phi) = F(\theta, \phi + C) \tag{3}$$

in which C is the angle through which the second antenna must be rotated in order to achieve congruence with the first. C depends on K, but neither depends on θ or ϕ.

Congruency implies that the original antenna would perform exactly the same at both frequencies, except for a rotation, C, in the azimuthal coordinate of its radiation pattern. If it develops that K is unrestricted, i.e.,

$$0 \leq K \leq \infty \tag{4}$$

then the original antenna must have pattern and impedance characteristics which are independent of frequency. The pattern may rotate in ϕ with frequency due to the parameter C, but its shape will be unaltered.

The nature of $F(\theta,\phi)$ may be deduced by equating the two equations obtained from differentiating (3) with respect to C and ϕ. This gives, with the aid of (1),

$$\frac{1}{K}\frac{dK}{dC} = \frac{1}{r}\frac{\partial r}{\partial \phi} \tag{5}$$

Since the left side of (5) is independent of θ and ϕ, it follows that

$$r = F(\theta,\phi) = e^{a\phi} f(\theta) \qquad \text{where} \quad a = \frac{1}{K}\frac{dK}{dC} \tag{6}$$

is a general solution, in which a is a parameter and $f(\theta)$ is a completely arbitrary function.

Equation (6) was first derived by V. H. Rumsey.[1] Any antenna shape whose surfaces can be described by functions of the form (6) should be theoretically independent of frequency. This equation requires an infinite structure in order to achieve frequency independence over an infinite spectrum of frequencies. However, it was found experimentally for certain structures that the current distribution along the antenna falls to a negligible value at some number of wavelengths from the feed point. Therefore, the antenna

can be truncated at this point without affecting the current distribution, and therefore, the characteristics of the antenna. The frequency for which this is done represents the low frequency limit of the antenna since the current distribution moves towards the feed point as the frequency is increased. The high frequency limit of the antenna occurs when the feed point ceases to look like a "point" due to the physical impossibility of modelling the structure to an indeterminately small size. As previously stated, the bandwidth can be increased simply by continuing the structure until the desired frequency is included within the range of the antenna.

2.2 The Equiangular Spiral Antenna

The equiangular spiral antenna was the first antenna of a practical size to exhibit the characteristics of the infinite structure.[9] The equation of the equiangular spiral may be obtained from (6) by letting

$$\frac{df(\theta)}{d\theta} = f'(\theta) = A\,\delta(\theta - \tfrac{\pi}{2}) \tag{7}$$

where A is an arbitrary positive constant and δ is the Dirac delta function. Substituting (7) in (6) yields

$$r = r_o e^{a(\phi - \phi_o)} \tag{8}$$

in the plane $\theta = \frac{\pi}{2}$, r being zero elsewhere. $r_o e^{-a\phi_o}$ is a substitution for A. Expression (8) is the equation of a planar equiangular (or logarithmic) spiral. If the angle ϕ is increased by one full turn, the radius vector, r is increased by the factor $e^{2\pi a}$. Hence, each turn of the spiral is identical with every

other turn except for a constant multiplier. The angle, ψ, between the radius vector, and the tangent to the equiangular spiral gives the rate of spiral and is a constant for a particular curve.

Since A is arbitrary, the choice can be made to fix r_0 and leave ϕ_0 as a parameter. If ϕ_0 is allowed to assume all values from 0 to ϕ_1 and all values from π to $\pi + \phi_1$, the antenna of Figure 1 results. Since (8) yields an infinite structure, the minimum and maximum radii, R_2 and R_1, must be specified for a practical antenna. These correspond to the upper and lower frequency limits of the antenna, respectively. Typical values for R_2 and R_1 are one eighth and one half wavelengths, respectively, at the upper and lower frequencies.

Two forms of this antenna have been used, the plane conductor antenna made of metallic arms suspended in free space, and the slot antenna consisting of spiral slots cut in a large conducting sheet.

The antenna may be fed at the centre by a balanced line. However, this causes some distortion of the fields because of the feed line. A preferred method is to imbed the coaxial feed cable in one arm of the spiral and connect the centre conductor to the other arm of the spiral as shown in Figure 2. This results in a perfectly balanced feed system. This method of feed, often referred to as the "infinite balun", is made possible by the rapid attenuation of the currents on the arms. It is the only form of the

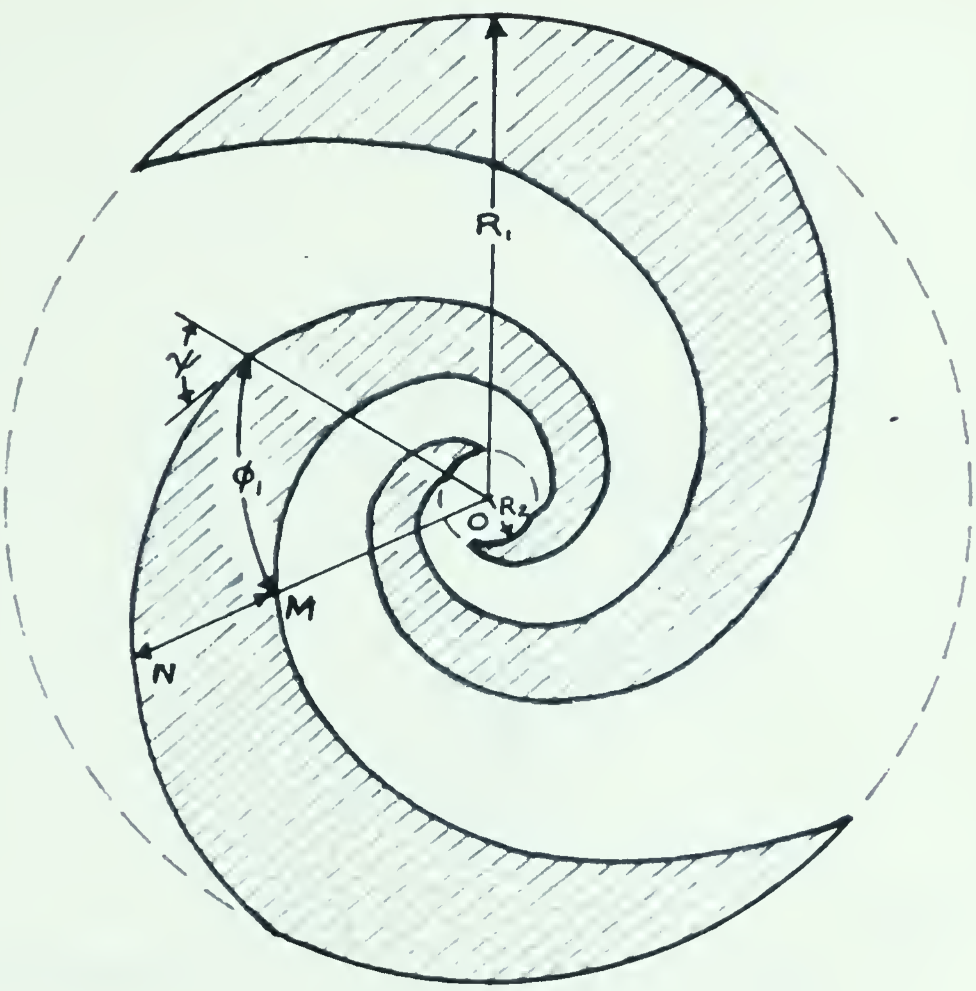

ψ =Rate of Spiral

$$r_1 = OM = r_o\, e^{a(\phi - \phi_1)}$$

$$r_2 = ON = r_o\, e^{a\phi}$$

$$\frac{r_2}{r_1} = e^{a\,\phi_1}$$

FIGURE 1

OUTLINE AND BASIC PARAMETERS
OF THE TWO ARM EQIANGULAR SPIRAL

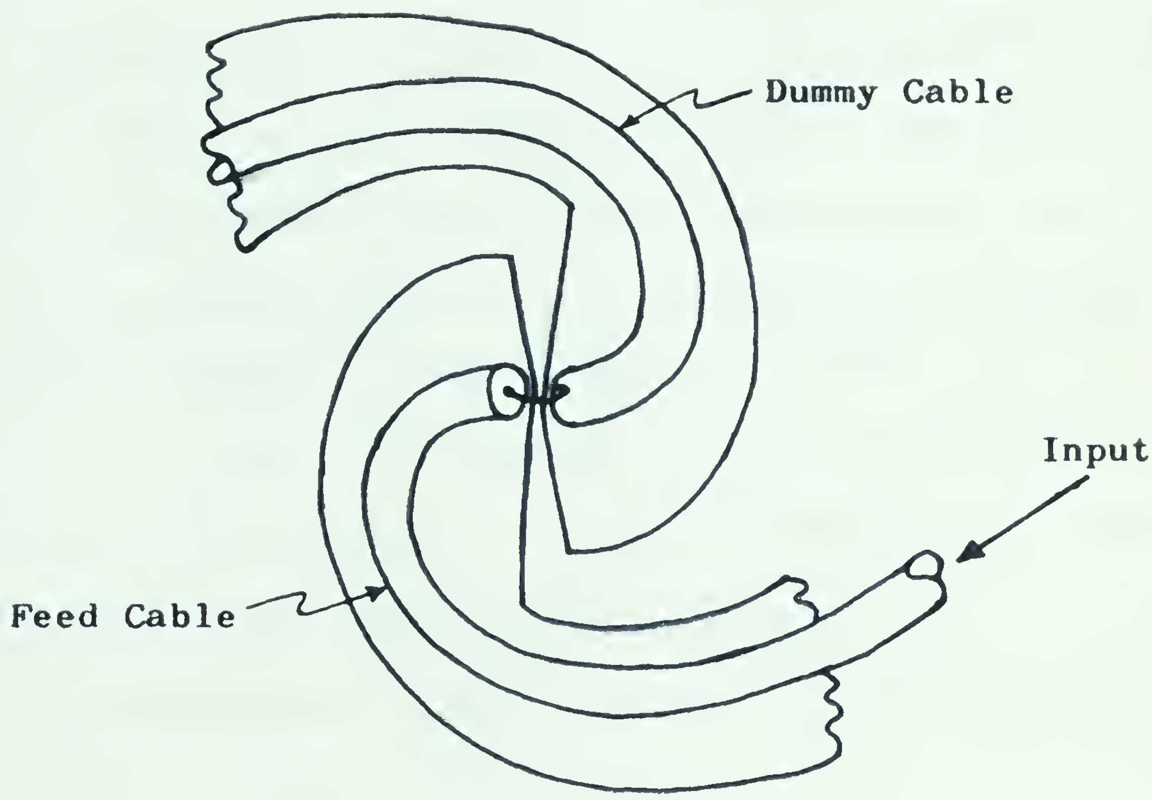

FIGURE 2

FEED REGION FOR A TYPICAL EQUIANGULAR SPIRAL SHOWING THE "INFINITE BALUN CONSTRUCTION"

presently known which permits full utilization of the "infinite" frequency properties of this antenna. To maintain symmetry, a dummy cable is sometimes soldered to the other arm of the spiral.

This antenna produces two equal broad lobes to the front and back of the structure, typical beamwidths being of the order sixty to one hundred degrees. The patterns do not change much with the parameters a and ϕ_1. They are nearly circular for high rates of spiral, but show some assymetry for low rates of spiral which produces a rotation effect as the frequency is varied. The field is practically circularly polarized over the operating range of the antenna.

A typical input impedance of 120 ohms with a VSWR of less than 2:1 over the frequency range is obtained for $\phi_1 = 90^\circ$.[10]

B. R. S. Cheo, V. H. Rumsey, and W. J. Welch have made a theoretical analysis of this antenna.[11] Design data is available.[10]

2.3 The Conical Equiangular Spiral Antenna

A slightly less restrictive choice of $f'(\theta)$ is given by

$$f'(\theta) = A\,\delta(\theta - \theta_0) \tag{9}$$

where θ_0 is any angle in the range $0 \leq \theta_0 \leq \frac{\pi}{2}$. Substituting in (6) yields

$$r = r_0 e^{a_1(\phi - \phi_0)} \tag{10}$$

where $A = r_0 e^{-a_1\phi_0}$ for the cone of revolution $\theta = \theta_0$, r being zero elsewhere. This is the equation of an equiangular spiral projected on to a cone of apex angle $2\theta_0$. As was done for the equiangular spiral antenna in the previous subsection the choice is made to fix r_0 and allow ϕ_0 to assume all values from 0 to ϕ_1 and all values from π to $\pi + \phi_1$. The outline for this particular type of

presently known which permits full utilization of the "possible" frequency properties of this antenna. To minimize asymmetry, a dummy cable is sometimes soldered to the other arm of the spiral.

This antenna produces two equal broad lobes to the front and back of the structure, typical beamwidths being on the order of one hundred degrees. The patterns do not change much with the parameters a and ψ_1. There are usually kinks for high values of spiral, but above some sensitivity for low values of spiral which produces a rotation effect as the frequency is varied. The field is practically circularly polarized over the operating range of the antenna.

A typical input impedance of the order with a VSWR of less than 2:1 over the frequency range is obtained for ψ_1 ...

R. H. S. Cheo, V. H. Rumsey, and W. J. Welch have made a theoretical analysis of this antenna.[?] Recent data is available.[10]

2.5 The Conical Equiangular Spiral Antenna

A slightly less restrictive choice of f' being given by

$$f'(\eta) = A\,\delta(\theta-\theta_0) \tag{9}$$

where θ_0 is any angle in the range $0 \le \theta_0 \le \frac{\pi}{2}$. Substituting in (?) yields

$$r = r_0\, e^{a(\phi-\psi_1)} \tag{10}$$

where $A = r_0 e^{-a\psi_1}$ for the cone of revolution $\theta=\theta_0$. In using here elsewhere. This is the equation of an equiangular spiral wrapped on to a cone of apex angle $2\theta_0$. As was done for the equiangular spiral antenna in the previous subsection the cutoff is made to fix r_0 and allow ψ_1 to assume all values from 0 to ψ_1 and all values from π to $\pi+\psi_1$. The outline for this particular type of

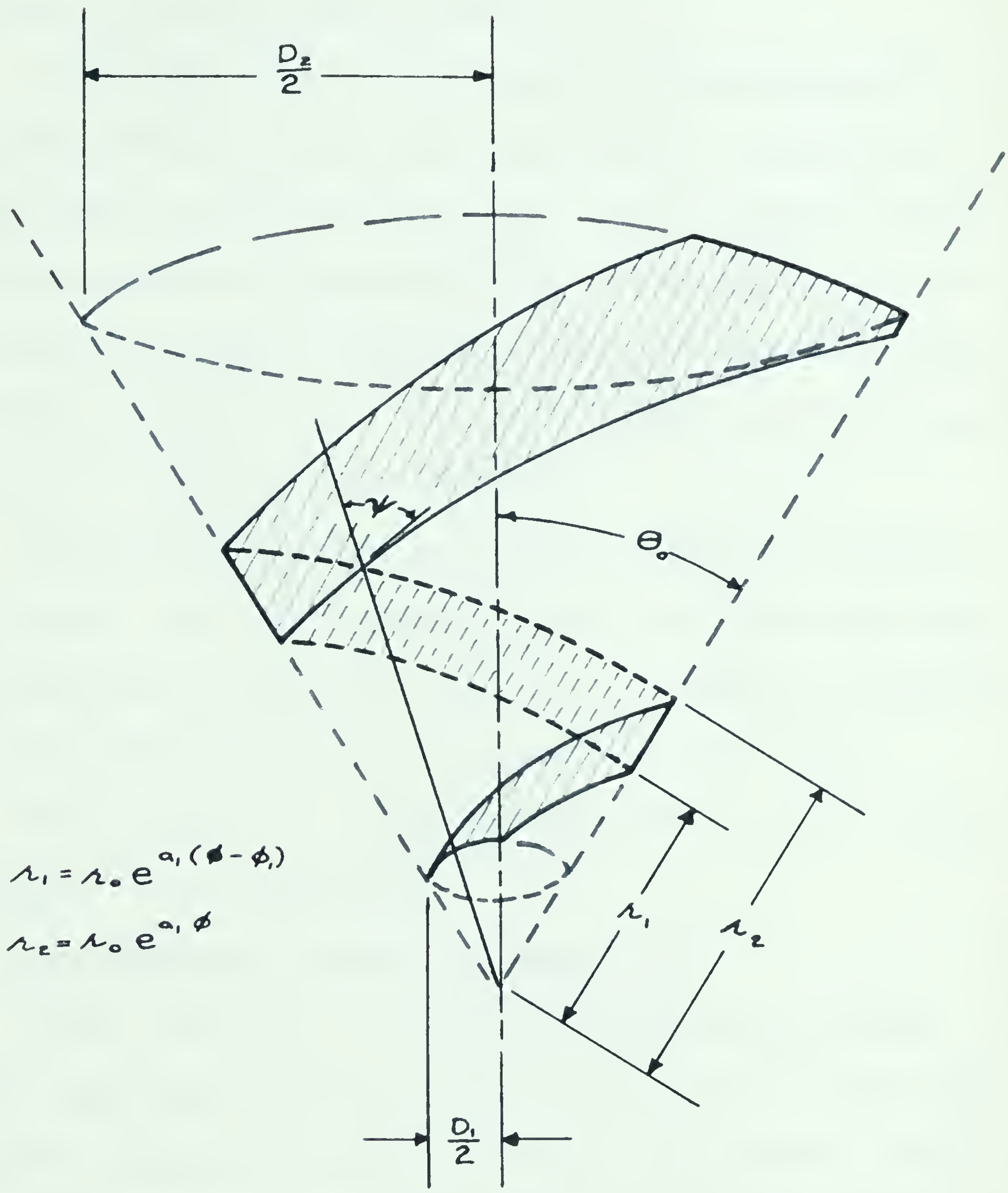

FIGURE 3

OUTLINE AND BASIC PARAMETERS OF
THE CONICAL EQUIANGULAR SPIRAL ANTENNA
(ONE ARM ONLY SHOWN)

antenna, shown in Figure 3, represents the projection of the planar spiral of Figure 1 on to the conical surface $\theta = \theta_0$. For the sake of clarity, only one arm is shown.

J. D. Dyson studied this antenna experimentally.[12] He found that the additional parameter, θ_0 , exerts a considerable influence on the shape of the radiation field. For the proper choice of θ_0 the pattern becomes unidirectional with the major lobe in the direction of the apex. The beamwidth varies widely with the parameters, typical values being 60° to 200° when ψ is varied from 82° to 45° ($\theta_0 = 10^\circ$ and $\phi_1 \approx 94^\circ$).[13]

The "infinite balun" previously described is used for the feed system. The mean impedance ranges from 153 to 130 ohms when the apex angle is varied from 60° to 20°. VSWR's of less than two to one are obtained over a six to one frequency range.

The design of this antenna is similar to that of the planar equiangular spiral antenna.[10]

2.4 Logarithmically Periodic Antennas

Since θ_0 in (9) is fixed for a particular antenna, the conical equiangular spiral antenna is essentially a two dimensional structure wrapped on a conical surface. If, however, θ_0 is allowed to assume all values from θ_1 to θ_2 $(0 \leq \theta_1 < \theta_2 \leq \frac{\pi}{2})$ the three dimensional conical screw results.

R. H. DuHamel conceived the idea of placing two conical screws apex to apex, collinearly, and taking the cut, ϕ = constant.[2] This yields the planar antenna of Figure 4. This concept is extremely

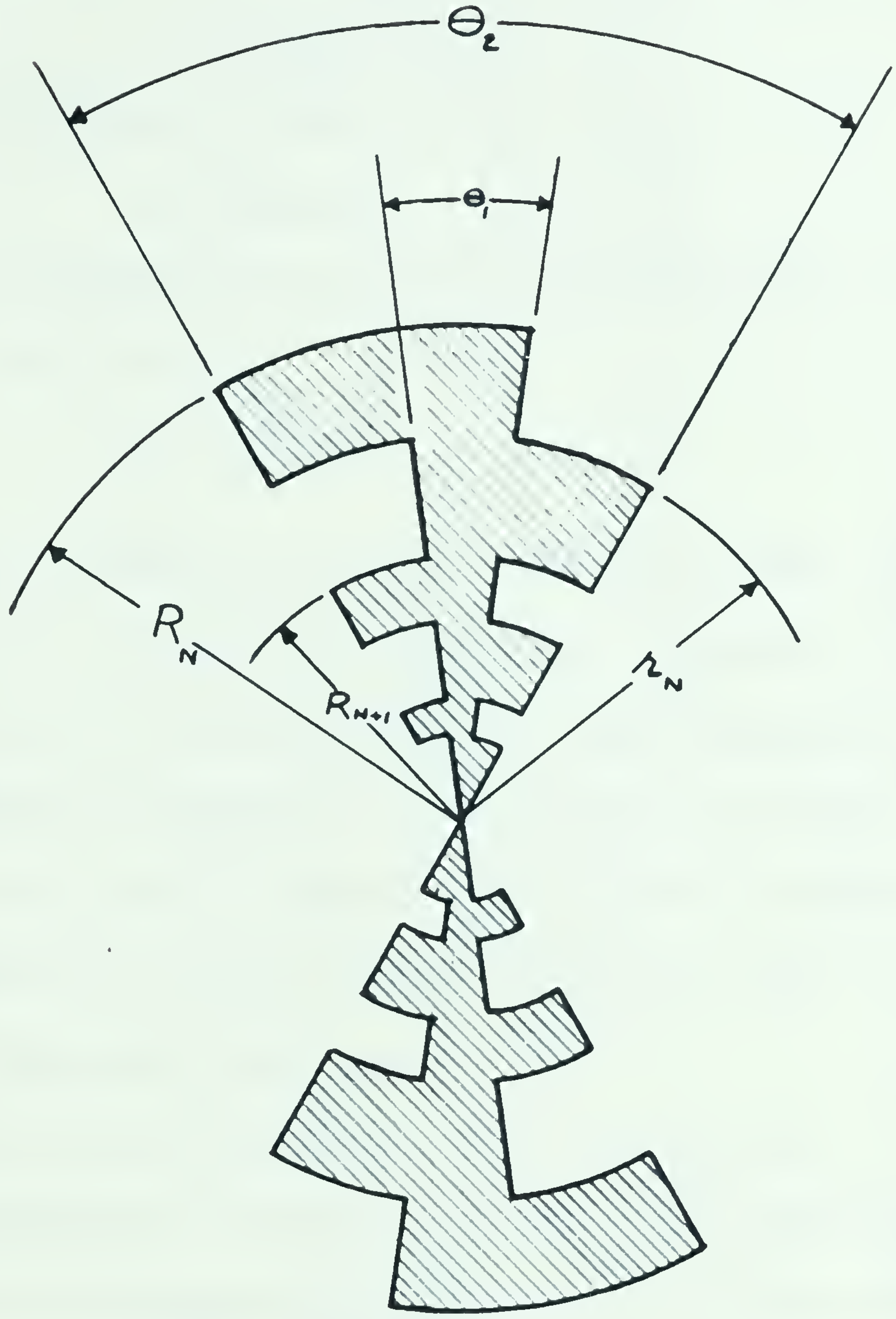

FIGURE 4

THE PLANAR SHEET CIRCULAR TOOTH
LOGARITHMICALLY PERIODIC ANTENNA

valuable since it provides a linearly polarized frequency independent antenna. The shape of these antennas can be described by

$$r = f(\theta) \tag{11}$$

A new antenna scaled to give

$$r = Kf(\theta) \tag{12}$$

will only be congruent to the original antenna for a discrete set of values for K given by

$$K = e^{2\pi n a_1} \tag{13}$$

where n is an integer and a_1 is defined in (10). Therefore, the properties of the antenna will repeat with period $2\pi a_1$. Hence, structures of this nature are called logarithmically periodic (or log periodic) antennas. If the variation of the impedance and pattern is small over a period, and therefore, all periods because of the repetitive characteristics, then the result is essentially a frequency independent antenna.

There is an infinite variety of choices for $f(\theta)$ and hence a corresponding infinite variety of log periodic structures. A theoretical study of the best choice for $f(\theta)$ seems to be nearly impossible and to date, the initial evaluation of these structures has been done experimentally. Some of the more successful structures are shown in Figure 5.

The parameters for this class of antennas are shown in Figure 6. The symbol Θ is used to define the apex angle since the symbol α, normally used in the literature, will be used to

variance where it produces a linearly polarized frequency independent

antenna. The shape of these antennas can be described by

$$\rho = f(\theta) \tag{11}$$

A new antenna scaled to give

$$[illegible] \tag{12}$$

will only be congruent to the original antenna for a discrete set

of values for K given by

$$[illegible] \tag{13}$$

where n is an integer and [illegible]. Therefore, the

properties of the antenna will [illegible]. Antenna

structures of this nature are called [illegible]

(or log periodic) antennas. If the variation of the [illegible]

pattern is small over a period, and [illegible]

of the repetition characteristics, then the result is [illegible]

frequency independent antenna.

There is an infinite variety of [illegible]

hence a corresponding infinite variety of [illegible] structures.

A theoretical study of the most [illegible]

impossible and to date, the initial evaluation of these structures

has been done experimentally. Some of the [illegible] structures

are shown in Figure 3.

The parameters for this class of antennas are shown in

Figure 4. The symbol [illegible]

the symbol K, normally used in the literature, [illegible]

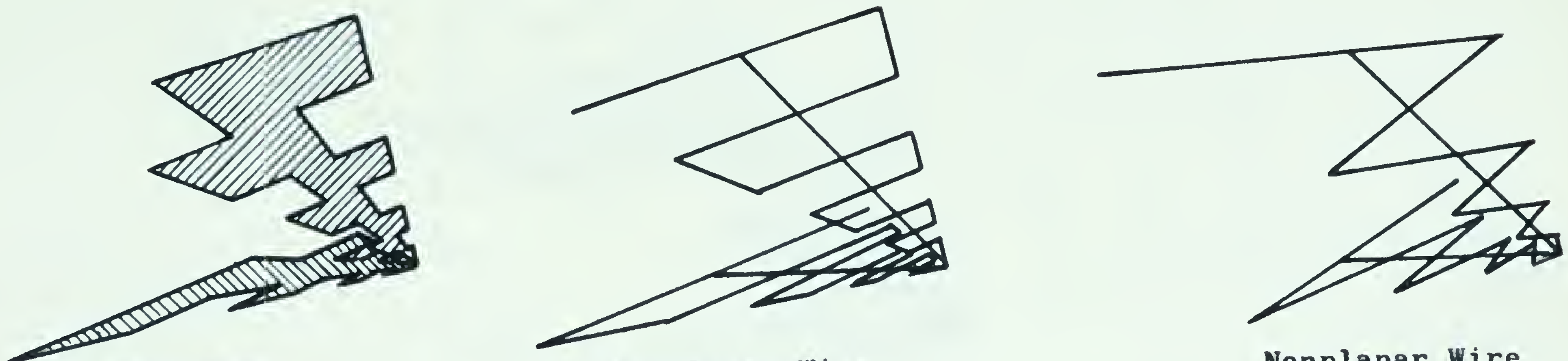

FIGURE 5

SEVERAL TYPES OF LOG PERIODIC ANTENNAS

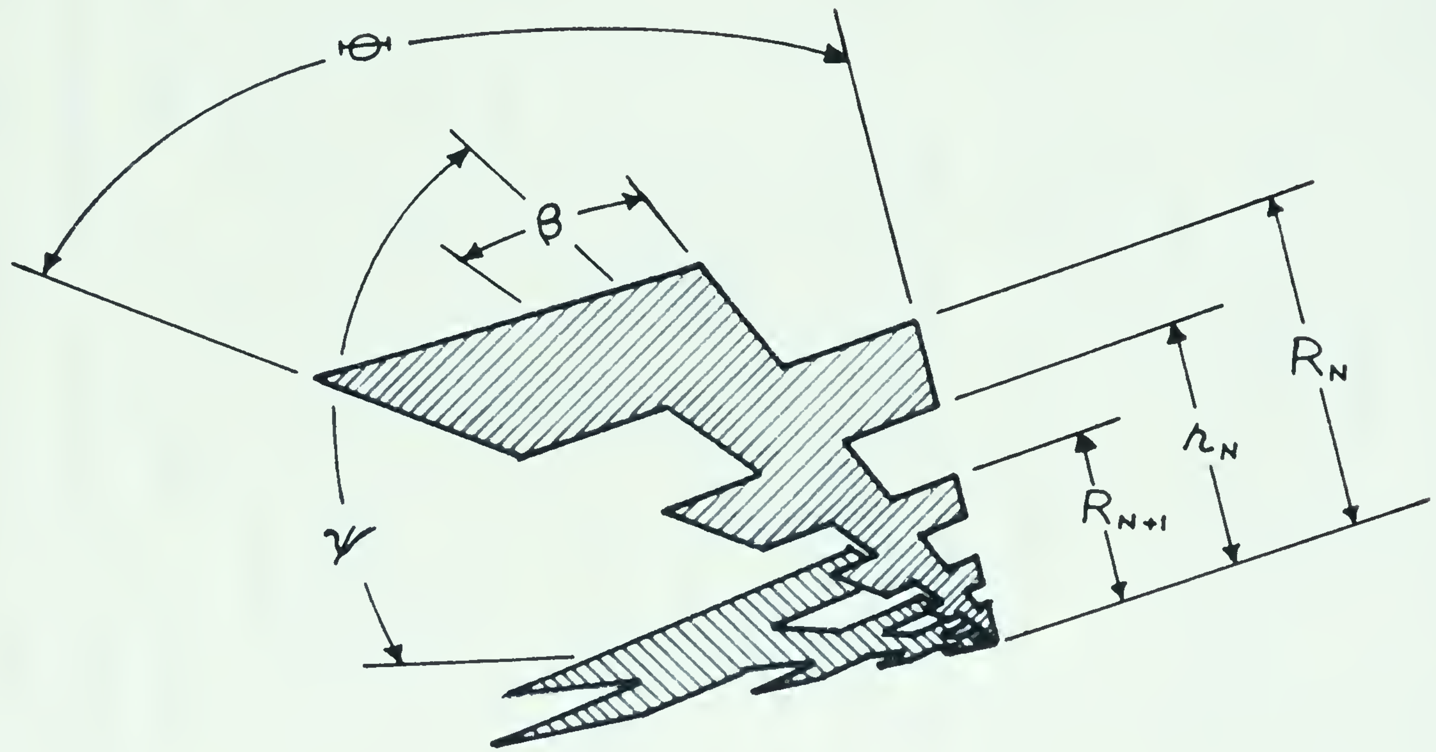

$$\tau' = \frac{R_{N+1}}{R_N}$$

$$r_N = \sqrt{\tau'}\, R_N$$

FIGURE 6

BASIC PARAMETERS OF THE LOG PERIODIC ANTENNA

denote the attenuation constant introduced later. The geometric ratio is defined as

$$\tau' = e^{2\pi a_1} = \frac{R_{N+1}}{R_N} \tag{14}$$

Since the radiation from these antennas is approximately centred on the teeth which are near a quarter wavelength in length, the upper and lower frequency limits of these antennas occur when the shortest and longest teeth are approximately a quarter wavelength long respectively.

Theoretically, the thickness of the sheets and the diameters of the wires should increase linearly with distance from the apex. In practice, this is not necessary for bandwidths less than five to one.[10] With tapering, bandwidths of twenty to one are easily achieved, and bandwidths of one hundred to one are feasible if the theoretical design is closely approximated.

The radiation patterns of the log periodic antennas shown in Figure 5 are similar for the same design parameters, τ', Θ and ψ. They give a unidirectional pattern pointing towards the apex. In general, higher gains are obtained by increasing τ' and ψ and decreasing Θ. If τ' is made too small, the patterns will break up excessively over a period. For the parameters $\tau' = 0.707$, $\Theta = \psi = 45^{\circ}$, a gain of 9.45 db. over an isotropic radiator is obtained for a wire tooth logarithmically periodic antenna. This particular antenna has a beamwidth of 66° for both the E and H planes, and a maximum sidelobe level of - 12.3 db.[14]

These antennas are fed at the apex either by a balanced line or the infinite balun structure previously described. Because of the left-right assymetry of these structures, the impedance has a periodicity of ½ ln($1/\tau$) compared to a periodicity of ln($1/\tau$) for the radiation patterns.[10] The input impedance varies widely with the various parameters, and as might be expected, the variation in the input impedance between various geometries with the same design parameters is greater than the variation in the radiation patterns.

Some design data is available in the literature for these antennas.[10,14]

The log periodic dipole antenna, shown in Figure 7 consists essentially of an array of dipoles whose lengths and spacings are arranged in a log periodic manner. This antenna has been investigated, both experimentally[15] and theoretically.[3] Design data, based on the theoretical analysis is available.[3] This antenna can be derived from the antenna of Figure 6 by letting the width of the teeth and the angles ψ and θ approach zero. The relation between the geometric ratios of the two antennas is given by

$$\tau = \sqrt{\tau'} \qquad (15)$$

The radiation and impedance characteristics of this antenna are similar to the other types of log periodic antennas.

The log periodic V antenna is an adaptation of the log periodic dipole antenna which takes advantage of the modal and directional characteristics of the conventional V antenna.[16] In the

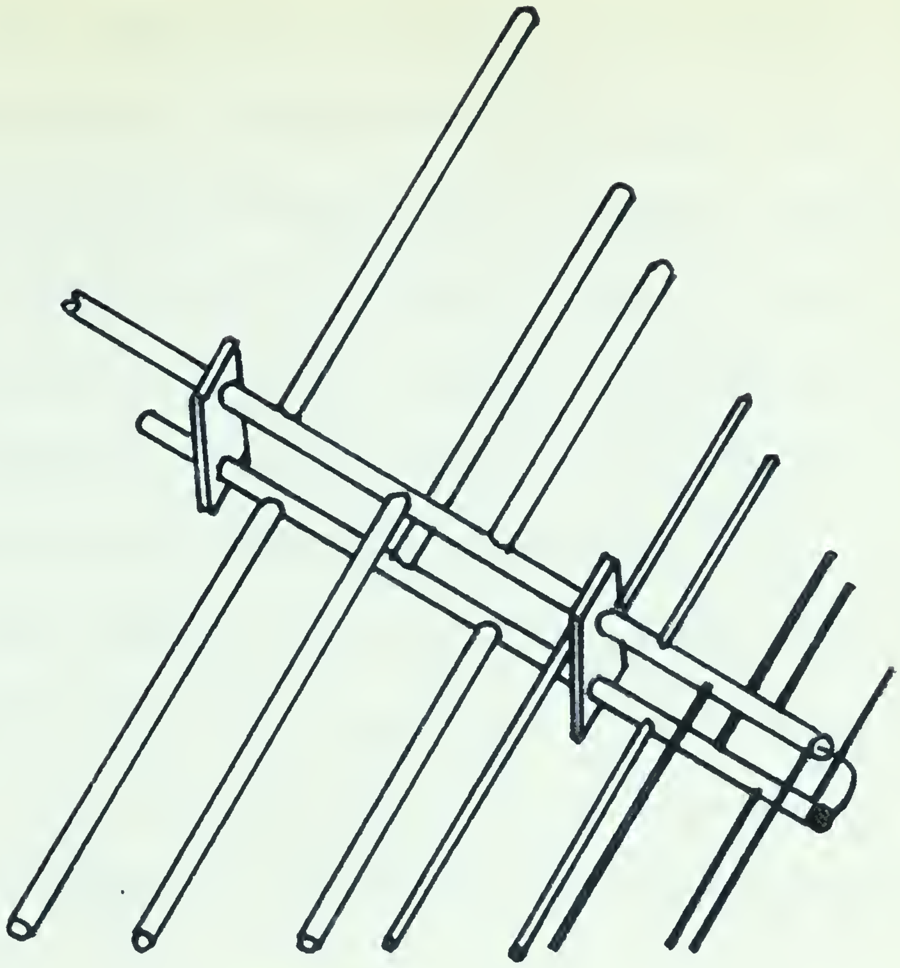

Sketch

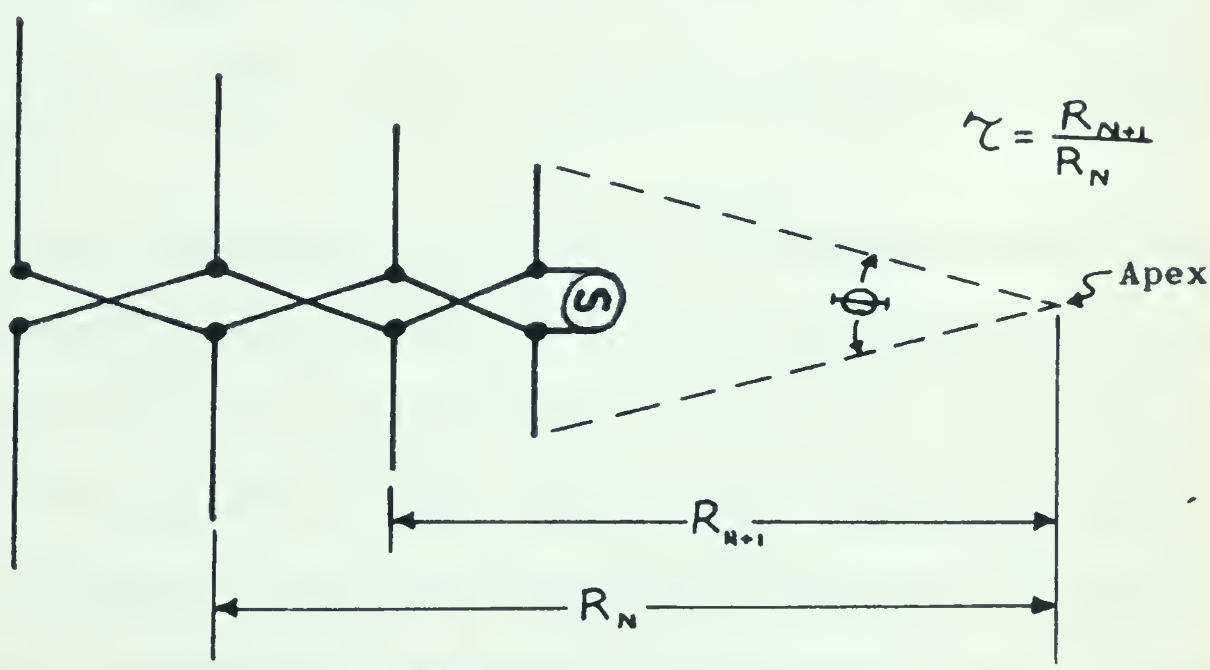

Schematic

FIGURE 7

THE LOG PERIODIC DIPOLE ANTENNA

lowest order mode, where the energy is radiated from the elements which are approximately half a wavelength long, its characteristics are similar to the log periodic dipole antenna. As the frequency is increased, the radiating region moves toward the apex. If the antenna is designed so that the longest elements are one and a half wavelengths long when the short elements are a half a wavelength long, then as the half wavelength radiating region moves off the antenna, the next higher mode consisting of the elements one and a half wavelengths long will be excited. As the frequency is increased further, this region of radiation will move toward the apex and will eventually be replaced by the two and a half wavelength mode of operation.

Gains as high as 18 db. over an isotropic source have been obtained in the higher modes of operation.[17] The main disadvantage of this antenna is that its characteristics deteriorate between modes.

2.5 Summary

The above description of frequency independent antennas has been, by necessity, quite brief and covers only the basic structures.

These antennas may be arrayed to give either an omnidirectional pattern or a high gain for both circular and linear polarization.[10,13,18]

The range of frequencies over which these antennas may be used is nearly unlimited. The lowest limit occurs when the elements become too large and hence difficult to build and support. The highest frequency boundary is usually determined by the accuracy with which the geometry of the structure can be modelled. In some

lowest order mode, where the current is radiating from the elements which are approximately half a wavelength long, the characteristics are similar to the log periodic [illegible]. As the frequency is increased, the radiating region moves toward the apex. If the antenna is designed so that [illegible] wavelengths long [illegible], then as the [illegible] antenna, the [illegible] half wavelengths long will [illegible]. As the frequency is increased further, [illegible] eventually [illegible] operation.

[illegible] obtained in the higher modes of operation. [illegible] of this antenna is that the [illegible].

2.5 Summary

The above description of frequency independent antennas has been, by necessity, quite brief [illegible]. These antennas can be designed to give [illegible] pattern or a high gain [illegible]. The range of frequencies [illegible] used is nearly unlimited. [illegible] become too large [illegible]. The highest frequency [illegible] with which the geometry of the structure can be achieved. [illegible]

applications, the high frequency limit may be determined by the power which the antenna is required to handle.

Numerous applications have been made of the principles outlined above to construct wideband antennas for special applications. Reference (7), in particular, contains a list of over seventy-five publications in its bibliography, many of which investigate specific applications for this class of antennas.

SECTION 3

3. DERIVATION OF THE RADIATION PATTERNS FOR LOG PERIODIC ANTENNAS

3.1 Review of Surface and Leaky Waves[19]

Surface and leaky wave antennas are part of the larger class of travelling wave antennas. A surface wave antenna supports a surface or trapped wave and does not radiate except at a discontinuity, for example, the termination of the structure. Therefore, the wave number along the structure is real. Conversely, the radiation from a leaky wave antenna occurs at all points along the structure so that the wave number along the structure is complex, containing an attenuation factor.

The relationship governing the parameters is the separability condition for the wave equation which is, in cartesian coordinates,

$$k_x^2 + k_y^2 + k_z^2 = k_o^2 \tag{16}$$

where the k's , called the wave numbers, are generally complex. For example,

$$\begin{aligned} k_i &= -j\gamma_i = \beta_i - j\alpha_i \\ \gamma_i &= j k_i = \alpha_i + j\beta_i \end{aligned} \tag{17}$$

where γ_i is the complex propagation constant, β_i is the phase constant (radians per wavelength) and α_i is the attenuation constant (nepers per wavelength), all in the i_{th} direction. The wave number, k_o , belongs to the medium in which the wave travels, and is given by

$$k_o = \omega\sqrt{\epsilon\mu} \tag{18}$$

where ω is the angular frequency, ϵ and μ are the dielectric and permeability constants of the medium respectively. In air, k_o is real.

Using this notation, the variation of the field strength in the i_{th} direction is given by

$$E_i = E_o e^{j(-k_i i + \omega t)} = E_o e^{-\gamma_i i + j\omega t} \tag{19}$$

Sometimes the time dependent term, $e^{j\omega t}$, is suppressed to shorten the expressions. If this is done, its presence is implied.

Consider a surface of infinite extent in the y direction supporting a surface wave propagating parallel to the surface in the z direction. For these conditions

$$k_y = 0 \qquad k_x = -j\alpha_x \tag{20}$$

since a surface wave decays exponentially away from an infinite surface. Substituting in (16) and equating the real and imaginary terms gives, taking $k_z = \beta_z - j\alpha_z$,

$$\beta_z^2 = k_o^2 + \alpha_x^2 \qquad \alpha_z = 0 \tag{21}$$

This means the signal is not attenuated as it propagates along the surface, and thus does not radiate.

If the above surface supports a leaky wave propagating in the z direction, the conditions become

$$k_y = 0 \qquad k_z = \beta_z - j\alpha_z \tag{22}$$

Substituting in (16) gives, taking $k_x = \beta_x - j\alpha_z$,

$$\begin{gathered} \beta_x^2 - \alpha_x^2 + \beta_z^2 - \alpha_z^2 = k_o^2 \\ \alpha_x\beta_x + \alpha_z\beta_z = 0 \end{gathered} \tag{23}$$

where ω is the angular frequency, ϵ, μ [illegible]
and permeability constants [illegible]
k_x is real.
Using this notation, [illegible]
the ξ_x direction is given by

$$E_1 = E_0 e^{[illegible]}$$

Sometimes the time dependent term, $e^{j\omega t}$ [illegible]
the expressions. [illegible]
Consider a [illegible]
expanding [illegible]
the z direction. [illegible]

$$[illegible]$$

since a surface wave [illegible]
surface. [illegible]
terms [illegible]

$$[illegible]$$

This means the signal [illegible]
along the surface, and thus does not radiate.
If the above surface supports [illegible]
the x direction, the conditions become

$$[illegible]$$

Substitution in (10) gives, taking [illegible]

$$[illegible]$$

Since α_z and β_z are of equal sign for attenuation of the wave in the direction of propagation along the surface and β_x is positive for propagation away from the surface, α_x must be negative. Therefore, the leaky wave field propagates with increasing amplitude away from the surface, becoming infinite at infinity in the direction transverse to the surface. In spite of this improper transverse behavior, leaky waves can be used to provide a valid representation of the fields for certain structures. To date, most antennas analysed using leaky waves have been open waveguide structures.

3.2 Interpretation of Near Field Measurements Made on a Log Periodic Antenna

R. L. Bell, C. T. Elfving, and R. E. Franks have made near field measurements on a triangular tooth antenna.[5] They found that two waves exist on these antennas.

The first, called the "transmission line wave" was found to be the transverse electromagnetic (TEM) two wire transmission line wave. This wave originates at the apex and propagates as a slow wave along the antenna without attenuation until it reaches the area where the teeth are approximately one quarter wavelength long. In this region, the wave is exponentially attenuated at a high rate and is thus effectively terminated.

Measurements of the currents on the teeth in this region were made and used to calculate the far field patterns. These

Since ωC_z and β_y are of equal sign for attenuation in the direction of propagation along the surface and β_x is positive for propagation away from the surface, α_x must be negative. Therefore, the leaky wave field propagates with increasing amplitude away from the surface, becoming infinite at infinity in the direction transverse to the surface. In spite of this improper behavior, leaky waves can be used to provide a valid representation of the fields for certain structures. To date, most antennas analyzed using leaky waves have been open waveguide structures.

3.4 Interpretation of Near Field Measurements Made on a Log Periodic Antenna

R. L. Bell, C. T. Elfving, and R. E. Franks have made near field measurements on a trapezoidal tooth antenna. They found that two waves exist on these antennas.

The first, called the "transmission line wave" was found to be the transverse electromagnetic (TEM) two-wire transmission line wave. This wave originates at the feed and propagates as a sine wave along the antenna without attenuation until it reaches the area where the teeth are approximately one quarter wavelength long. In this region, the wave is exponentially attenuated at a high rate and is thus effectively terminated.

Measurements of the currents on the teeth in this region were made and used to calculate the far field patterns. These

agreed with the measured patterns indicating that the energy was radiated from those elements. Therefore, this region was designated the "active region" of the antenna.

The second wave, named the "radiation wave", originates in the active region, and propagates toward the apex. Inside the active region, it builds up exponentially in the direction of propagation. Outside this region, it propagates with the speed of light toward and beyond the apex, its magnitude decreasing inversely with distance in front of the antenna. This wave becomes the far field at a suitable distance in front of the antenna.

Contour plots for this antenna have been published[5] and are reproduced in Figure 8. To aid in interpreting the radiation wave as a leaky wave, the near field contours for a Yagi-Uda antenna six wavelengths in length have been reproduced from the literature in Figure 9.[20]

It has been shown that a Yagi-Uda structure will support a travelling wave and that a long Yagi-Uda antenna can be treated as a surface wave antenna.[21,22] The hypothesis was made that the cross-sectional area of the field at the end of the antenna represents the effective aperture for the antenna. This approach assumes no direct radiation from the feed and no reflection from the end of the antenna. If the antenna is long enough for the surface wave to become established, the above solution represents the dominant mode of radiation.

As can be seen from Figure 9, the Yagi-Uda antenna supports

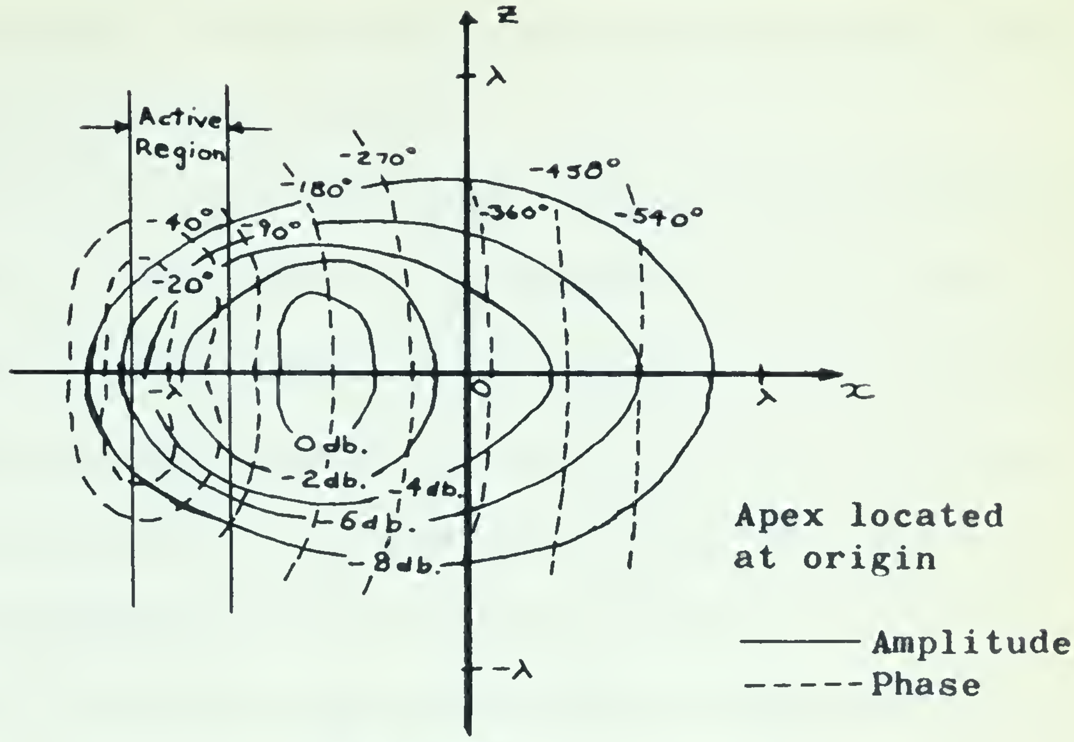

FIGURE 8

THE RADIATION WAVE FOR A LOG PERIODIC ANTENNA

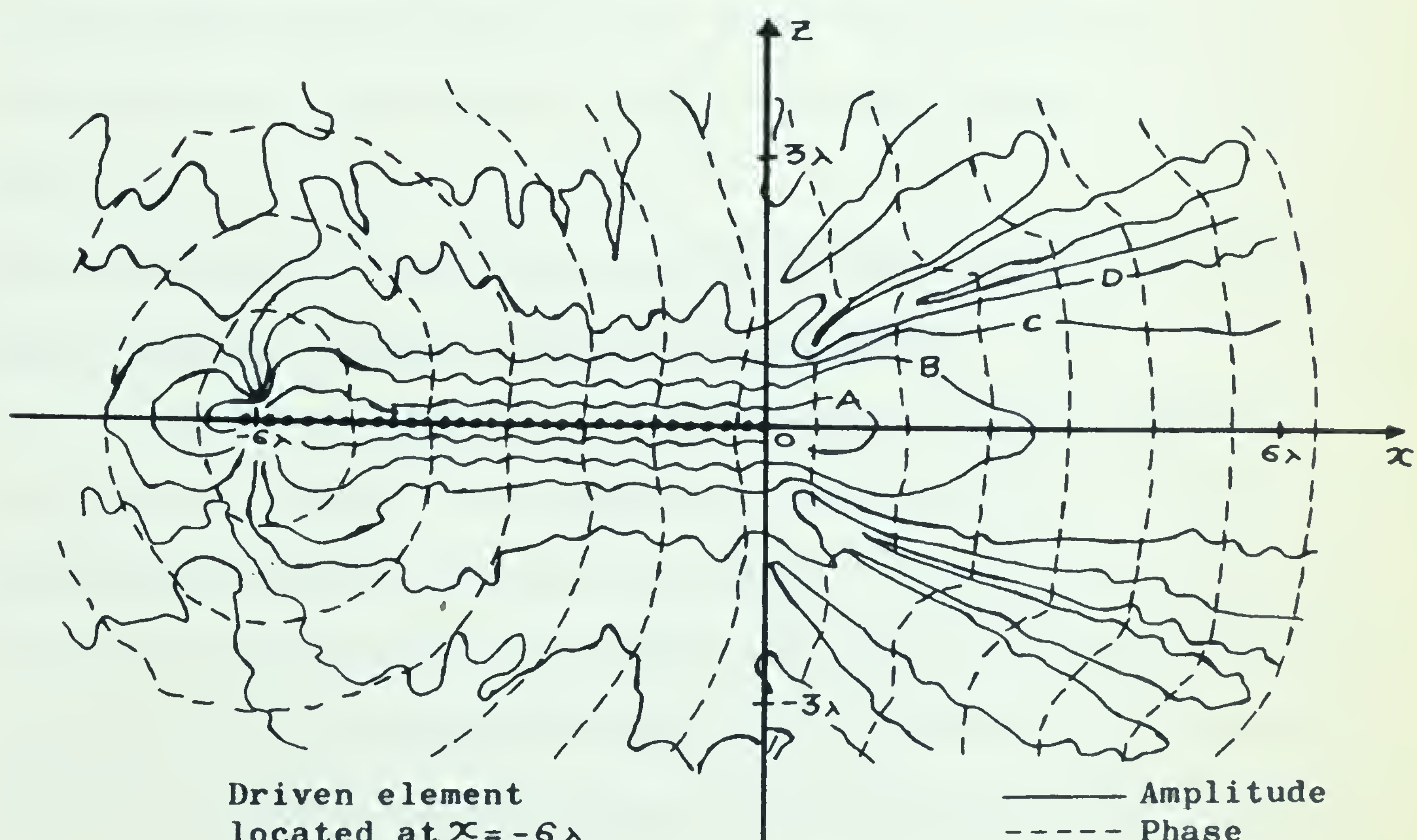

FIGURE 9

NEAR FIELD CONTOURS FOR A YAGI-UDA ANTENNA

a surface wave which forms an equi-phase aperture distribution at the end of the antenna. In front of the antenna, the wave begins to take the form of a diverging wave.

Comparison of the radiation wave for the log periodic antenna, shown in Figure 8, to the field of the Yagi-Uda antenna shows that the radiation wave does not behave as a surface wave in the active region. Instead, the magnitude of this wave increases along the centreline of the antenna in the direction toward the apex and decays in the perpendicular direction away from the centreline of the structure. Its phase progression has two components. The first is along the centreline of the antenna in the direction toward the apex and the second is perpendicular to the centreline in the direction away from the antenna. This behavior is the same as that described on Page 24 for a leaky wave. Therefore, the radiation wave can be treated as a leaky wave inside the active region.

3.3 Derivation of the Radiation Patterns for the Log Periodic Dipole Antenna ($\gamma = 0$) in Terms of Leaky Waves

It has been shown in the literature that the radiation patterns for a leaky wave antenna can be calculated from the approximate aperture distribution which is determined only by the leakage of energy along the structure.[23,24] In this section the approximate radiation pattern for the log periodic dipole antenna will be derived using this concept. The hypothesis will be made that the effective radiating aperture is located at the front of

the active region in the plane perpendicular to the antenna structure and that the radiation wave, which passes through this plane, makes up the aperture field.

Consider the log periodic dipole antenna shown in Figure 10. The antenna is oriented along the x axis with its elements parallel to the y axis (into and out of page). The active region covers the range $0 \leq x \leq a$. For mathematical expediency, the assumption is made that

$$k_y = 0 \tag{24}$$

This is true if the structure is infinite in the y direction. Physically an infinite structure can be obtained by arraying other identical antennas along the y axis. If there is no mutual coupling between the antennas, the shape of the radiation pattern in the $x-z$ plane will not be affected, and so the calculated radiation pattern in the $x-z$ plane obtained using this approach will be a good approximation to the actual patterns. Thus the problem has been effectively reduced from three dimensions to two dimensions. This simplification allows the fields to be described by exponential rather than Bessel functions.

It was shown in the previous subsection that the radiation wave for a log periodic antenna can be treated as a leaky wave inside the active region. Therefore, the following conditions hold in the region bounded by $0 \leq x \leq a$ and $0 \leq z \leq \infty$,

$$\begin{aligned} k_x &= -j\gamma_x = \beta_x + j\alpha_x = -j\gamma_R = \beta_R + j\alpha_R \\ k_z &= -j\gamma_z = \beta_z - j\alpha_z \end{aligned} \tag{25}$$

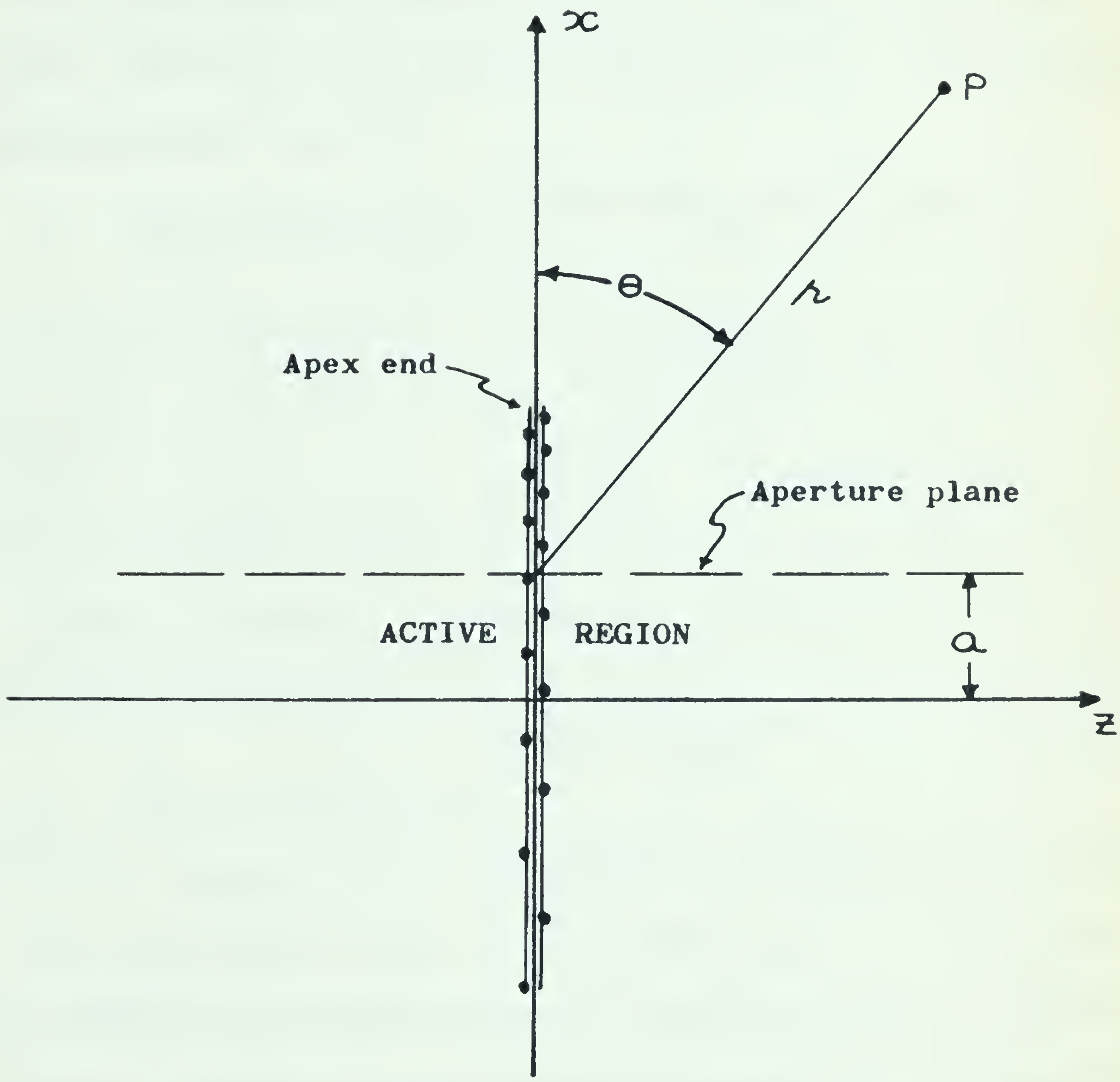

FIGURE 10

COORDINATE SYSTEM USED TO
CALCULATE THE RADIATION PATTERNS
FOR THE LOG PERIODIC DIPOLE ANTENNA

assuming $k_y = 0$. γ_R ($= \gamma_x$) is the complex propagation along the centreline of the antenna and thus describes the properties of the radiation wave in the direction along the boom. Equation (25) is readily obtained from Figures 8 and 10. The electric field intensity, parallel to the antenna elements in the active region, is obtained from (19) and (25)

$$E_y(x,z) = E_o e^{-z(\alpha_z + j\beta_z)} e^{x(\alpha_x - j\beta_x)} \tag{26}$$

where the time dependence, $e^{j\omega t}$, is suppressed. E_o, the amplitude of the fields at $x = z = 0$ is not needed since only the shape of the radiation fields will be considered. If required, it could be computed by equating the total input power to the radiated power.

Since the antenna is symmetrical about the x axis, the component of the electric field is given by

$$E_y(x,z) = E_o e^{-|z|\gamma_z - x\gamma_x} \tag{27}$$

in the active region, bounded by $0 \le x \le a$, $-\infty \le y \le \infty$, and $-\infty \le z \le \infty$.

The hypothesis is made that the aperture is in the plane $x = a$, $-\infty \le y \le \infty$ and $-\infty \le z \le \infty$ which is perpendicular to the axis of the antenna. This parallels the approach used for the long Yagi-Uda antenna previously described. Therefore, the aperture distribution is given by

$$E_y(a,z) = E_o e^{-|z|\gamma_z} e^{-a\gamma_x} = E_a e^{-|z|\gamma_z} \tag{28}$$

For $x > a$ the electric field $E_y(x, z)$ may be found using the bilateral Laplace transform[23] (equivalent to a Fourier transform[25])

$$E_y(x, z) = \int_c \mathcal{E}_y(\gamma_z') \, e^{-\gamma_x' x - \gamma_z' z} \, d\gamma_z' \tag{29}$$

and

$$\mathcal{E}_y(\gamma_z') = \frac{1}{2\pi j} \int_{-\infty}^{\infty} E_y(a, z) \, e^{\gamma_x' a + \gamma_z' z} \, dz \tag{30}$$

where $\gamma_x'^2 = -k_o^2 - \gamma_z'^2$ and $E_y(a, z)$ is given by (28).

In the following analysis, the parameters describing the radiation wave in the active region, γ_z and γ_x (or γ_R) will be treated as constants. This is not necessarily true for the actual antenna since there is some variation of the far field radiation patterns as the frequency is swept over a period of the antenna. It was observed during the measurements presented in Appendix B that the position of the standing wave on the transmission line field shifted through 360° as the frequency was swept over a period. Therefore, it is reasonable to assume that the position of the variations in the radiation wave making up the aperture distribution will also vary periodically with frequency and will cause the periodic variations in the far field patterns. However, the variations of the far field patterns, and thus, the effect of the variations in the radiation wave, are small over the useable range of the antenna's parameters so that the patterns obtained by assuming γ_z and γ_x (or γ_R) are constants will represent the average shape of the radiation patterns. Substituting (28) into (30) gives[23]

$$\mathcal{E}_y(\gamma_z') = \frac{1}{2\pi j}\int_{-\infty}^{\infty} E_a e^{-|z|\gamma_z} e^{\gamma_x' a + \gamma_z' z}\, dz \tag{31}$$

$$= \frac{E_a e^{\gamma_x' a}}{2\pi j}\left[\int_{-\infty}^{0} e^{(\gamma_z + \gamma_z')z}\, dz + \int_{0}^{\infty} e^{(-\gamma_z + \gamma_z')z}\, dz\right]$$

$$= \frac{E_a e^{\gamma_x' a}}{2\pi j}\left[\frac{1}{\gamma_z + \gamma_z'} - \frac{1}{-\gamma_z + \gamma_z'}\right]$$

$$\mathcal{E}_y(\gamma_z') = \frac{E_a \gamma_z e^{\gamma_x' a}}{j\pi\left[\gamma_z^2 - \gamma_z'^2\right]} \tag{32}$$

In (32), $\gamma_x' = j(k_o^2 + \gamma_z'^2)^{1/2}$, but $\gamma_z = \alpha_z + j\beta_z$ is a constant. Therefore, substituting (32) into (29) gives

$$E_y(x, z) = \frac{E_a \gamma_z}{j\pi}\int_c \frac{e^{-\gamma_x'(x-a) - \gamma_z' z}}{\gamma_z^2 - \gamma_z'^2}\, d\gamma_z' \tag{33}$$

This integral may be solved using the saddle-point method of approximation outlined in Appendix A.[23,26] In order to simplify the mechanics of using this method, the complex γ_z' plane is transformed into the complex ϕ' plane using the transformation

$$\gamma_z' = jk_o \sin\phi' \tag{34}$$

where

$$\gamma_z' = \alpha_z' + j\beta_z' \qquad \phi' = \sigma' + j\eta' \tag{35}$$

Also, the rectangular coordinates x, z are changed to the cylindrical coordinates r, θ where θ is measured from the x axis. Therefore, (33) becomes

$$E_y(r, \theta) = \frac{E_a \gamma_z k_o}{\pi}\int_{C_o} \frac{e^{-jk_o r\cos(\phi' - \theta)}\cos\phi'}{k_o^2 \sin^2\phi' + \gamma_z^2}\, d\phi' \tag{36}$$

The contour C_o in the complex ϕ' plane may be deformed into a steepest descent contour, SDC, passing through the saddle-point at $\phi' = \theta$. The integral may now be evaluated assymptotically to yield the far field radiation pattern, given by

$$E_y(r, \theta) = E_a \gamma_z k_o \left(\frac{2}{\pi k_o r}\right)^{1/2} e^{-j(k_o r - \pi/4)} f_1(\theta) \tag{37}$$

where the pattern function, $f_1(\theta)$, is

$$f_1(\theta) = \frac{\cos\theta}{k_o^2 \sin^2\theta + \gamma_z^2} \tag{38}$$

The details for the above transformation and integration are given in Appendix A.

A slightly more convenient form of (38) can be obtained in order to simplify the calculation of the radiation fields. The relation

$$\gamma_x^2 + \gamma_z^2 + k_o^2 = 0 \tag{39}$$

can be obtained from (16) and (17) on Page 23. Substituting (39) in (38) yields

$$f_1(\theta) = \frac{-\cos\theta}{k_o^2 \cos^2\theta + \gamma_x^2} = \frac{-\cos\theta}{k_o^2 \cos^2\theta + \gamma_R^2} \tag{40}$$

since $\cos^2\theta + \sin^2\theta = 1$. The angle θ is measured from the x axis as shown in Figure 10.

In the above derivation, the radiation patterns of the individual elements making up the antenna were not considered. Hence, (40) represents the group pattern for the log periodic dipole antenna. Since the radiation pattern of a dipole is isotropic in the H plane, (40) also represents the H plane radiation pattern for

the log periodic dipole antenna. To obtain the E field pattern, the unit patterns of the individual elements must be considered. An exact solution for these unit patterns would be very difficult to obtain because the lengths of the elements vary and mutual coupling must be accounted for. However, measurements made on a wire triangular tooth log periodic antenna indicated that the current distribution over each tooth is approximately sinusoidal so that mutual coupling between the teeth has little effect on the shape of the current distribution on the individual teeth.[5] Since the active region is approximately centred on the elements which are near a half wavelength long and the radiation patterns for dipoles near this length are practically identical to the pattern of a half wave dipole, the E field pattern for this antenna can be approximated by multiplying the group pattern by the unit pattern for a half wave dipole. The pattern function of a half wave dipole with a sinusoidal distribution is given by[27]

$$f_d(\theta) = \frac{\cos(\pi/2 \sin\theta)}{\cos\theta} \tag{41}$$

Therefore, the pattern function for the E field of the log periodic dipole antenna is given by

$$f_2(\theta) = \frac{-\cos(\pi/2 \sin\theta)}{k_o^2 \cos^2\theta + \gamma_R^2} \tag{42}$$

3.4 Generalization to Other Types of Log Periodic Antennas ($\psi \neq 0$)

Although it is necessary to feed two half structures, or booms, of the log periodic antennas against each other or against ground in order to obtain wideband operation, R. H. DuHamel and

D. G. Berry have shown, using special measuring techniques, that each half structure produces a unidirectional beam pointing in the direction of its centreline.[18] In order to explain the variation of the H field radiation pattern for the complete antenna as the angle, ψ, between the booms is changed, a reasonable approach would be to assume that each boom radiates independently of the other. Therefore, the overall pattern of the complete antenna can be calculated if the direction of each half structure and the position of the centre of radiation on each boom is known. Although this approach neglects the effects of mutual coupling between the booms, it has still been found to give good results.[10,18]

The H field radiation pattern for a log periodic antenna may be calculated by considering Figure 11.[18] In space, the total radiation pattern is given by the vector addition of the radiation fields from the booms. If the phase reference point is taken to be the apex of the antenna, then the pattern function for the H field is given to be

$$f_3(\theta) = f_1(\theta - \psi/2)\, e^{-j2\pi \ell_1} + f_1(\theta + \psi/2)\, e^{-j2\pi \ell_2} \tag{43}$$

The lengths, ℓ_1, and ℓ_2, are given by

$$\begin{aligned} \ell_1 &= d\cos(\theta - \psi/2) \\ \ell_2 &= d\cos(\theta + \psi/2) \end{aligned} \tag{44}$$

where d is the distance from the apex of the antenna to the centre of radiation on each boom, measured in wavelengths. For the special case where $\psi = 0$, the patterns for the overall antenna should be identical to those of each individual boom, providing the effects of

[illegible] have shown, using several measuring techniques, that each beam radiates [illegible] in the direction of its [illegible].[17] In order to explain the deviations of the H-field radiation pattern [illegible] between the beams [illegible] would be to assume that each beam radiates independently of the other. Therefore, the overall pattern of the complete antenna can be evaluated by [illegible] of beams with [illegible] and the position of the center of radiation of each beam is known. Although this approach neglects the effects of mutual coupling between the beams, it has still been found to give good results.[11,18]

The H-field radiation pattern for a two-element antenna can be calculated by considering Figure 31.[19] As shown, the total radiation pattern is found by the [illegible] of the radiation fields from the beams. If the [illegible] point is taken at the apex of the antenna, then the pattern function for the H-field is given by

[illegible]

The [illegible] are given by

[illegible]

[illegible]

where [illegible] is the distance from the apex of the antenna to the center of radiation on each beam, measured in wavelengths. For the [illegible] case where [illegible] = 0, the patterns for the overall antenna [illegible] identical in terms of each [illegible], providing the effects of

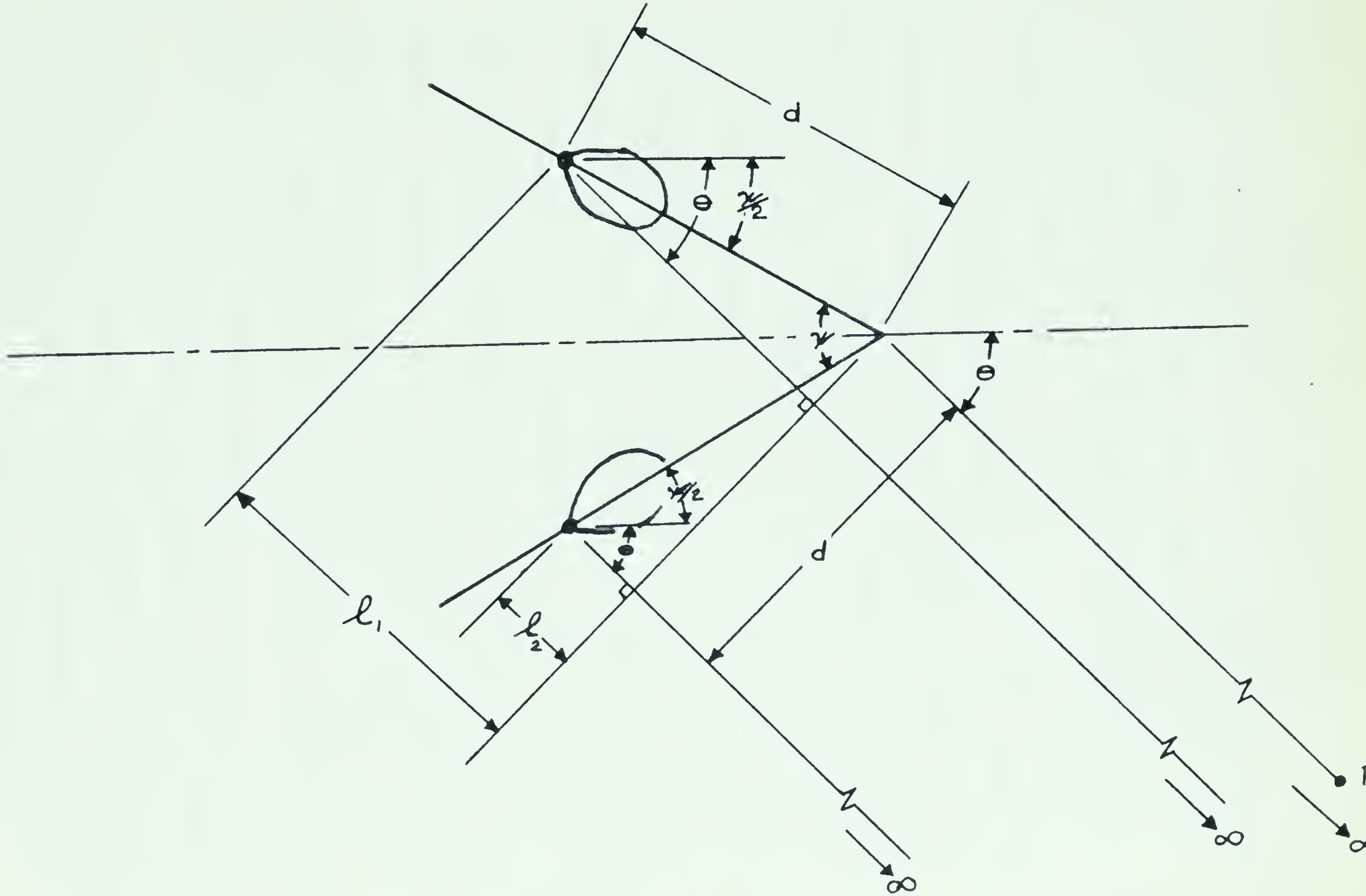

FIGURE 11

GEOMETRY FOR CALCULATING THE H FIELD PATTERN OF A LOG PERIODIC ANTENNA

mutual coupling are ignored. It has been observed that the radiation patterns of the log periodic dipole antenna ($\psi = 0$) and the wire trapezoidal tooth half structure with equivalent parameters do agree closely.[10] Therefore, the pattern function, $f_1(\theta \pm \frac{\psi}{2})$, in (43) for each boom is given by (40) of the previous subsection making the substitution $\theta \pm \psi/2$ for θ.

In the previous subsection, the hypothesis was made that the "effective aperture" for these antennas occurs at the front of the active region, which is roughly centred on the elements one half wavelength long. However, in order to apply (43), the exact location of the phase centre of the radiation from each boom must be known. This information is available in the literature and is reproduced in Figure 12 for the wire trapezoidal tooth structure.[10] It was found that d (measured in wavelengths) is essentially independent of frequency. For apex angles less than 60° and in the range of geometric ratios for which the patterns do not break up excessively over a period, d is also independent of the geometric ratio. Thus, Figure 12 can be applied to any antenna whose parameters meet the above restrictions.

It has been observed that the E field beamwidth is reasonably constant as the angle, ψ, between the booms is varied from 0° to 90° and so (42) can be used to calculate the E field pattern for a log periodic antenna if ψ is not too large.[10]

3.5 Relationships Between the Radiation and Transmission Line Waves

It has been shown that the transmission line wave terminates in the active region, and the radiation wave originates therein.

mutual coupling are ignored. It was shown however that the radiation patterns of the log periodic dipole antenna ($\psi = 0$) and the wire trapezoidal tooth half structure with equivalent parameters do agree closely.[15] Therefore, the pattern function, $F(\theta,\phi)$, in (43) for each beam is given by (44) of the previous subsection making the substitution $\Theta = 90°$, ($\psi = 0$).

In the previous subsection, the hypothesis was made that the "effective aperture" (or linear-arrangement element) of the log periodic is the active region, which is roughly centered at the element one-half wavelength long. However, in order to apply (43), the exact location of the phase center of the radiation from each beam must be known. This information is available in the literature and is reproduced in Figure 12 for the wire trapezoidal tooth structure.[19] It was found that d_l (measured in wavelengths) is essentially independent of frequency. The apex angles from 10° to 45° and the range of geometric ratios for which the structure is not excessively over a period, d_l is also independent of the geometric ratio. Thus, Figure 12 can be applied to any antenna whose parameters meet the above restrictions.

It has been observed that the E field magnitude is reasonably constant as the angle, ψ, between the beams is varied from 0° to 90° and so (43) can be used to calculate the E field pattern for a log periodic antenna if ψ is not too large.[20]

3.6 Relationships between the Radiation and Transmission Line Modes

It has been shown that the transmission line mode radiates in the active region, and the radiation mode originates there.

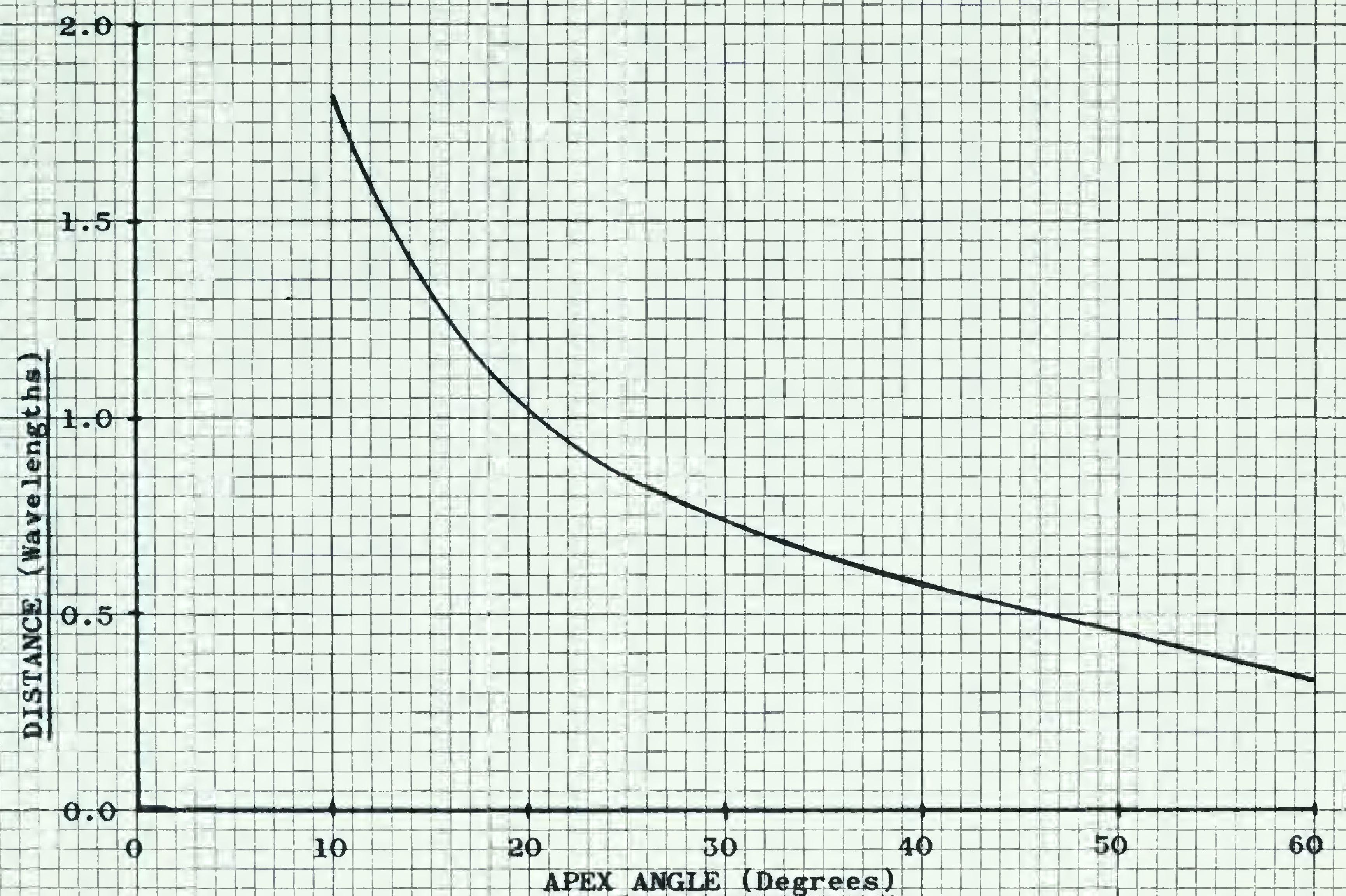

FIGURE 12

DISTANCE (d) FROM APEX TO PHASE CENTRE

FOR A WIRE TRAPEZOIDAL TOOTH LOG PERIODIC HALF STRUCTURE

Therefore, the current distribution on the teeth in this region serves as the common boundary between the two waves.[5]

To simplify the problem of finding the relations between the radiation and transmission line waves, it is convenient to consider an end fire array whose elements have identical input impedances and spacings. For normal excitation, the phase progression along the transmission line field and the currents in the elements would be equal. However, as can be seen from Figure 7 on Page 20, the feed system for log periodic antennas produces an additional 180° phase shift between the elements. If the elements are spaced σ wavelengths apart, the phase shift of the transmission line wave between elements will be $\beta_T \sigma$ radians with the result that the phase shift between the currents on these elements will be given by $\beta_R \sigma = \beta_T \sigma - \pi$.[4] β_R is the phase constant of the currents on the elements. The assumption is made that the phase progression of the radiation wave is equal to that of the currents on the elements so that β_R can also be considered as the phase constant of the radiation wave. Therefore, the phase relationship between the transmission line and radiation waves is given by

$$\beta_R = \beta_T - \pi/\sigma \tag{45}$$

for an array of elements having equal input impedances and spacings.

Since the active region for log periodic antennas is short, the variation in the spacings between the elements will be small and an average value can be used.[4] If σ is taken to be the

spacing between the half wavelength element and the next closer element to the apex of the antenna, the result[3]

$$\sigma = \frac{1 - \tau}{4 \tan \frac{\Theta}{2}} \tag{46}$$

is obtained from the geometry of the log periodic dipole antenna shown in Figure 7 on Page 20. Using this approximation, it has been found that (46) gives a good representation for the phase shift of the currents on the elements of a log periodic dipole antenna even though the input impedances of the elements do vary over the active region.[3]

For successful log periodic antennas σ is normally small so that β_R is negative with respect to β_T , and the radiation wave propagates back toward the apex. This explains why log periodic antennas behave as backward wave structures.[4]

In the active region, it can be seen from measurements presented in the literature that the currents on the elements build up very quickly near the front of the active region and then decay at nearly the same rate as the transmission line wave toward the rear of the region.[3] Since these currents act as the source of the radiation wave the phase progression and distribution of the wave will be similar to that of the currents in the elements. Since the phase progression of the elements is toward the apex, the wave will appear to start at the rear of the active region and propagate toward the apex, building up at the same rate as the currents on the elements. Near the front of the active region, the currents on the

elements drop off rapidly, and have little effect on the radiation wave. Once established, the wave continues to propagate toward and beyond the apex, and becomes the far field at a suitable distance in front of the antenna. Therefore, the decay of and build up of the transmission line and radiation waves, respectively, are approximately equal and the relationships between the two waves are given by

$$\alpha_R = \alpha_T \tag{47}$$

and (45) to a first order approximation. α_R and α_T are the attenuation constants for the radiation and transmission line waves, respectively, in the active region.

3.6 Summary

It was shown in this section that the radiation mechanism of the log periodic class of antennas can be analysed in terms of leaky waves.

Three basic assumptions were made which greatly simplified the analysis. The first was that each half structure radiates independently of the other. Although this approach ignores the effects of mutual coupling between the booms, it has been found to give a good approximation to the measured patterns.[18] Therefore, only one boom need be considered in the leaky wave analysis. The overall pattern can then be obtained by adding the radiation from the two booms vectorially in space. The second simplification made was to assume $k_y = 0$, therefore, reducing the problem to two dimensions.

This allowed the fields to be described in terms of exponential functions. The third premise was that the radiating aperture for each half structure occurs at the front of the active region and is in the plane perpendicular to the boom. The radiation wave, which passes through this plane, was assumed to make up the aperture field distribution.

The far field pattern for each boom may be obtained from the aperture distribution using a bilateral Laplace transform. This transform is valid in the half plane $x > a$, and therefore, the solutions obtained are valid over the range $-\frac{\pi}{2} < \theta < \frac{\pi}{2}$ and will not predict the radiation in the rear quadrants.

The E and H field pattern functions for each boom or for the log periodic dipole antenna ($\psi = 0$) were found to be

$$f_2(\theta) = \frac{-\cos(\pi/2 \sin\theta)}{k_o^2 \cos^2\theta + \gamma_R^2} \tag{42}$$

and

$$f_1(\theta) = \frac{-\cos\theta}{k_o^2 \cos^2\theta + \gamma_R^2} \tag{40}$$

respectively. The azimuth angle, θ , is measured from the extended centreline of the boom. γ_R is the complex propagation constant of the radiation wave along the boom and k_o is the wave number of free space.

The H field pattern function for other types of log periodic antenna ($\psi \neq 0$) was found to be

$$f_3(\theta) = f_1(\theta - \psi/2)\, e^{-j2\pi \ell_1} + f_1(\theta + \psi/2)\, e^{-j2\pi \ell_2} \tag{43}$$

where

$$\ell_1 = d \cos(\theta - \psi/2)$$
$$\ell_2 = d \cos(\theta + \psi/2) \qquad (44)$$

The distance, d , from the apex of the antenna to the centre of radiation on each boom, measured in wavelengths, may be obtained from Figure 22. The azimuth angle, θ , is measured from the extended centreline of the antenna as shown in Figure 11.

The relations between the radiation field and the transmission line field were found to be

$$\alpha_R = \alpha_T \qquad (47)$$

and

$$\beta_R = \beta_T - \frac{\pi}{\sigma} \qquad (45)$$

where

$$\sigma = \frac{1 - \tau}{4 \tan \frac{|\Theta|}{2}} \qquad (46)$$

for the log periodic dipole antenna, or

$$\sigma = \frac{1 - \sqrt{\tau}}{4 \tan \frac{|\Theta|}{2}} \qquad (48)$$

for the other types of log periodic antenna. (48) is obtained from (46) using (15) on Page 19.

If the angle, ψ , between the booms is less than 90°, the pattern function for the E field can be approximated by (42) with reasonable accuracy.[10]

Using the above equations, the shape of the far field patterns can be obtained for the log periodic class of antennas if the properties of the transmission line field are known. These can

be obtained either theoretically or experimentally. In this thesis they will be found experimentally using the measuring procedure outlined in the next section.

SECTION 4

4. MEASURING TECHNIQUES

In the previous section, the far field radiation patterns for the log periodic antenna were derived in terms of the attenuation and phase constants of the transmission line field in the active region of the antenna.

The attenuation constant may be obtained by plotting the relative strength of the transmission line field in decibels versus the distance from the apex of the antenna in wavelengths and taking the slope of the curve in the active region. If this is done, the attenuation constant is given by

$$\alpha_T = -\frac{\text{Slope}}{8.68} \tag{49}$$

where α_T is expressed in nepers per wavelength. Similarly, the phase constant is found by plotting the relative phase shift of the transmission line field in degrees versus the distance from the apex of the antenna in wavelengths and taking the slope of the resulting curve in the active region. The phase constant is then given by

$$\beta_T = -\frac{\text{Slope}}{57.3} \tag{50}$$

where β_T is expressed in radians per wavelength. Therefore, the relative magnitude and phase of the transmission line field must be measured along the antenna before the radiation patterns can be calculated.

4.1 Requirements of the Measuring System

Since both the transmission line and radiation fields exist along the antenna, the measurement of each individual field is rather difficult. It has been found that both these fields contain components parallel and perpendicular to the elements except in the plane equidistant between the two booms.[5] In this plane, the electric part of the transmission line field, perpendicular to both this plane and the elements, is parallel to the plane containing the booms. The radiation field is parallel to the elements in this plane. Therefore, the sampling probe must have the proper polarization to a high degree of accuracy in order to sample the desired field.

The system used to make the measurements must give accurate results over a wide range of signal levels since the transmission line field decays about 20 db. in the active region.

A desireable, although not essential, property of the measuring system is that it can be used over a reasonably wide frequency range. If the measurements are made on a log periodic dipole antenna having a particular value of geometric ratio, τ , and apex angle, Θ , the same structure can be used for smaller apex angles simply by cutting the elements to the required lengths. Since it is necessary to measure the properties of the transmission line field over a large range of antenna parameters, a wide band measuring system will greatly reduce the time required for assembling the structures.

4.1 Requirements of the Measuring System

Since both the transmission line and radiation fields exist along the antenna, the measurement of each individual field is rather difficult. It has been shown that both these fields contain components parallel and perpendicular to the elements except in the plane containing the antenna and the booms.[7] In this plane, the electric part of the transmission line field, perpendicular to the wire plane and the elements, is parallel to the plane containing the booms. The radiation field is parallel to the elements in this plane. Therefore, the measuring probe must have its proper polarization to a high degree of accuracy in order to sample the desired field.

The probe used to make the measurements must also measure accurately over a wide range of signal levels since the transmission line field ranges about 20 db. in the active region.

A desirable, although not essential, property of the measuring system is that it can be used over a reasonably wide frequency range. If the measurements are made on a log periodic dipole antenna having a particular value of geometric ratio, τ, and apex angle, 2α, the same structure can be used for another apex angle simply by cutting the elements to the required lengths. Since it is necessary to measure the properties of the transmission line field over a large range of antenna parameters, a wide band measuring system will greatly reduce the time required for fabricating the structures.

The final requirement is that the frequency at which the measurements are to be made lies within the ranges 400 mc. to 1,000 mc. and 1,900 mc. to 4,000 mc. in order to use the equipment available. The range between 1,900 mc. and 3,500 mc. is the most attractive since the antenna structures will be of a convenient size to handle, but will not become too small for the required physical tolerances to be maintained.

Direct probing of the fields by a dipole is unsatisfactory since a significant portion of the signal is picked up by the outer conductor of the coaxial lead. This results in the measurement of a very high standing wave caused by the vector addition of the transmission line field and the radiation field picked up by the outer conductor. It is possible to eliminate the induced currents produced by these fields on the outer conductor by using chokes.[19] However, the space between the booms is rather limited so that this method is not too practical unless a relatively low frequency is used.[5]

Since only one boom is used for the feed system, the other boom may be slotted and the cable to the probe run inside the boom.[3] When the angle between the booms is zero, such as for the log periodic dipole antenna, the probe is very nearly symmetrically located between the booms and good results are obtained. This requires that the inner diameter of the boom be large enough to allow the feed cable to move freely and effectively limits the upper frequency at which the measurements can be made to about 500 mc.

Therefore, this method is not entirely satisfactory.

4.2 Description of Measuring System

The method finally settled on was to mount a single boom over a horizontal ground plane and use a vertical probe extending through the ground plane to make the measurements. Since the ground plane is located symmetrically between the boom and its image, the probe will only sample the transmission line field. This type of probe can be used over a wide frequency range. No currents will be induced in the feed cable as it is located below the ground plane.

Placing a single half structure over an infinite ground plane is analogous to rotating one of the booms about its centreline through an angle of 180° since the image antenna is the mirror image of the actual boom. The phase of the energy radiated by the rotated antenna is effectively reversed with the result that a null occurs along the extended centreline of the boom (or the ground plane) for the far field radiation pattern. However, it has been observed that the E field radiation pattern is unchanged when this rotation is made so that the effects of mutual coupling between the booms are small.[14] Therefore, the results obtained using the ground plane should be identical to those obtained for the complete antenna providing the ground plane is infinite in extent. However, it was observed that the magnitude of the standing wave of the transmission line field was larger than that obtained for the complete antenna. The reason for this apparent discrepancy is that the reflection of energy out of the active region from the booms adds in phase when

they are mirror images. For the normal antenna, the reflections are 180° out of phase and tend to cancel so that the standing wave is reduced. A similar phenomenon has been observed for the variation of the input impedance[14] which is of the same magnitude as the standing wave on the transmission line field.[5] Thus, this method of measuring might be considered as giving a more accurate picture of the actual transmission line field for a single boom than the measurements made on the complete antenna.

The ground plane used was a sheet of aluminum eight feet long and four feet wide. Absorbing material was piled around the edges of the plane to make it appear infinite in extent to the antenna. A photograph of the ground plane and absorbing material is shown in Figure 13. One piece of absorbing material was removed allowing the antenna to be seen from the rear.

A close up photograph of a typical antenna half structure, with parameters $\tau = 0.81$ and $\Theta = 20^{\circ}$, mounted over the ground plane is shown in Figure 14. The half structure is soldered to the centre conductor of a type UG-290/U panel jack mounted on a small aluminum bracket. This is shown in the right hand side of Figure 14. The feed cable from the generator runs up through a hole in the ground plane and is connected to the panel jack, thus, exciting the antenna. Probing holes were drilled in the ground plane at intervals of one half centimeter directly under the boom. The probe can be seen located in the ground plane near the rear of the antenna.

they are mirror images. For the normal antenna, the reflections are 180° out of phase and tend to cancel so that the standing wave is reduced. A similar phenomenon has been observed for the variation of the input impedance[14] which is of the same magnitude as the standing wave on the transmission line field.[7] Thus, this method of measuring might be considered as giving a more accurate picture of the actual transmission line field for a single boom than the measurements made on the complete antenna.

The ground plane used was a sheet of aluminum eight feet long and four feet wide. Absorbing material was piled around the edges of the plane to make it appear infinite in extent to the antenna. A photograph of the ground plane and absorbing material is shown in Figure 13. The piece of absorbing material was removed allowing the antenna to be seen from the front.

A close up photograph of a typical antenna half structure, with parameters $\tau = 0.82$ and $2\psi = 30°$, mounted over the ground plane is shown in Figure 14. The half structure is connected to the center conductor of a type UG-290/U panel jack mounted on a small aluminum bracket. This is shown in the right half of Figure 14. The feed cable from the transmission line is brought through a hole in the ground plane and is connected to the panel jack, thus exciting the antenna. Probing holes were drilled in the ground plane at intervals of one half centimeter directly under the boom. The probe had to be inserted in the ground plane under the boom of the antenna.

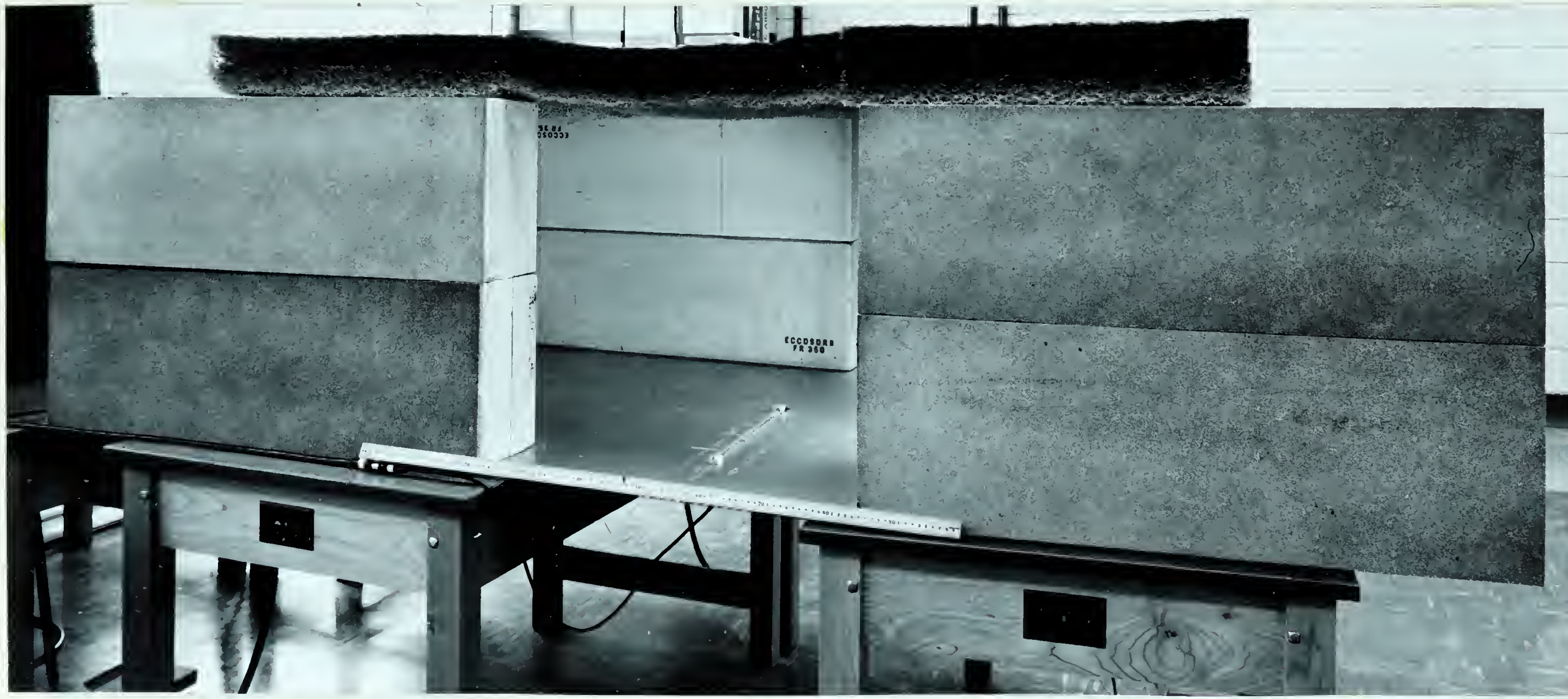

FIGURE 13

GROUND PLANE USED FOR MEASURING

TRANSMISSION LINE CHARACTERISTICS

FIGURE 14

HALF STRUCTURE MOUNTED OVER GROUND PLANE

SHOWING DETAILS OF FEED SYSTEM

Figure 15 shows a view of the bottom side of the ground plane with the probe assembly in place. The probe is held in place by four aluminum strips bolted to the ground plane and running parallel to the holes. For each pair of strips, the one next to the ground plane is slightly farther from the holes than the top piece so that a small lip is formed which holds the probe assembly in place. The probe can be quickly removed by twisting it clockwise until the plate of the assembly clears the lips and then lifting it out of the hole. To insert the probe in another hole, the procedure is reversed. The feed from the generator is located behind the vertical plate.

The probe assembly is shown in Figure 16. The ruler shows the relative size of the probe in inches. The assembly consists of a short length of RG-142/U rigid coaxial cable, a type UG-89/U connector, a small aluminum plate and a small piece of tin. The cable is soldered to the piece of tin which is in turn bolted to the aluminum plate, thus, holding the assembly together. The connector is placed on the other end of the rigid cable and allows the signal to be coupled to a conventional coaxial cable. To insure maximum rigidity and stability, the connectors were taped together.

The circuit used to make the measurements is shown in Figure 17. A photograph of the circuit is shown in Figure 18. The relative phase along the antenna is determined by adjusting the position of the probe on the slotted line and the variable power divider to achieve a null on the receiver.

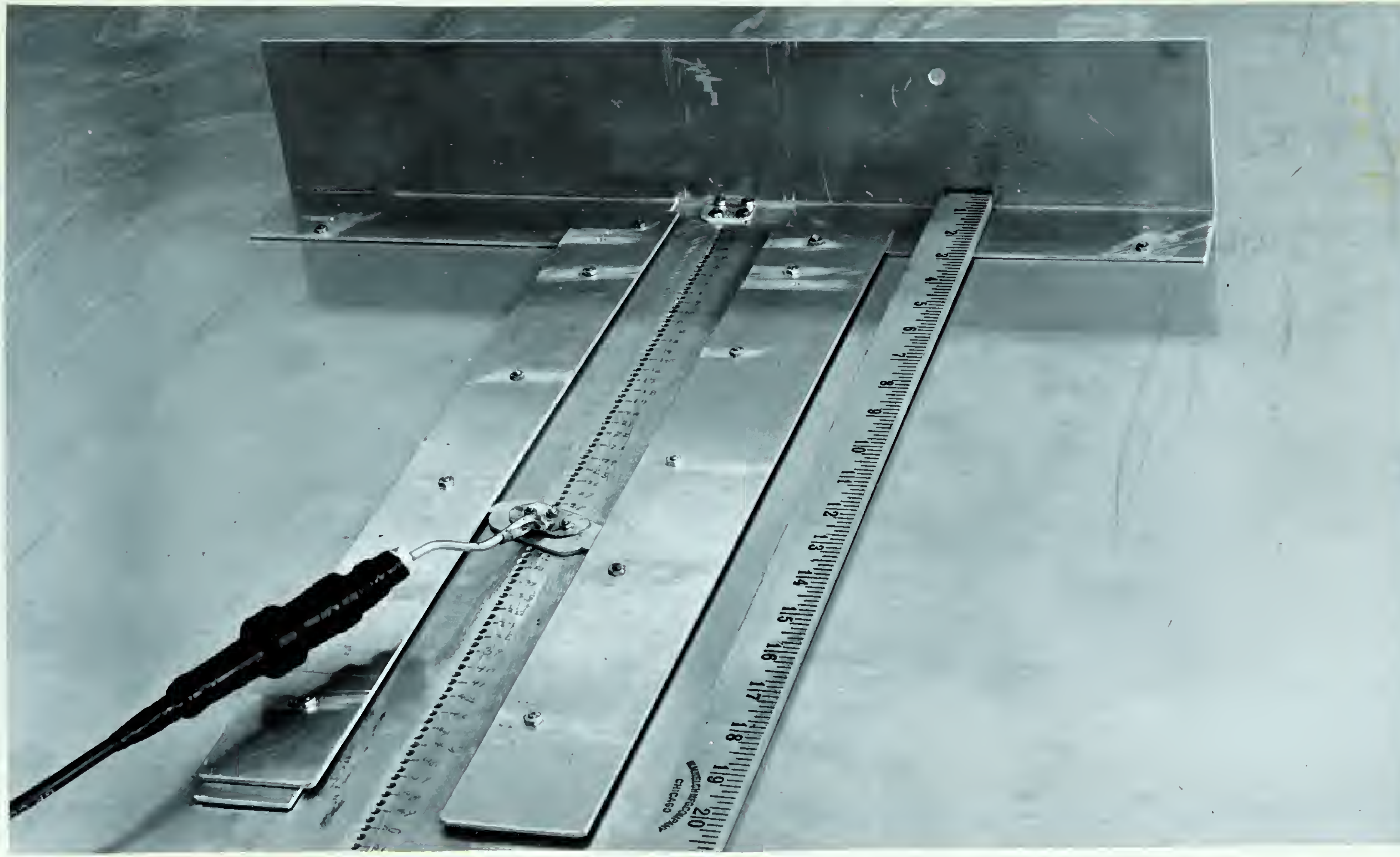

FIGURE 15

BOTTOM SIDE OF GROUND PLANE

WITH PROBE ASSEMBLY IN PLACE

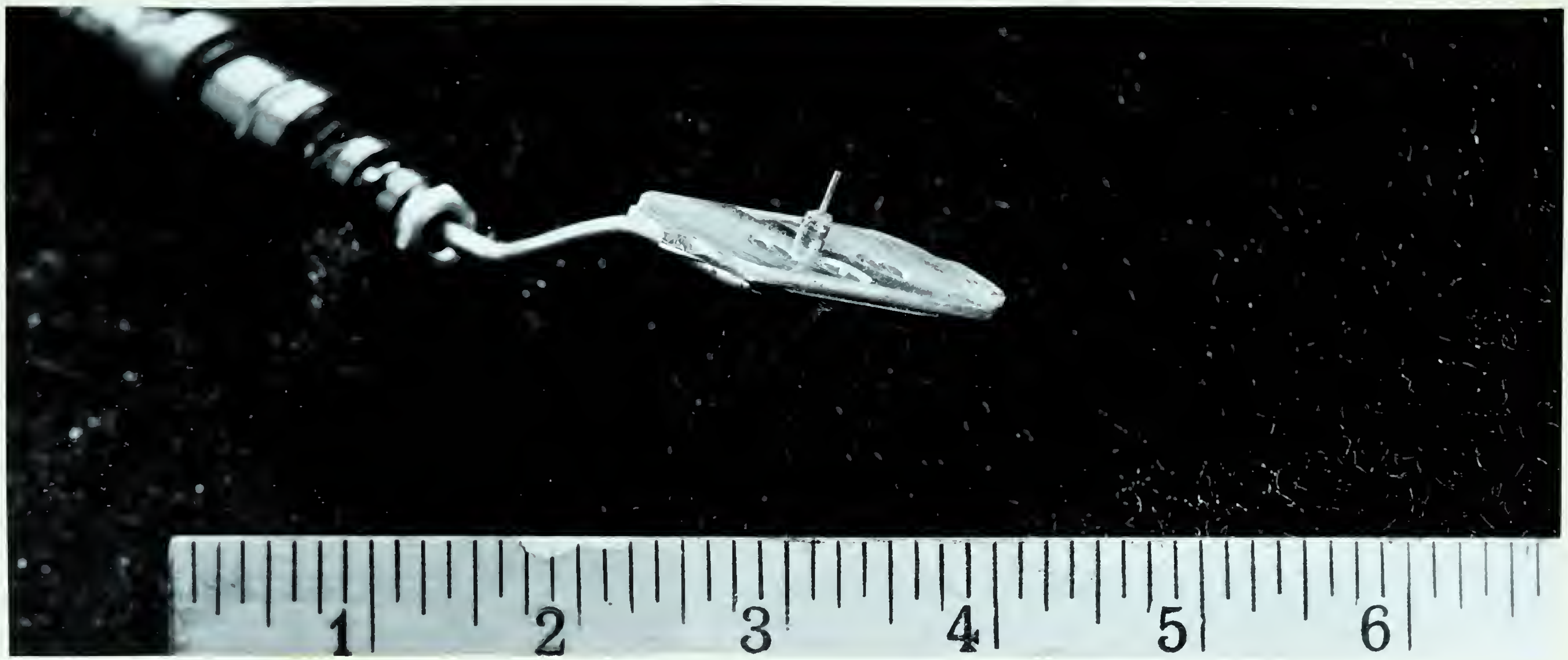

FIGURE 16

PROBE ASSEMBLY

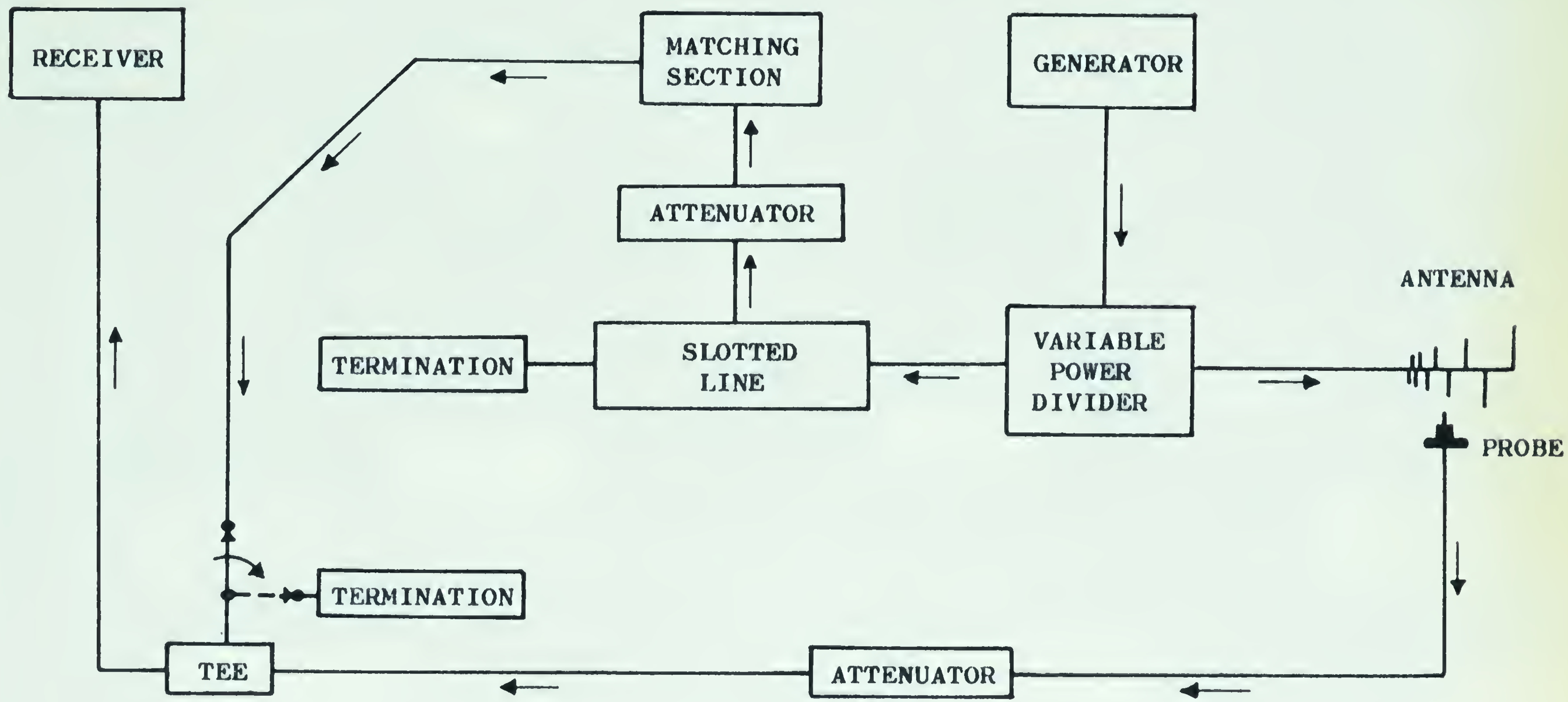

FIGURE 17

CIRCUIT USED FOR PHASE
AND AMPLITUDE MEASUREMENTS

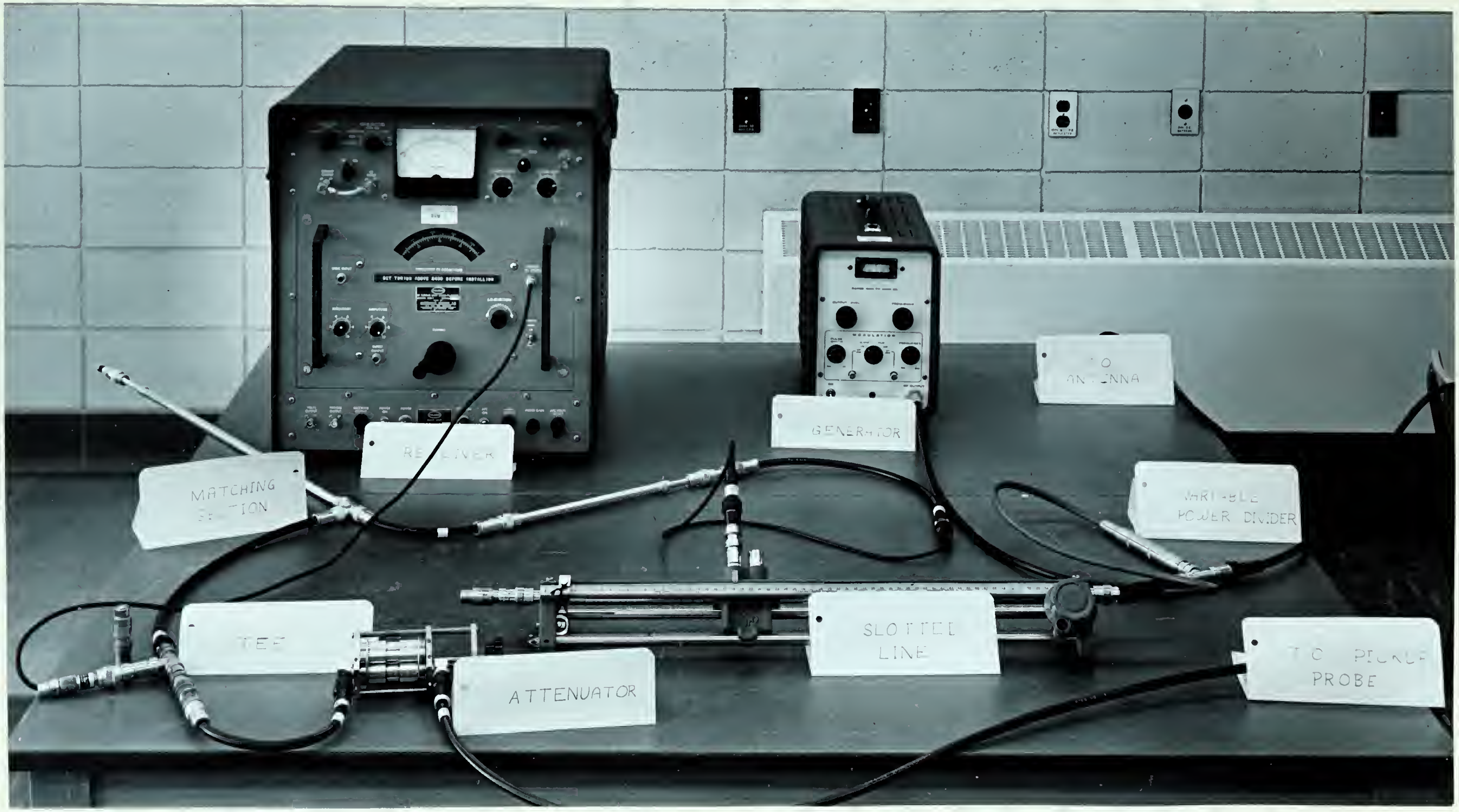

FIGURE 18

EQUIPMENT USED FOR THE MEASUREMENTS

If the slotted line is terminated in its characteristic impedance then the signal will propagate down the line with the speed of light. Therefore, as the slotted line probe is moved along the line, the phase of the signal will vary $2\pi\ell$ radians where ℓ is the distance the slotted line probe moves, measured in wavelengths. If the signal levels from the pickup probe sampling the antenna fields and from the probe on the slotted line are equal in magnitude at the tee, a very sharp null will occur on the receiver when these two signals are 180° out of phase at the tee. As the sampling probe is moved along the antenna, the distance the probe on the slotted line must be moved to maintain the null condition will give the phase shift of the field on the antenna.

To measure the signal level picked up by the sampling probe, the cable from the slotted line probe was replaced by a standard termination at the tee connector.

4.3 Evaluation of Measuring Circuit

The circuit shown in Figure 17 has several rather critical requirements if accurate results are to be obtained.

Since the variation of the signal level along the antenna exceeds 30 db. and a nulling technique was used to measure the phase, the detecting device must be capable of accurately measuring signal levels over a very wide range. The generator used, a PRD Electronics Corporation Type S712 signal source, has a maximum output of about 100 milliwatts and so the detector must possess high sensitivity. Fortunately, such a receiver, the Polaroid

If the slotted line is terminated in its characteristic impedance then the signal will propagate down the line with the speed of light. Therefore, as the slotted line probe is moved along the line, the phase of the signal will vary 2π radians where λ is the distance the slotted line probe moves, measured in wavelengths. If the signal levels from the pickup probe sampling the antenna fields and from the probe on the slotted line are equal in magnitude at the tee, a very sharp null will occur on the detector when these two signals are 180° out of phase at the tee. As the sampling probe is moved along the antenna, the distance the probe on the slotted line must be moved to maintain the null condition will give the phase shift of the field on the antenna.

To measure the signal level picked up by the sampling probe, the cable from the slotted line probe was replaced by a matched termination at the tee connector.

4.3 Evaluation of Measuring Circuit

The circuit shown in Figure 17 has several rather exacting requirements if accurate results are to be obtained.

Since the variation of the signal level along the antenna exceeds 30 db, and a nulling technique was used to measure the phase, the detection device must be capable of accurately measuring signal levels over a very wide range. The Polytechnic Research and Development type signal source, and a output of about 100 milliwatts and high sensitivity. Fortunately, such a receiver, the

Electronics Corporation Model R-B1 Microwave Receiver with Plug in Unit RW-T, was available. This receiver will measure signal levels over a 70 db. range. It was found that the maximum signal on the antenna usually gave a deflection of over 50 db. on the receiver so that a reserve exceeding 10 db. was available for making the phase measurements even at the lowest signal levels on the antenna. Very sharp nulls, as deep as 40 db., could be obtained while making the phase measurements in the high signal level region of the antenna. For lower signal levels, the depths of these nulls were determined primarily by the signal level.

Any reflections occurring in the circuit will be constant at a particular frequency and hence will appear as a standing wave for the phase measurements. For example, if the lines leading to the tee at the receiver have a VSWR of 1.1:1 the maximum possible error in the phase reading is $\pm 5.5^{o}$, providing both signals are equal in magnitude. It was possible to match one line to the above tolerance using a General Radio type 874-G10 attenuator pad and a Microlab AT-13N Turret Attenuator. The second line could not be matched to this tolerance using the remaining General Radio and Microlab attenuators so that a matching unit consisting of attenuators and a single stub match made up of two Microlab series SR adjustable lines was used. The required matching tolerance was then met at each frequency by adjusting the lengths of the adjustable lines.

Any variation from a linear phase shift, such as caused by

Electronics Corporation model D-81 Microwave Receiver with plug in Unit RF-5, was available. This receiver will measure signal levels over a 70 db. range. It was found that the maximum signal in the antenna usually gave a deflection of over 50 db. on the receiver so that a complete [illegible] of 50 db. was available for making the phase measurements even at the lowest signal levels in the antenna. Very sharp nulls, as deep as 40 db., could be obtained while making the phase measurements in the high signal level region of the antenna. For lower signal levels, the depths of these nulls were determined primarily by the signal level.

Any reflections occurring in the circuit will be constant at a particular frequency and hence will appear as a standing wave for the phase measurements. For example, if the lines leading to the tee at the receiver have a VSWR of 1.1:1 the maximum possible error in the phase reading is ± 5.7°, provided both signals are equal in magnitude. It was possible to match the line to the [illegible] tolerance using a General Radio type 874-[illegible] tuner and a [illegible] CT-138 Tunable attenuator. The [illegible] line could not be matched to this tolerance using the [illegible] and [illegible] attenuators so that a [illegible] consisting of attenuator and a single stub tuner made up of two [illegible] 50 adjustable lines was used. The required matching tolerance was then set at each frequency by adjusting the location of the appropriate lines.

Any variation from a linear phase shift, such as caused by

reflections, along the slotted line will also cause an apparent standing wave to appear on the phase measurements. A General Radio type 874-LBA slotted line and a type 874 WS termination was used for this part of the circuit. The standing wave measured at the input of the slotted line was found to be less than 1.1:1 for the frequencies at which the measurements were made. Therefore, the total phase error due to mismatch will not exceed $\pm$ 8.5^{o} provided the signal levels in the two lines connected to the tee are equal in magnitude.

Since fairly high standing waves were found to exist on the transmission line field, the effects of the above mismatches were hardly noticeable during the course of the measurements.

The above tolerance on the phase measurements will rise rapidly if the magnitude of the signals in the lines connected to the tee are not kept equal. An equally important reason for maintaining equal signal levels in the lines is that the null broadens rapidly if the signals are not nearly equal. Therefore, the inclusion of the variable power divider in the circuit is a necessity since the signal level along the antenna varies over a very wide range. However, the phase delay through the power divider must remain constant as the attenuation is changed if the readings are to have any meaning. The output of the power divider used, a General Radio Type 874-GA adjustable attenuator, can be varied over a range of 120 db., which is more than adequate for the attenuation requirements. Basically it consists of a waveguide

structure operating in the cuttoff region of the $TE_{1,1}$ mode. The output signal is obtained from a pickup loop. Since the waveguide operates in the cuttoff region, the signal picked up by the loop varies rapidly for small displacements of the loop, and of equal importance for this application, the phase shift through the device remains constant as the position of the loop is changed.

An attempt was made to calibrate the overall system. This was done by replacing the antenna with a length of brass welding rod short circuited by a vertical aluminum plate placed at the end of the rod in the plane perpendicular to the rod. Since there were no elements on the rod, the signal propagated down the rod with the speed of light, and was reflected by the plate causing a high standing wave to exist along the rod. The results are shown in Figures 19 and 20. The measured standing wave ratio along the line was about 9:1. The theoretical curve for this standing wave ratio was drawn to assist in evaluating the measurements. Since some perturbation of the fields were observed at the short circuiting plate, the zero position for the horizontal ordinate was displaced to the null one half wavelength from the plate. As can be seen, the results are satisfactory for both the magnitude and phase measurements.

During the early stages of the measurements, some difficulty was encountered due to direct radiation from the feed. The feed system shown in Figure 14, on Page 52, was evolved and found to give satisfactory results. Figure 21 shows the signal level of the

FIGURE 19

SYSTEM CALIBRATION FOR

FIELD STRENGTH MEASUREMENTS

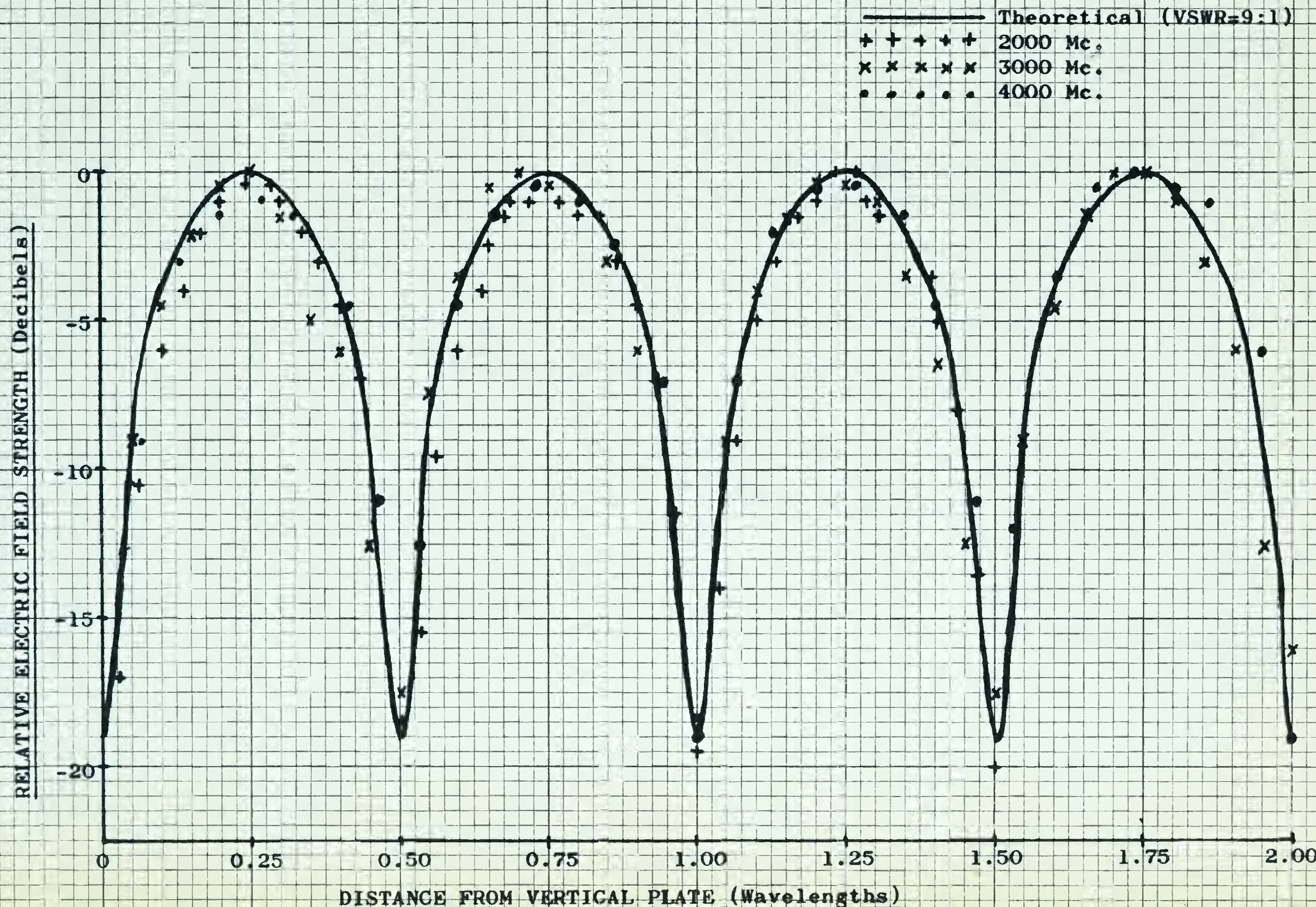

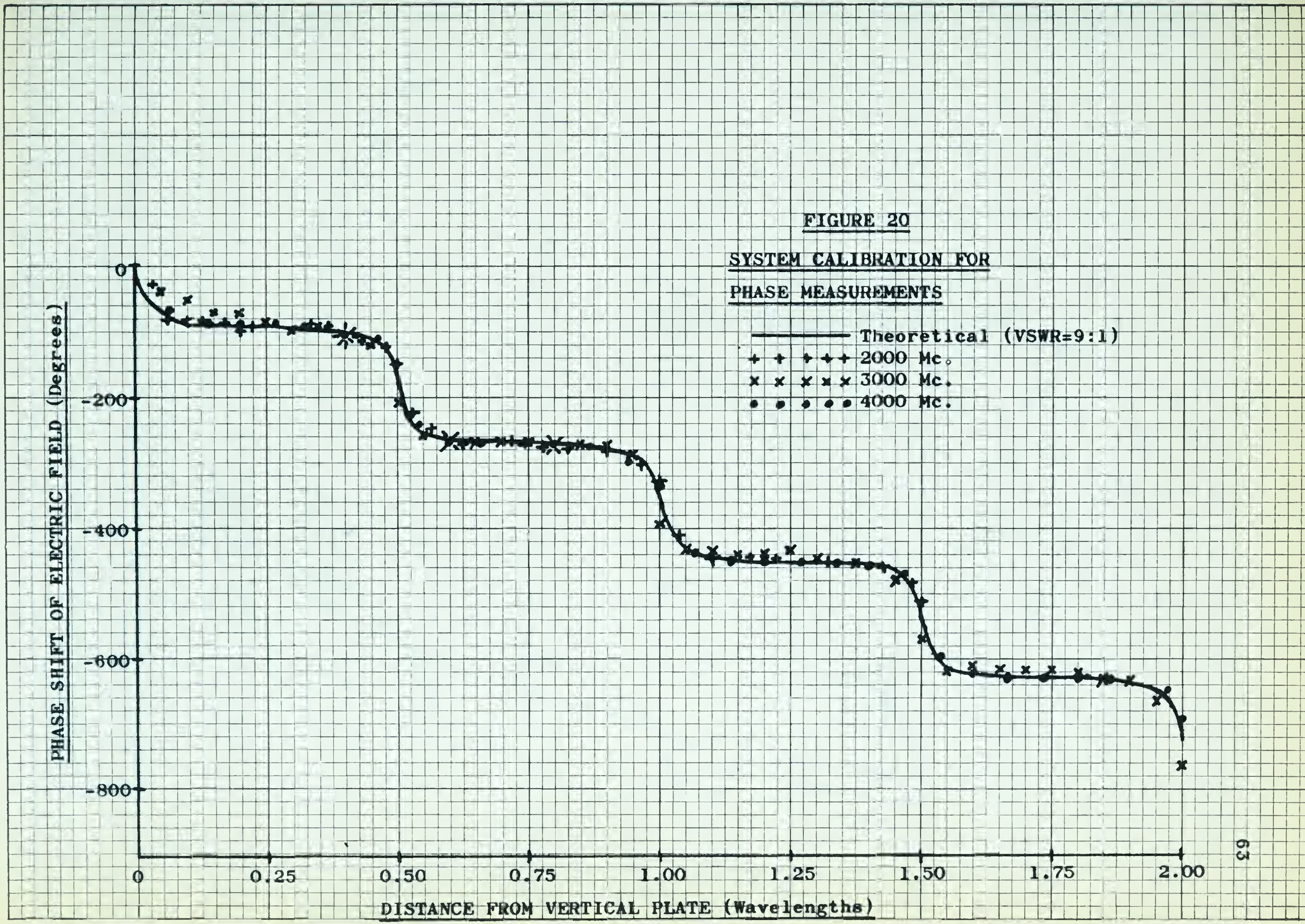

FIGURE 20

SYSTEM CALIBRATION FOR

PHASE MEASUREMENTS

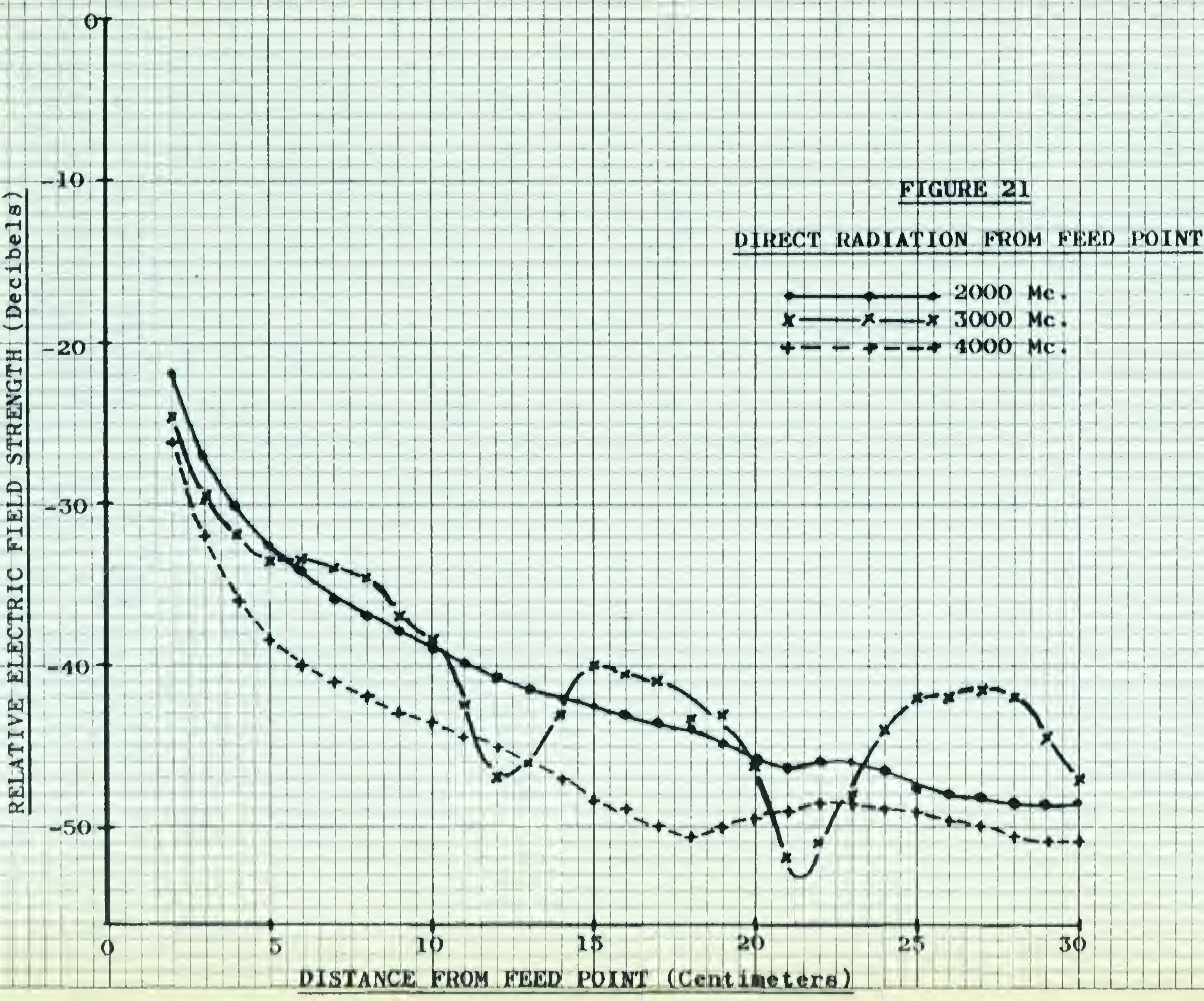
FIGURE 21
DIRECT RADIATION FROM FEED POINT
2000 Mc.
3000 Mc.
4000 Mc.
RELATIVE ELECTRIC FIELD STRENGTH (Decibels)
0
-10
-20
-30
-40
-50
DISTANCE FROM FEED POINT (Centimeters)
0
5
10
15
20
25
30

direct radiation from the feed system with the antenna removed. The zero decibel level was taken to be the maximum signal measured with an antenna half structure soldered in place. As can be seen, the direct radiation is quite low and was found to have little effect on the measurements, with the possible exception of the area to the rear of the active region where the transmission line field is highly attenuated. Fortunately, the measurements made in this region are of no importance in this thesis.

4.4 Radiation Pattern Measurements

In order to evaluate the theory, it is necessary to compare the shape of the calculated radiation patterns to those obtained experimentally.

The equipment for an antenna range was purchased during this semester, and a temporary installation set up for use in conjunction with the undergraduate laboratories. It was found to give very good results for measurements made in the azimuth plane.

A photograph of the receiving site is shown in Figure 22. A wooden structure with absorbing material tied to it was built around the turntable in order to minimize reflections from the walls of the room. The turntable is a Scientific-Atlanta Inc. Medium Duty Azimuth Positioner, Model PMA-5R and the recorder is a Scientific-Atlanta Inc. Series APR-20 Rectangular Recorder.

A Hewlett Packard Model 420A crystal detector was used with the recorder. The calibration of the crystal detector-recorder combination was checked using the receiver as a standard. Based on

FIGURE 22

TEMPORARY ANTENNA RANGE RECEIVING SITE

a linear scale, it was found that the variations between the two were insignificant over the frequency range required for the pattern measurements.

The transmitting site was located at the other end of the room, a distance of about thirty feet. It consisted simply of an S band horn and the generator used for the measurements of the transmission line characteristics.

SECTION 5

5. RESULTS

5.1 Presentation of Measured Data for Transmission Line Field

Measurements were made on the log periodic dipole antenna to determine the characteristics of the transmission line field for the parameters $\tau = 0.95$, 0.89, and 0.81. The apex angle, Θ, for each of the above geometric ratios, τ, was varied in steps of five degrees over the useable range of the antenna (measured VSWR of input impedance less than 2:1[15]).

The log periodic dipole antenna was chosen since the apex angle for a particular geometric ratio could be varied simply by cutting the elements to the proper lengths. Therefore, it was neccessary to build only three structures which represented a considerable saving in time and materials. This antenna does represent a simplification of the other types of log periodic antennas. However, the pattern of the complete log periodic antenna can be calculated using array theory once the pattern of each half structure has been determined using the leaky wave theory.

A length of brass welding rod 0.241 cms. in diameter was used for the boom. The half structure was mounted one centimeter above the ground plane as shown in Figure 14 on Page 52. Therefore, the characteristic impedance of the equivalent twin lead transmission line for the complete antenna, Z_o, is 340 ohms.[28] Number 14 copper wire was used for the elements which were soldered to the boom. Thus, the length to diameter ratio of the half wavelength

5. RESULTS

5.1 Interpolation of Measured Data for Transmission Line Plots

Measurements were made on the log periodic dipole antenna to determine the characteristics of the transmission line plots for the parameters τ = 0.90, 0.80, and 0.91. The apex angle, 2α, for each of the above geometric ratios, τ, was varied in steps of five degrees over the useful range of the antenna (variance [illegible] of input impedance less than 2:1[10]).

The log periodic dipole antenna was simple since the apex angle for a particular geometric ratio could be varied simply by cutting the elements to the proper lengths. Therefore, it was necessary to build only three structures which represented a considerable saving in time and materials. This antenna type represents a simplification of the other types of log periodic antennas. Further, the pattern of the complete log periodic antenna can be calculated using array theory once the pattern of each half structure has been determined using the image [illegible].

A length of brass tubing, [illegible] 0.[illegible] [illegible], was used for the boom. The half structure was mounted [illegible] above the ground plane as shown in Figure [illegible] on Page [illegible]. Therefore, the characteristic impedance of the equivalent two-wire transmission line for the complete antenna, Z_o, is [illegible] ohms.[illegible] Number [illegible] copper wire was used for the elements which were soldered to the boom. Thus, the length to diameter ratio of the half [illegible]

element varied from 46.1 at 2000 mc. to 26.4 at 3500 mc.

The measured results for the transmission line field are presented graphically in Appendix B. The position along the boom is measured from the apex of the antenna in wavelengths. The advantage of using this method is that the position of the half wave element for each graph remains fixed for all frequencies. Therefore, if there is no variation of the fields as the frequency is varied over a period, all the curves for a particular τ and θ will be superimposed.

As previously stated, Bell, Elfving and Franks found that the VSWR of the transmission line wave was equal to the VSWR of the input impedance.[5] Isbell has measured the input impedance of log periodic antennas and found the VSWR to be less than 2:1 over the range of parameters for which the curves in Appendix B were made.[15] While the VSWR for various antenna parameters follows the trend of Isbell's impedance measurements, it is much greater than 2:1. This apparent discrepancy can be explained as follows: The measurements presented in Appendix B were made on a single boom mounted over a ground plane, which causes a mirror rather than complimentary image. The reflections from this mirror image are in phase with those from the real boom and so a large VSWR is obtained. For the actual antenna, the booms are complimentary, so that the reflections from them are 180° out of phase and tend to cancel. This results in the lower VSWR measured for the actual antenna. DuHamel and Ore have reported input impedance VSWR's of the

order 5:1 to 8:1 if the elements are located less than a half wavelength from the ground plane.[14] A series of input measurements was made for τ = 0.89 and various apex angles. The VSWR's for the input impedance measurements agreed with those of the transmission line wave.

It was noticed that the position of the standing wave of the curves repeated with a period of $2 \ln(1/\tau)$. Thus, if the frequency is changed from f to $\tau^{1/2} f$, the position of the standing waves for the two frequencies will be 90° apart in terms of the transmission line field wavelength. This procedure was found to greatly aid in measuring the slope of the curves. The measurements for τ = 0.95 are at random frequencies because they were made before the advantages of this property were realized. A ground plane could not be used for τ's much less than 0.81 since the VSWR of the transmission line wave is nearly as large as the drop in the signal level in the active region. Fortunately, log periodic dipole antennas with τ's less than 0.8 break up excessively as the frequency is varied over a period.[3] Therefore, this value represents the lower limit of τ.

A vertical line was drawn on each graph at the position of a hypothetical half wavelength element in order to give a reference point.

The results of the measurements presented in Appendix B for the transmission line field are given in Figures 23 and 24. They follow general trends which could have been predicted intuitively.

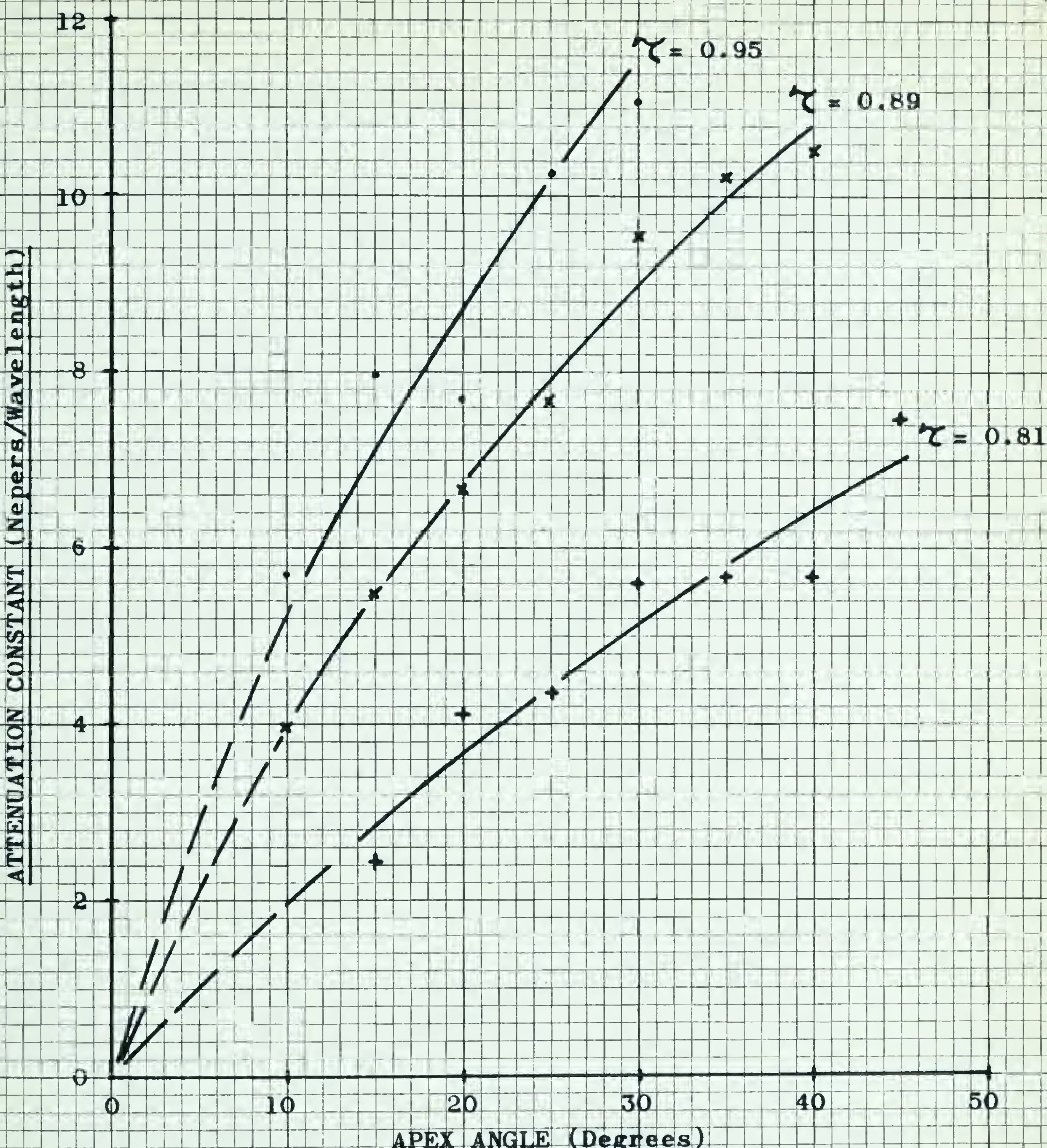

FIGURE 23

ATTENUATION CHARACTERISTICS

OF TRANSMISSION LINE FIELD

FOR LOG PERIODIC DIPOLE ANTENNA

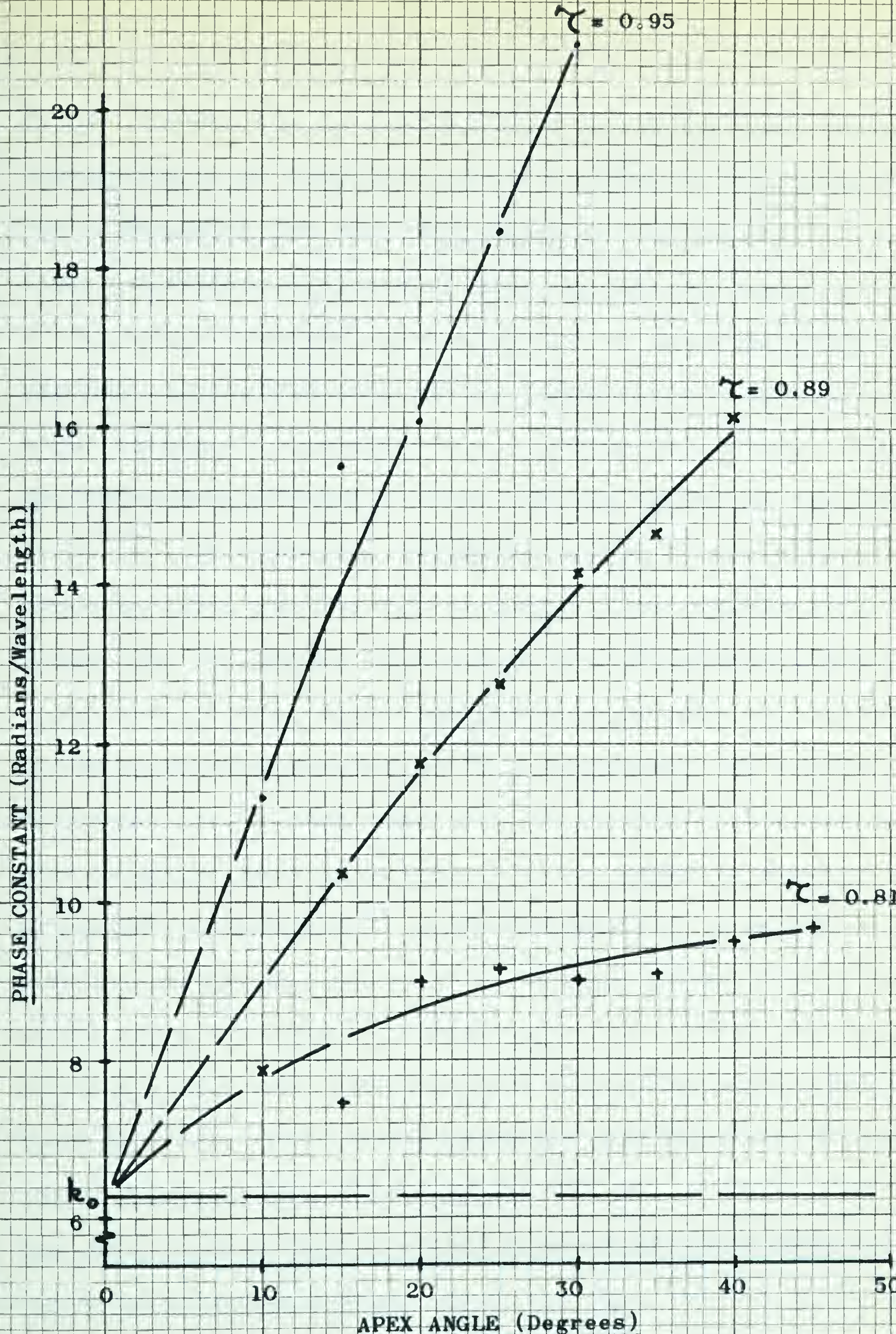

FIGURE 24

PHASE CHARACTERISTICS OF TRANSMISSION LINE FIELD FOR LOG PERIODIC DIPOLE ANTENNA

In the limiting case as the apex angle approaches zero, the antenna degenerates to an infinite parallel transmission line along which the transmission line wave will propagate with the velocity of light and without attenuation. Thus, as the apex angle is decreased, it is expected that the attenuation and the phase constants will decrease, approaching zero and k_0 respectively in the limiting case as the apex angle approaches zero. This trend was observed and so the curves were extended to these limiting cases. As the geometric ratio, τ , is increased, more elements will be closer to a half a wavelength long and they will be spaced closer together with the result that the antenna will radiate more efficiently. The resulting higher rate of decay of the transmission line wave will yield a higher attenuation constant as τ is increased. For a given length of element, it has been found that the velocity of the wave passing over parasitic elements is reduced as the number of elements per wavelength is increased.[22] A similar result is to be expected for directly excited elements so that the phase constant should increase as the geometric ratio is increased for a particular apex angle. The same points could also be argued by considering the limiting cases as the geometric ratio approached zero for which α_T and β_T approach zero and k_0 respectively.

5.2 Comparison of Calculated and Measured Radiation Patterns for Log Periodic Dipole Antenna

The shapes of the far field radiation patterns were calculated using the theory of Section 3 and Figures 23 and 24. In order to

In the limiting case as the mesh width approaches zero, the antenna degenerates to an infinite parallel transmission line along which the transmission line mode will propagate with the velocity of light and without attenuation. Thus, as the mesh width is decreased, it is expected that the attenuation and the phase constants will decrease, approaching zero and β_0 respectively in the limiting case as the apex angle approaches zero. This trend was observed when the angles were extended to lower limiting values. As the geometric ratio, τ, is increased, more elements will be placed in a half-wavelength long and they will be spaced closer together with the result that the antenna will radiate more efficiently. The preceding discussion of means of the transmission line mode will yield a larger attenuation constant as τ is increased. For a given length of element, it has been found that the velocity of the wave passing over periodic elements is reduced as the number of elements per wavelength is increased.[23] A similar result is to be expected for linearly periodic elements so that the phase constant should increase as the geometric ratio is increased for a particular mesh width. The same result would also be arrived by considering the limiting cases as the geometric ratio approaches zero (at which α and β approach zero and β_0 respectively).

<u>5.2 Comparison of Calculated and Measured Radiation Patterns for Log-Periodic Zig-zag Antennas</u>

The shapes of the far-field radiation patterns were calculated using the theory of Section 3 and figures 20 and 21. In order to

obtain the most meaningful comparison, the elements were made from the same size wire as those used to measure the attenuation and phase constants. The same frequencies were also used in an attempt to minimize the effect of changing the height to diameter ratio of the elements. Unfortunately, the RG-142/U rigid coaxial cable which is most suitable for constructing the boom carrying the feed cable has a diameter of 0.355 cms. Further, it is not practical to separate the booms two centimeters because this separation is not small compared to the wavelengths used and would have a noticeable effect on the H plane radiation pattern. Therefore, a separation of 0.6 cms. was used. This resulted in a Z_0 of 140 ohms for the antennas used to make the pattern measurements compared to 340 ohms for the structure used to measure the characteristics of the transmission line field.

It has been found that increasing Z_0 tends to broaden the beamwidth very slightly.[3] However, this effect is negligible compared to the degree of accuracy obtained using the theory developed in this paper.

Calculated and measured far field patterns for several parameters are shown in Figures 25 to 33. A comparison of the calculated and measured half power beamwidths is shown in Figures 34 and 35 for the E and H planes respectively. Since the calculated patterns do not account for any variations, they can be thought of as representing the average radiation pattern. Therefore, the far field patterns were measured at several frequencies over a period

obtain the most meaningful measurements, the elements were made from the same size wire as those used to measure the attenuation and phase constants. The same precaution was also taken in an attempt to minimize the effect of element tip height to diameter ratio of the elements. Unfortunately, the unshielded RG-8/U coaxial cable which in most instances for constructing the yagi carrying the feed cable has a diameter of 0.405 cms. However, it is not practical to separate the boom two centimeters because this separation is not small compared to the wavelengths used and would have a noticeable effect on the H-plane radiation pattern. Therefore, a separation of 0.6 cms. was used. This resulted in b = for the same for the antennas used to make the pattern measurements presented in this and for the structure used to measure the characteristics of the illuminating line field.

It has been found that increasing tends to broaden the beamwidth very slightly.[5] However, this effect is negligible compared to the degree of accuracy obtained using the theory developed in this paper.

Calculated and measured far-field patterns for several parameters are shown in Figures 58 to 73. A comparison of the calculated and measured half power beamwidths is shown in Figures 74 and 75 for the E and H planes respectively. Since the calculated patterns do not account for any variations that may be present in representing the measured radiation pattern. Therefore, the far field patterns were measured at several frequencies over a period

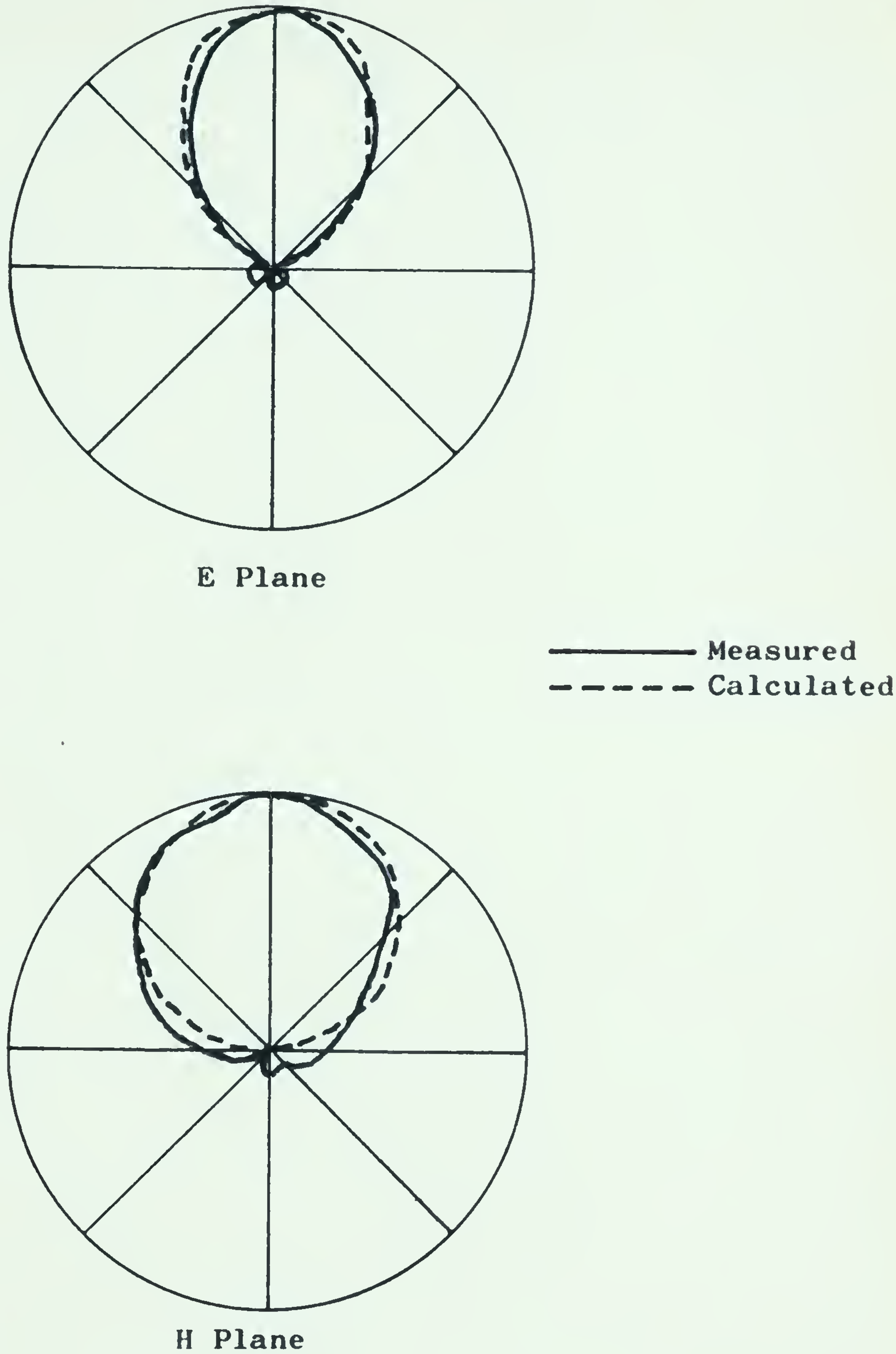

FIGURE 25

RADIATION PATTERNS OF LOG PERIODIC

DIPOLE ANTENNA FOR τ =0.95 AND Θ =30°

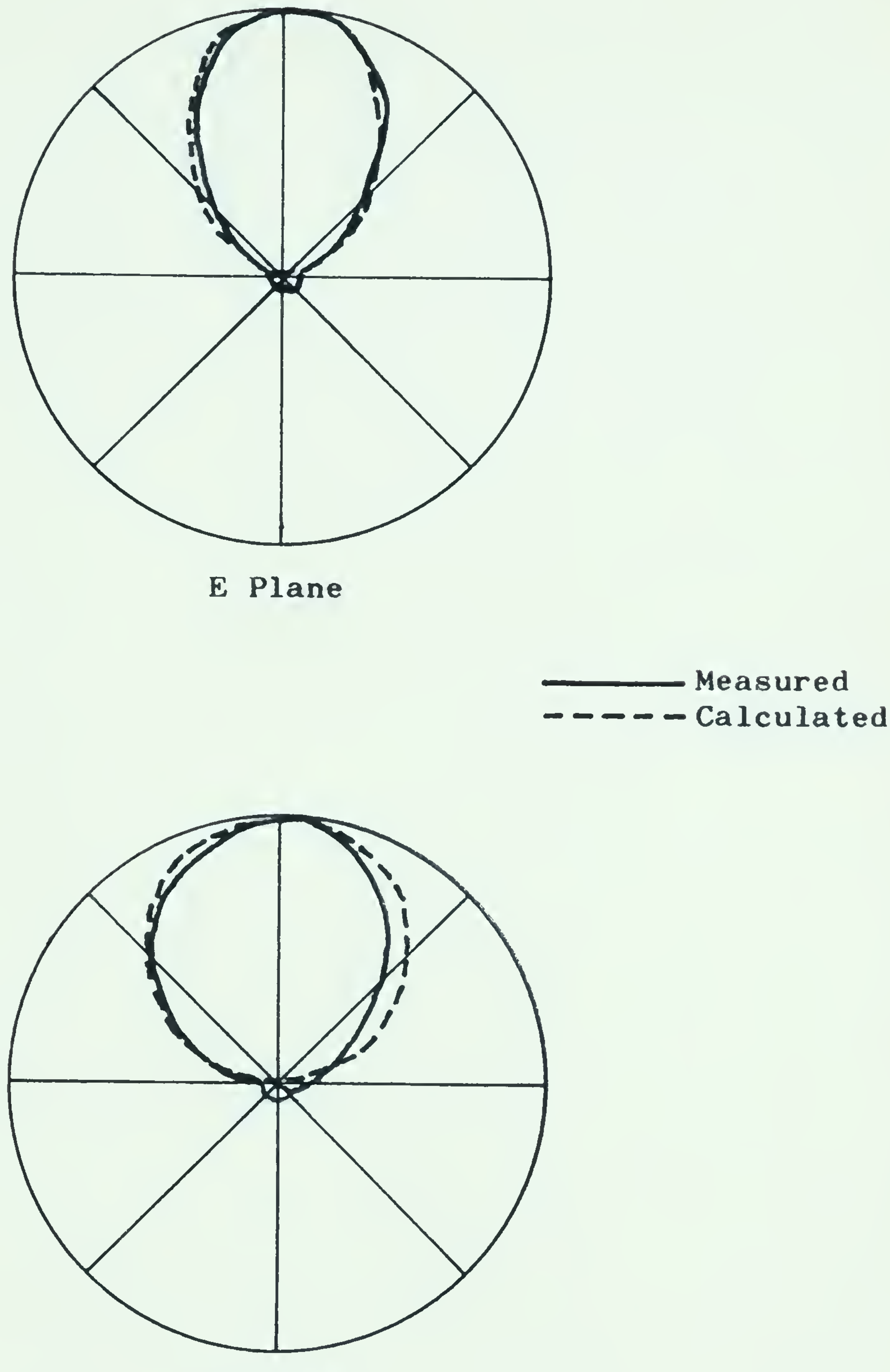

FIGURE 26

RADIATION PATTERNS OF LOG PERIODIC

DIPOLE ANTENNA FOR τ = 0.95 AND Θ = 20°

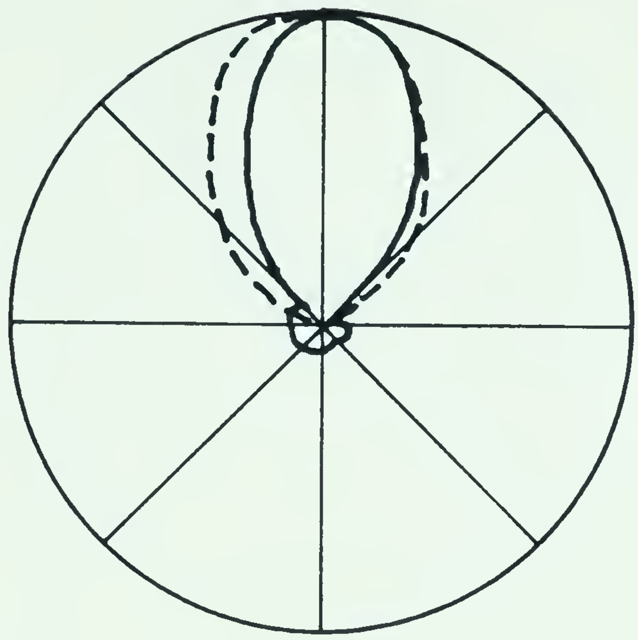

E Plane

——— Measured
- - - - Calculated

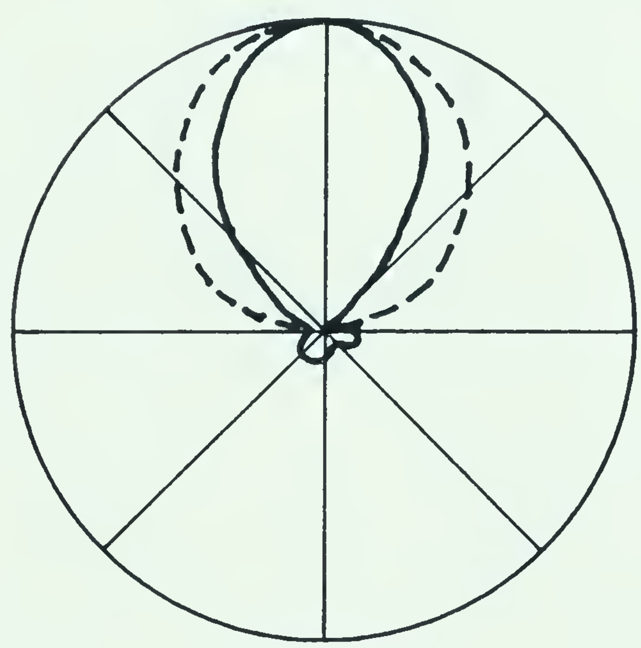

H Plane

FIGURE 27

RADIATION PATTERNS OF LOG PERIODIC DIPOLE ANTENNA FOR $\tau = 0.95$ AND $\Theta = 10^{\circ}$

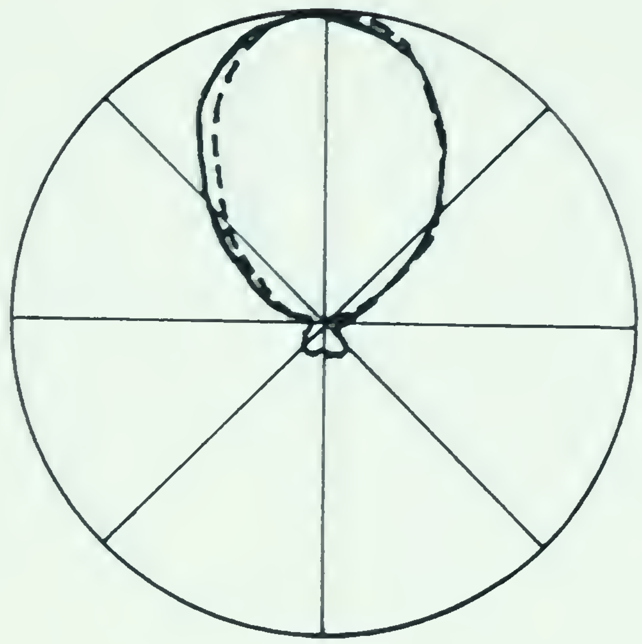

E Plane

——— Measured
- - - - Calculated

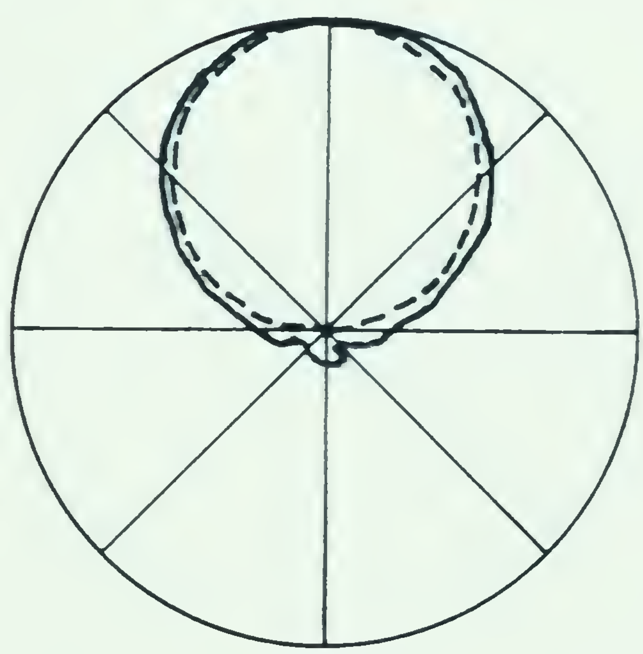

H Plane

FIGURE 28

RADIATION PATTERNS OF LOG PERIODIC
DIPOLE ANTENNA FOR $\tau = 0.89$ AND $\Theta = 40^{\circ}$

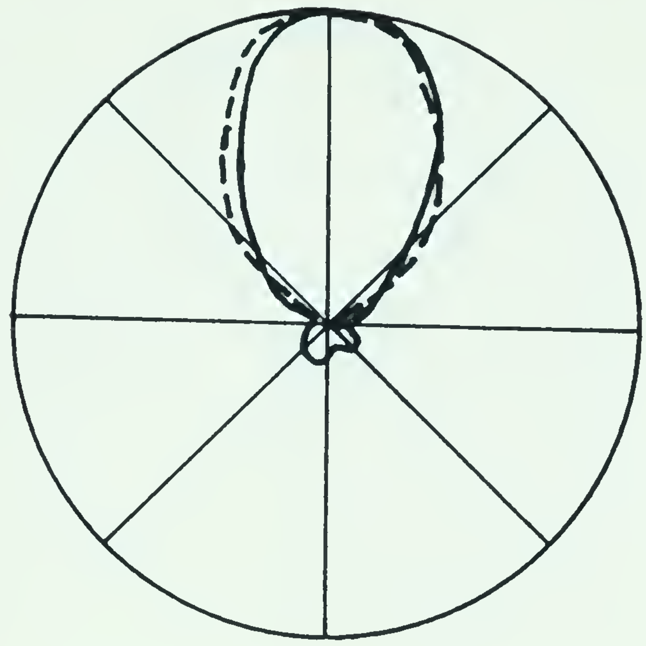

E Plane

——— Measured
– – – – Calculated

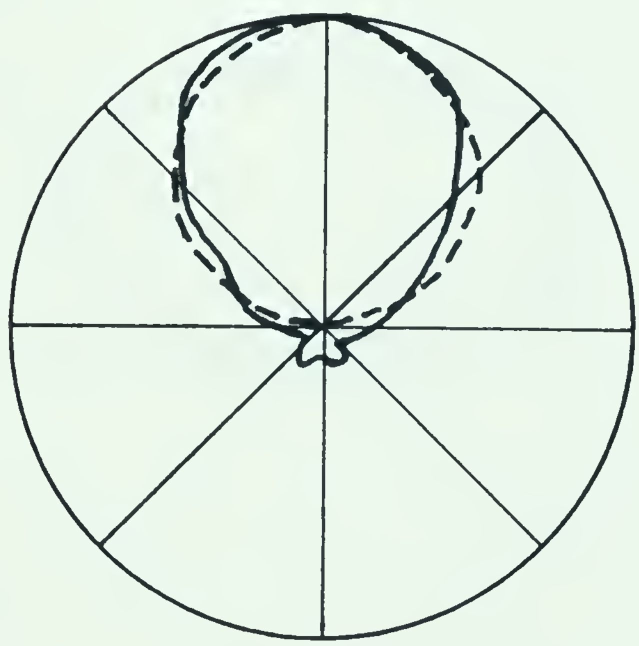

H Plane

FIGURE 29

RADIATION PATTERNS OF LOG PERIODIC

DIPOLE ANTENNA FOR $\tau = 0.89$ AND $\theta = 25^\circ$

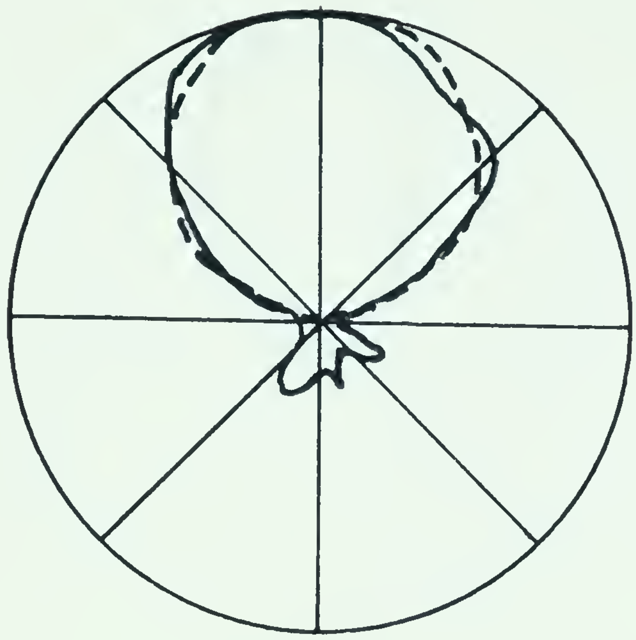

E Plane

——— Measured
- - - - Calculated

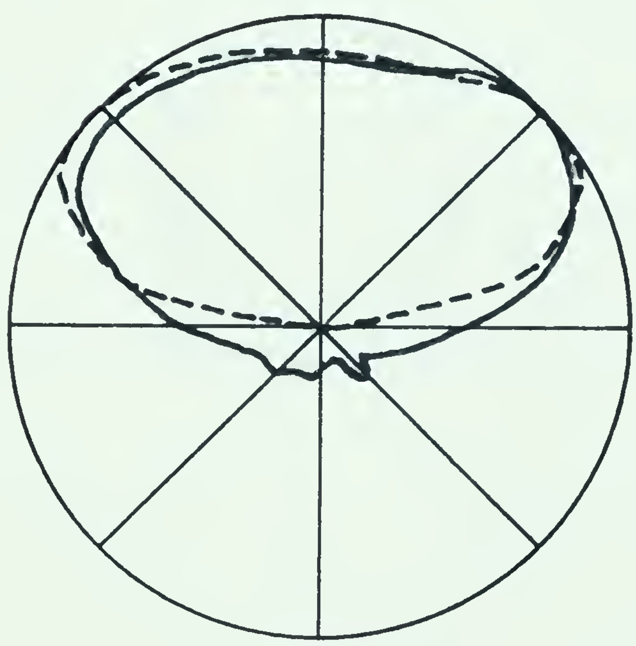

H Plane

FIGURE 30

RADIATION PATTERNS OF LOG PERIODIC DIPOLE ANTENNA FOR $\tau = 0.89$ AND $\theta = 10^{\circ}$

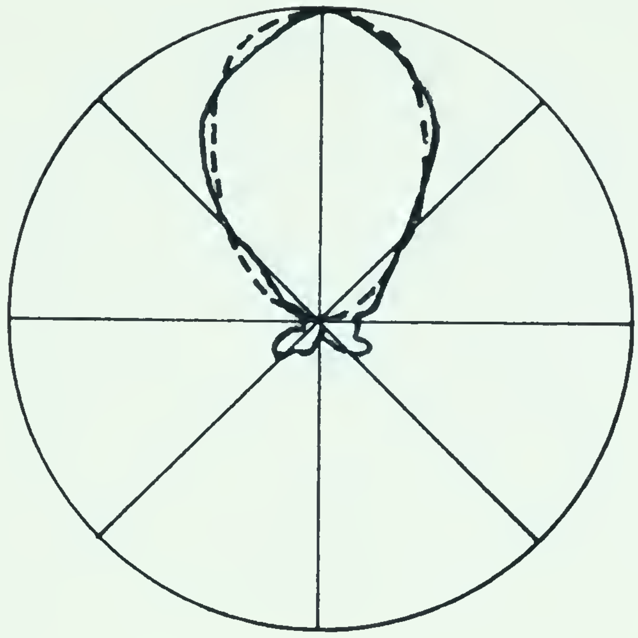

E Plane

———— Measured
- - - - - - Calculated

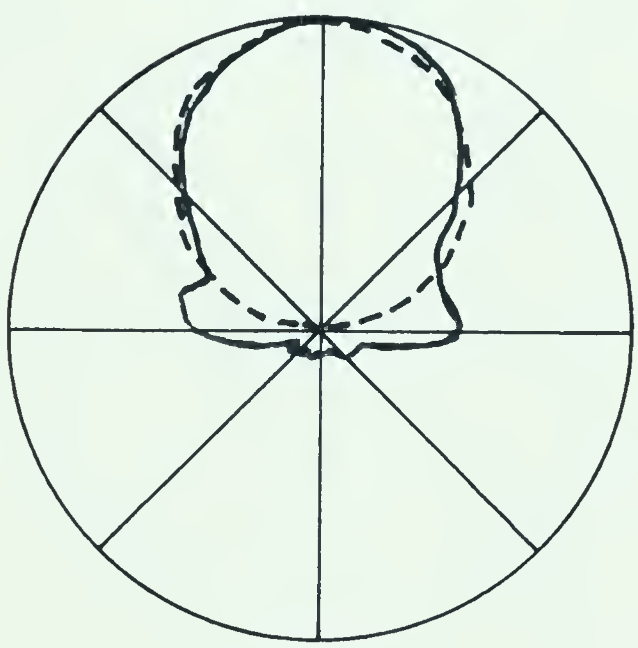

H Plane

FIGURE 31

RADIATION PATTERNS OF LOG PERIODIC
DIPOLE ANTENNA FOR $\tau = 0.81$ AND $\Theta = 40^{\circ}$

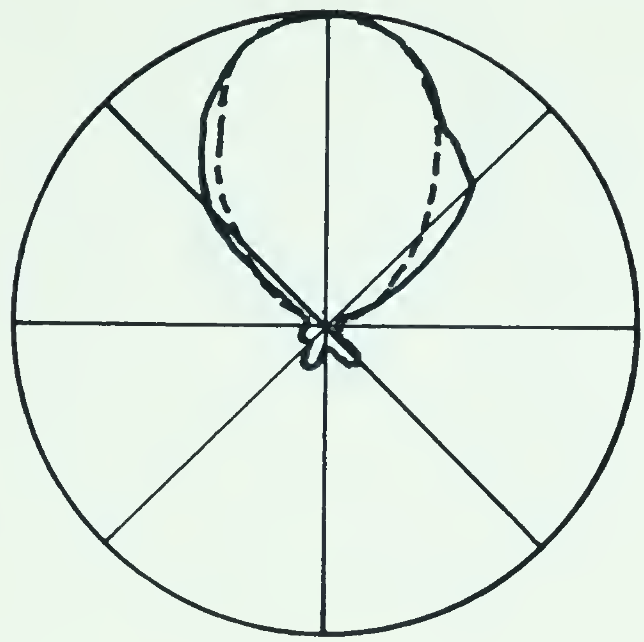

E Plane

——— Measured
– – – Calculated

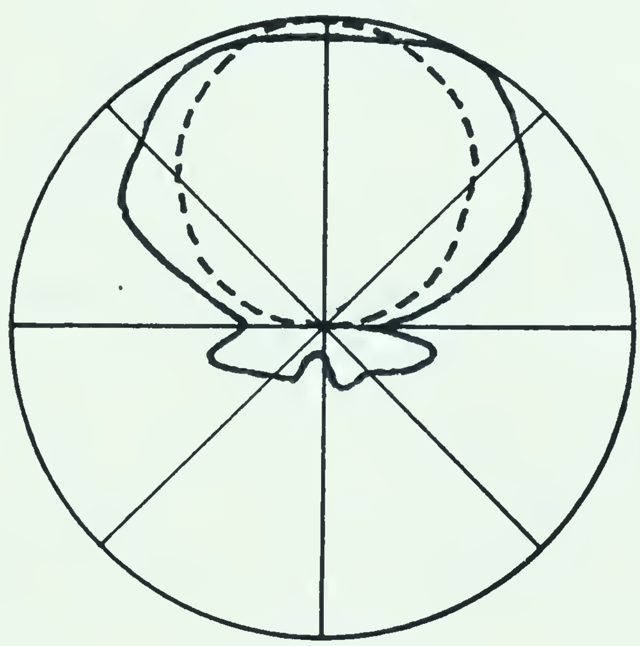

H Plane

FIGURE 32

RADIATION PATTERNS OF LOG PERIODIC
DIPOLE ANTENNA FOR $\tau = 0.81$ AND $\Theta = 30^{\circ}$

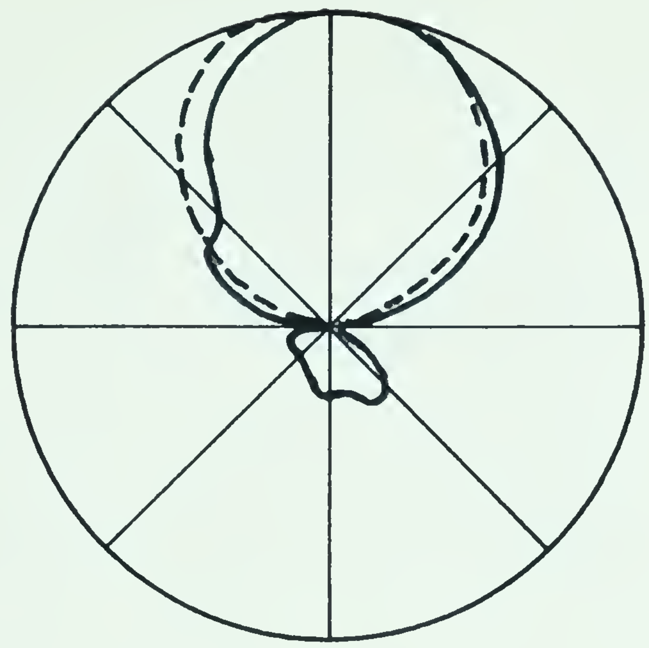

E Plane

——— Measured
- - - - Calculated

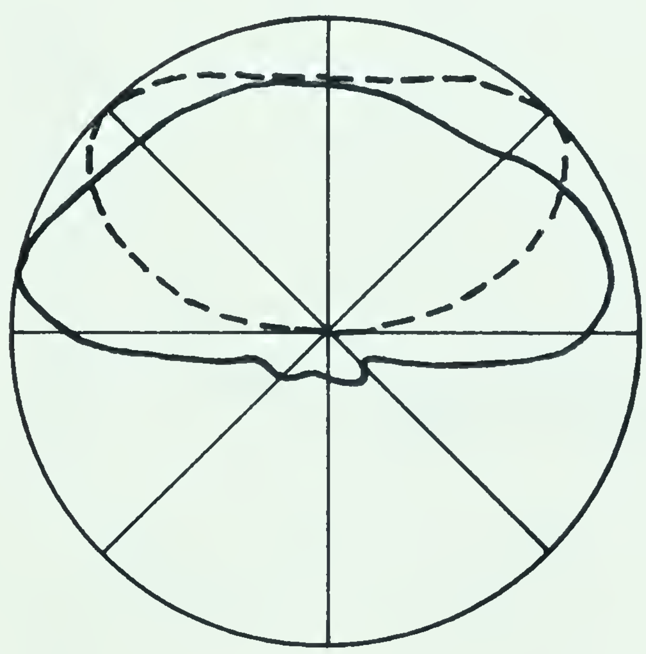

H Plane

FIGURE 33

RADIATION PATTERNS OF LOG PERIODIC

DIPOLE ANTENNA FOR $\tau = 0.81$ AND $\Theta = 20^{o}$

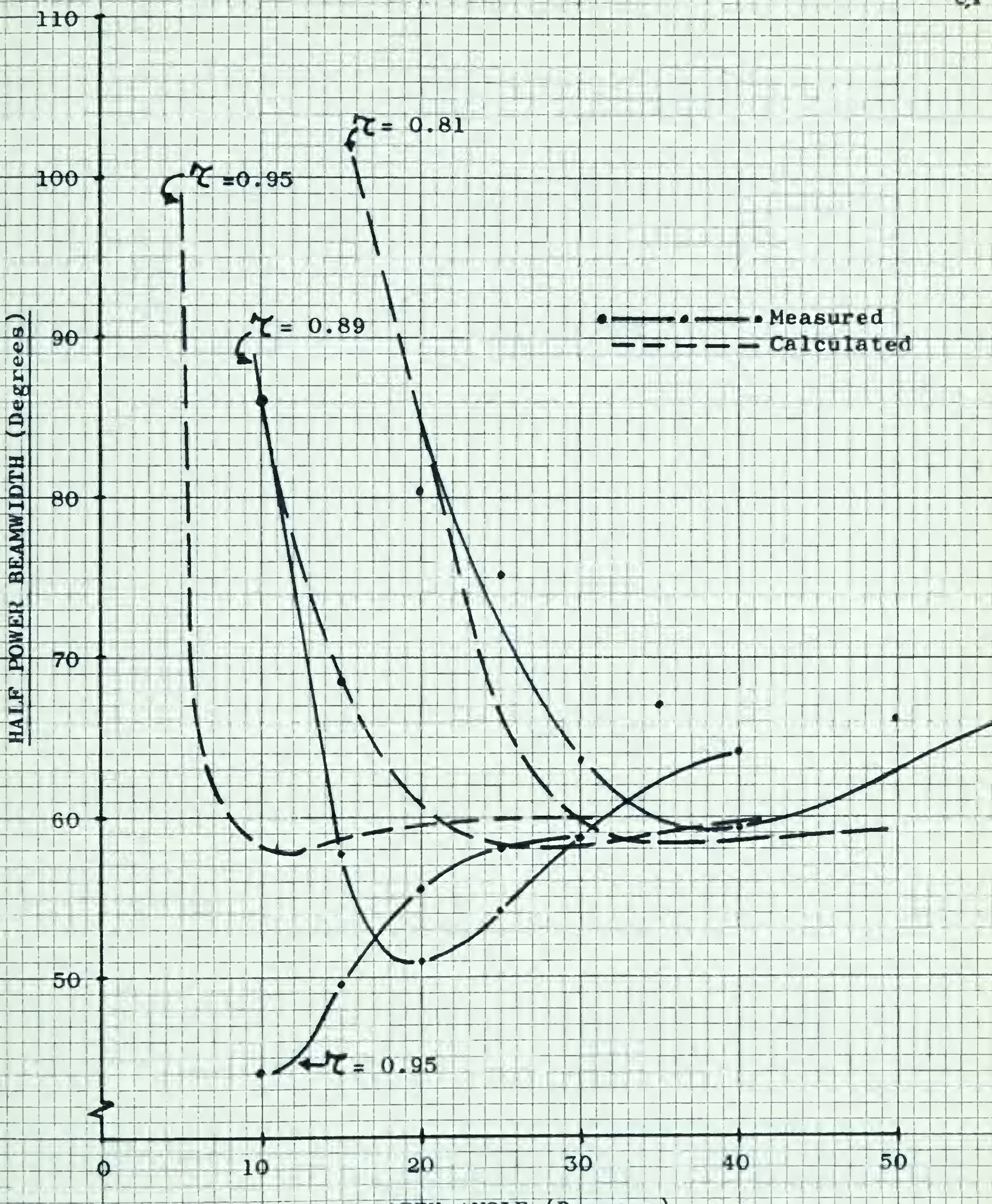

FIGURE 34

E PLANE HALF POWER BEAMWIDTH

FOR LOG PERIODIC DIPOLE ANTENNA

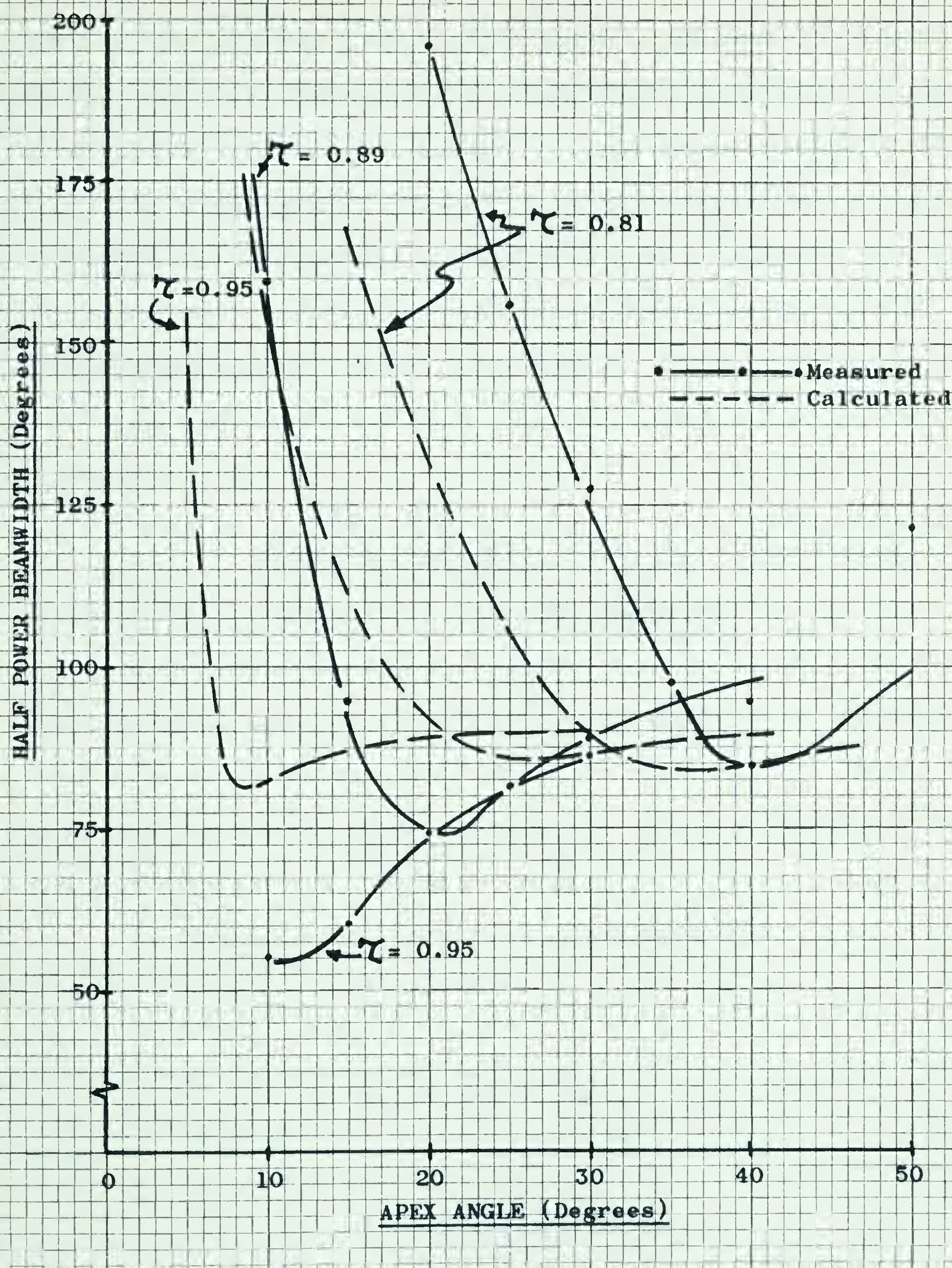

FIGURE 35

H PLANE HALF POWER BEAMWIDTH

FOR LOG PERIODIC DIPOLE ANTENNA

and averaged to obtain the measured results presented in Figures 25 to 35. The variations of the patterns over a period were found to be quite small within the useable range of antenna parameters.

An examination of Figures 34 and 35 reveals that the minimum beamwidth for each geometric ratio occurs at a different apex angle. For larger apex angles, the beamwidth increases slowly and for smaller apex angles, it increases rapidly.

The effects of the leaky wave pole can be seen from the expression

$$f_1(\theta) = \frac{-1/k_o^2 \cos\theta}{\left(\cos^2\theta - \frac{\beta_R^2 - \alpha_R^2}{k_o^2}\right) - j\,\frac{2\beta_R\alpha_R}{k_o^2}} = \frac{-1/k_o^2 \cos\theta}{(\cos^2\theta - A) - jB} \tag{51}$$

which is the H plane pattern function. Equation (51) can be readily obtained by combining (25) and (40) on Pages 29 and 34 respectively. When the denominator is at a minimum, the magnitude of $f_1(\theta)$ will tend to be a maximum depending on the value of $\cos\theta$. It can be seen that the minimum of the denominator occurs at $\cos\theta = \pm A^{1/2}$ and the sharpness of this minimum is determined by the magnitude of B.

In Section 3, the assumptions were made that

$$\alpha_R = \alpha_T \tag{47}$$

and

$$\beta_R = \beta_T - \pi/\sigma \tag{45}$$

where

$$\sigma = \frac{1-\tau}{4\tan\frac{|\Theta|}{2}} \tag{46}$$

Using these equations and Figures (23) and (24), it is readily seen that the magnitudes of both α_R and β_R increase as the apex angle

are averaged to obtain the measured results presented in Figures 25 to 30. The variations of the patterns over a period were found to be quite small within the probable range of optical parameters.

An examination of Figures 31 and 32 reveals that the minimum beamwidth for each geometric ratio occurs at a different apex angle. For larger apex angles, the beamwidth increases slowly and for smaller apex angles, it increases rapidly.

The effects of the leaky wave pole can be seen from the expression

$$F_1(\theta) \simeq \frac{-k_1^2 \cos\theta}{\left(\cos^2\theta - \frac{\alpha^2-\beta^2}{k_1^2}\right) - j\frac{2\alpha\beta}{k_1^2}} = \frac{-k_1^2 \cos\theta}{(\cos^2\theta - A) - jB} \quad (51)$$

which is the θ plane pattern function. Equation (51) can be readily obtained by combining (25) and (40) on pages 35 and 51 respectively. When the denominator is at a minimum, the magnitude of $F_1(\theta)$ will tend to be a maximum depending on the value of $\cos\theta$. It can be seen that the minimum of the denominator occurs at $\cos^2\theta = A$ and the sharpness of this minimum is determined by the magnitude of B.

In Section 3, the assumptions were made that

$$\alpha_s = \alpha_1 \quad (47)$$

and

$$\beta_s = \beta_1 - \frac{\pi}{a} \quad (49)$$

where

$$a = \frac{1-\tau}{4\cos\frac{\varphi}{2}} \quad (40)$$

Using these equations and Figures (23) and (24), it is readily seen that the magnitudes of both α_s and β_s increase as the apex angle

is widened. The magnitude of β_R varies faster than the magnitude of α_R and for large apex angles, the magnitude of β_R is much larger than that of α_R. Therefore, the magnitudes of A and B are proportional to the apex angle, being large for wide apex angles and small for narrow apex angles.

For wide apex angles, both A and B are large so the denominator of (51) is nearly constant for all azimuth angles. As a result, the theory predicts that the H plane pattern function will assymptotically approach a cosine distribution for very large apex angles.

This distribution can also be predicted intuitively as a first order approximation to the actual antenna having a large apex angle. In the limit as the apex approaches 180°, all the elements of the antenna will be located vanishingly close to the apex with the result that the spacings between the elements will be very small. Therefore, the net effect of the elements in the active region will be essentially that of a single half wavelength dipole. The elements to the rear of the active region, which are longer, will not be excited (providing they are of a non-resonant length). Thus, the structure can be simplified to that of a driven half wavelength dipole located immediately in front of a longer non-resonant element which acts as a reflector. For the idealized case, the reflector will create a perfect image dipole located vanishingly close to the driven element. In the H plane, these two idealized dipoles form a Hertzian dipole pair whose pattern function is given by a cosine

distribution.[27]

As the apex angle is reduced, both A and B in (51) decrease. In this region A is still greater than unity so that the minimum of the denominator occurs at the azimuth angle $\theta = 0^{\circ}$. Since the magnitude of B is proportional to the apex angle, the beamwidth gradually decreases as the apex angle is reduced. To a first order approximation, the minimum beamwidth for a particular geometric ratio, τ, occurs at the azimuth angle for which A = 1, or

$$\beta_R^2 - \alpha_R^2 = k_o^2 \tag{52}$$

It is easily seen that B will be large for this apex angle unless α_R is very small. Since the active region for successful log periodic structures is fairly short, α_R must be reasonably large in order to have the energy in the transmission line wave efficiently transferred to the radiation wave. Thus, as often happens in engineering problems, the two requirements are contradictory and a compromise must be made.

The variations of A and B with respect to the apex angle were found to have secondary effects on the patterns, and it was found that the minimum beamwidth for a particular geometric ratio occurred at a slightly wider apex angle than that given by (52).

With a further reduction in the apex angle, both A and B continue to decrease in magnitude. In this region A is less than unity and the azimuth angle for which the denominator of (51) is a minimum begins to scan toward broadside. B becomes rather small and this minimum can become quite sharp with the result that the

maximum value of $f_1(\theta)$ also scans towards broadside. Good examples of this behavior are shown in Figures 30 and 33.

Although Figures 25 to 35 show that the calculated patterns agree with those obtained experimentally with a reasonably good degree of accuracy, the theory does have some failings. First, the measured patterns do not assymptotically approach a cosine distribution for large apex angles. Figures 34 and 35 show that the beamwidth in this region is inversely proportional to the geometric ratio and does not assymptotically approach a single beamwidth for all geometric ratios as the theory predicts. Figures 25 and 28 are examples of the patterns in this region and show that the theory is valid to a first order approximation. Surprisingly, both the measured and calculated patterns reveal that this region begins for apex angles much smaller than the limiting case of 180°. As might be expected from the qualitative analysis given above, the apex angle for which this region begins is inversely proportional to the geometric ratio. Structures built in this region of the parameters are not too practical since the VSWR of the input impedance is fairly high.[15] The curves presented in Figures 34 and 35 extend approximately over the range for which the measured VSWR of the input impedance is less than 2:1 and reasonably good agreement between the measured and calculated beamwidths is obtained. The impedance measurements indicate that the VSWR will increase rapidly for larger apex angles outside the range shown in Figures 34 and 35.[15]

For small apex angles, the pattern maximum scans toward

broadside as previously described. This can also be predicted intuitively from the relationship

$$\beta_R = \beta_T - \frac{\pi}{\sigma} \tag{45}$$

For small apex angles, σ becomes large so that β_R can become zero and might even have the same sign as β_T for certain parameters. When β_R is zero, all the elements are excited in phase. This is the condition for broadside radiation from other types of antennas. Figure 33 reveals that the measured patterns tend to support this reasoning. Because of the cosine term in the numerator of (51), the theory cannot predict broadside radiation although it certainly does predict the scanning of the maximum toward broadside. However, the measured far field patterns break up rather badly for these small apex angles as the frequency is varied over a period, and so the antennas are not of any practical use in this region.

Figure 36, for $\tau = 0.81$ and $\Theta = 15^\circ$, shows the break up of the patterns in this region of the parameters. The patterns were measured over a period and found to fall within the crosshatched area between the two curves. It was observed that this break up of the patterns occurred rather suddenly. The measured patterns for $\tau = 0.81$ and $\Theta = 20^\circ$ showed a much smaller variation as the frequency was changed. The variations of the patterns for most of the other parameters would have only caused a thickening of the line if the patterns were drawn to the same scale used in Figure 36.

As might be expected, the shape of the measured E plane

broadside as previously described. This can also be predicted intuitively from the relationship

$$\frac{\psi}{\omega} - \Theta_r = \Theta_a$$

For small apex angles, σ becomes large so that Θ_a can become zero and might even take the same sign as Θ_r for certain parameters. When Θ_a is zero, all the elements are excited in phase. This is the condition for broadside radiation from other types of antennas. Figure 55 reveals that the measured patterns tend to support this reasoning. Because of the cosine term in the numerator of (11), the theory cannot predict broadside radiation although it certainly does predict the scanning of the maximum toward broadside. However, the measured far field patterns break up rather badly for these small apex angles as the frequency is varied over a period, and so the antennas are not of any practical use in this region.

Figure 56, for $\tau = 0.81$ and $\psi = 15^\circ$, shows the break up of the patterns in this region of the parameters. The patterns were measured over a period and found to fall within the cross-hatched area between the two curves. It was observed that this break up of the patterns occurred rather suddenly. The measured patterns for $\tau = 0.71$ and $\psi = 20^\circ$ showed a much smaller variation as the frequency was changed. The variations of the patterns for most of the other parameters would have only caused a thickening of one line if the patterns were drawn to the same scale used in Figure 55. As might be expected, the shape of the measured E plane

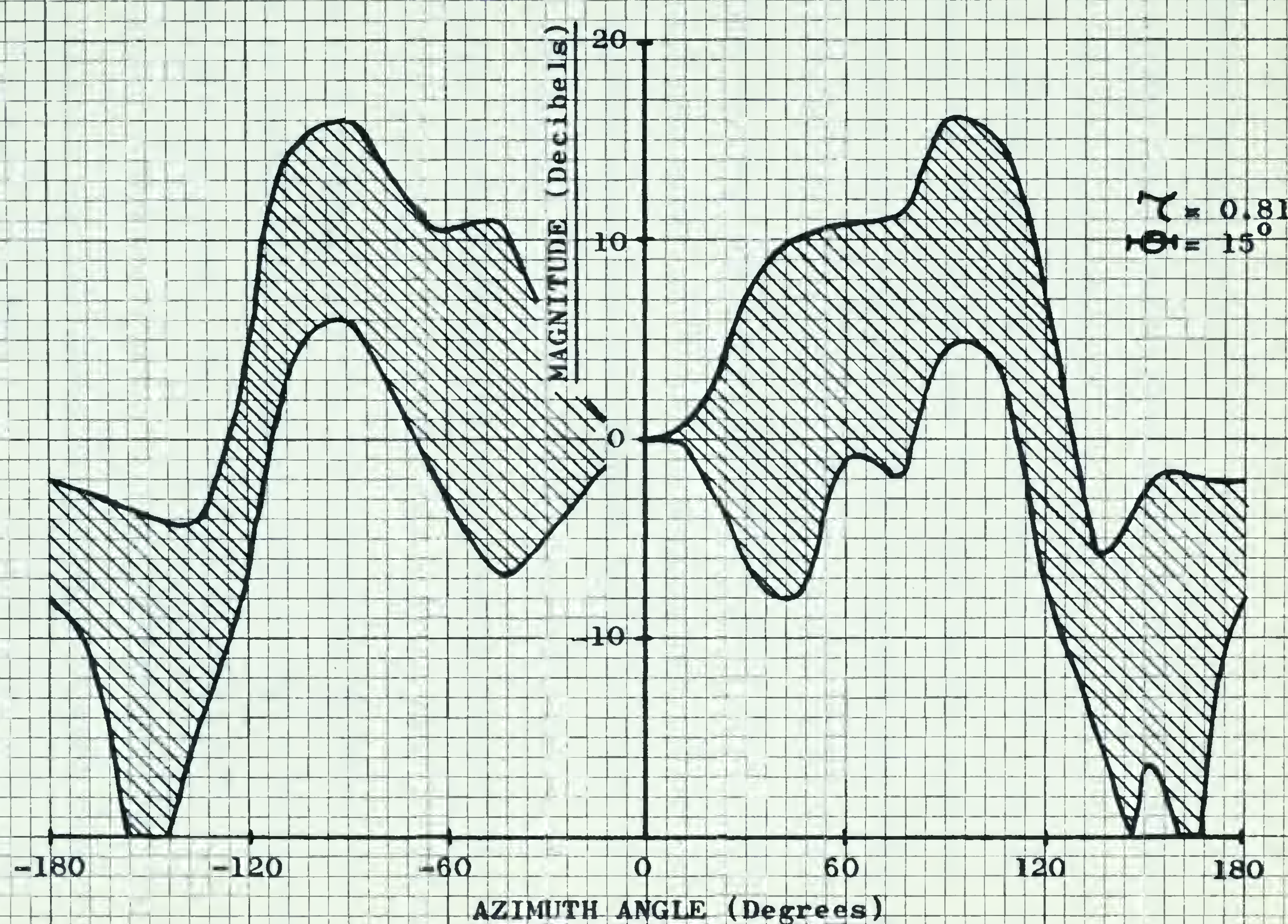

FIGURE 36

VARIATION OF H PLANE PATTERN

FOR A LOG PERIODIC DIPOLE ANTENNA

patterns show better agreement with the calculated patterns than the H plane patterns do. This is because the unit pattern of the individual elements does not permit radiation in the direction broadside to the array.

The experimental data shown in Figures 34 and 35 reveals that the minimum obtainable beamwidth, for a particular choice of τ , varies inversely with the parameter τ , being about 25^{o} narrower for $\tau = 0.95$ than $\tau = 0.81$ in the H plane. The calculated curves show that the minimum obtainable beamwidth for the three values of τ used are nearly equal. This represents a rather serious failure since the conclusion to be drawn from these curves is that any value of τ in the above range can be used to obtain the minimum beamwidth (or maximum gain) for this class of antennas as long as the proper apex angle is used. This, of course, is an incorrect conclusion as the measurements clearly show. It is believed that these erroneous results are due to the assumptions made in Section 3 relating the characteristics of the radiation wave to transmission line wave, and are not a basic deficiency of the leaky wave approach. While the assumptions made relating the two waves are valid as first order approximations, the actual relationship between the two waves is undoubtedly more complicated than that given by (45) and (47).

Since the transform used is valid only in the half plane to the front of the antenna, no information is given regarding the pattern shape in the rear quadrants. However, Figures (25) to (33)

patterns show better agreement with the calculated patterns than the H plane patterns do. This is because the unit pattern of the individual elements does not permit radiation in the direction broadside to the array.

The experimental data shown in Figures 34 and 35 reveals that the minimum obtainable beamwidth, for a particular choice of τ, varies inversely with the parameter τ, being about 29° narrower for $\tau = 0.95$ than $\tau = 0.91$ in the E plane. The extrapolated curves show that the minimum obtainable beamwidth for the three values of τ used are nearly equal. This represents a rather serious failure since the conclusion to be drawn from these curves is that any value of τ in the above range can be used to obtain the minimum beamwidth (or maximum gain) for this class of antennas as long as the proper apex angle is used. This, of course, is an incorrect conclusion as the measurements clearly show. It is believed that these erroneous results are due to the assumptions made in Section 2 relating the characteristics of the radiating wave to transmission line wave, and are not a basic deficiency of the leaky wave approach. While the assumptions made relating the two waves are valid as first order approximations, the actual relationship between the two waves is undoubtedly more complicated than that given by (35) and (47).

Since the transform used is valid only in the half plane in the front of the antenna, no information is given regarding the pattern shape in the rear quadrants. However, Figures (29) to (33)

show little energy is radiated to the rear of this antenna in the useable region of its parameter, so that this deficiency is not too important. If it is desired to predict the front to back ratio of these antennas, a more sophisticated theory will be required.

SECTION 6

6. CONCLUSIONS

The object of this thesis was to provide an analytic solution of the far field radiation patterns for the log periodic class of antennas. Within certain limitations, this goal was obtained by considering them to behave as a leaky wave device.

It has been shown by DuHamel and Berry that each half structure radiates by itself with the result that the pattern of the complete antenna can be obtained using array theory if the pattern functions of each boom are known. This approach neglects the effects of mutual coupling, but it has been shown that these effects have only a small influence on the shapes of the radiation patterns.[18]

The radiation pattern for each half structure was obtained by hypothesising the existence of a radiating aperture at the front of the active region in the plane perpendicular to the half structure. The approximate aperture distribution was obtained by considering the radiation wave to behave as a leaky wave in the active region. The far field pattern was found from this aperture distribution using a transform technique. This procedure did not consider the half wave dipoles from which the radiation wave originated so that this pattern represented the group pattern. Since dipoles are isotropic in the H plane, this pattern gave the H plane pattern function for the half structure. The assumption was made that the unit pattern for the elements is that of a half wave dipole. The product of the group pattern and this unit pattern gave the E plane

6. CONCLUSIONS

The object of this thesis was to provide an analytic solution of the far field radiation patterns for the log periodic class of antennas. Within certain limitations, this goal was obtained in considering them to behave as a leaky wave device.

It has been shown by DuHamel and Berry that each half structure radiates by itself with the result that the pattern of the complete antenna can be obtained using array theory if the pattern functions of each half are known. This approach neglects the effects of mutual coupling, but it has been shown that these effects have only a small influence on the shapes of the radiation patterns.[15]

The radiation pattern for each half structure was obtained by hypothesizing the existence of a radiating aperture at the front of the active region in the plane perpendicular to the half structure. The approximate aperture distribution was obtained by considering the radiating wave to behave as a leaky wave in the active region. The far field pattern was found from this aperture distribution using a transform technique. This procedure did not consider the half wave dipoles from which the radiation was originating so that this pattern represented the group pattern. Since dipoles are isotropic in the H plane, this pattern gave the H plane pattern function for the half structure. The assumption was made that the unit pattern for the elements is that of a half wave dipole. The product of the group pattern and this unit pattern gave the E plane

pattern function. The pattern function of the complete structure was then obtained using array theory.

Assumptions were made relating the radiation wave to the transmission line wave so that the far field pattern functions of these antennas can be calculated if the characteristics of the transmission line wave are known.

These characteristics were obtained experimentally for a log periodic dipole antenna and used to calculate the far field patterns. It was found that each value of the geometric ratio, τ, had a corresponding apex angle, Θ, for which minimum beamwidth was obtained. It was found that this minimum beamwidth occurs approximately at the apex angle for which the relation

$$\beta_R^2 - \alpha_R^2 = k_o^2 \tag{52}$$

is satisfied. The beamwidth for this apex angle was found to be directly proportional to the magnitude of α_R. It was observed that this property effectively limits the minimum beamwidth, or maximum gain, which can be obtained from this antenna since the magnitude of α_R must be fairly large for frequency independent operation to take place.

The calculated far field patterns were found to show reasonably good agreement with the main beam of patterns obtained experimentally. This agreement demonstrates that the actual radiation patterns for these antennas can be approximated by the pattern obtained using aperture theory where the aperture field is computed

using leaky wave theory. While this approach gives only the approximate aperture distribution, the far field patterns thus calculated have been found to show exceedingly close agreement with the actual patterns if the magnitude of the attenuation constant is small.[23,24] For the log periodic class of antennas, reasonably good agreement was also obtained using this simplified aperture distribution, although the correlation was not as good as that obtained for structures with small attenuation constants. In the case of log periodic antennas, where the magnitude of the attenuation constant is fairly large, the influence of other factors on the shape of the radiation patterns becomes significant. This occurs because the effect of the leaky wave pole is inversely proportional to the magnitude of the attenuation constant. However, the generally good agreement obtained demonstrates that the leaky wave mode plays the dominant role in determining the far field radiation patterns of these antennas.

One main failure of the theory was noted. This was that the minimum obtainable beamwidths for various values of τ were approximately equal and did not vary inversely with τ as was experimentally observed. This failure of the theory was attributed to the assumptions made relating the characteristics of the transmission line and radiation waves.

It was also noted that if the front to back ratio of these antennas is required, a more sophisticated theory would have to be used since the transform is valid only for the half plane in

using leaky wave theory. While this approach gives only the approximate aperture distribution, the far field patterns thus calculated have been found to show exceedingly close agreement with the measured patterns if the magnitude of the attenuation constant is small.[21,28] For the log periodic class of antennas, reasonably good agreement was also obtained using this simplified aperture distribution, although the correlation was not as good as that obtained for structures with small attenuation constants. In the case of log periodic antennas, where the magnitude of the attenuation constant is fairly large, the influence of other factors on the shape of the radiation patterns becomes significant. This occurs because the effect of the leaky wave mode is increasingly proportional to the magnitude of the attenuation constant. However, the generally good agreement obtained demonstrates that the leaky wave mode plays the dominant role in determining the far field radiation patterns of these antennas.

One main failure of the theory was noted: This was that the minimum obtainable beamwidths for various values of τ were approximately equal and did not vary inversely with τ as was experimentally observed. This failure of the theory was attributed to the assumptions made regarding the characteristics of the transmission line and radiation zones.

It was also noted that if the trend to [illegible] antennas is required, a more sophisticated theory would have to be used since the transform is valid only for the half plane to

front of the antenna.

The conclusion was made that the radiating patterns for the log periodic antenna can be obtained analytically from the properties of the transmission line field by considering this antenna to behave as a leaky wave device.

BIBLIOGRAPHY

BIBLIOGRAPHY

1. V. H. Rumsey, "Frequency Independent Antennas," 1957 IRE National Convention Record, Part 1, pp. 114-118.

2. R. H. DuHamel and D. E. Isbell, "Broadband Logarithmically Periodic Antenna Structures," Technical Report No. 19, Antenna Laboratory, University of Illinois, May, 1957.

3. R. L. Carrel, "Analysis and Design of the Log - Periodic Dipole Antenna," Technical Report No. 52, Antenna Laboratory, University of Illinois, October, 1961.

4. P. E. Mayes, G. A. Deschamps and W. T. Patton, "Backward-Wave Radiation From Periodic Structures and Application to the Design of Frequency Independent Antennas," Technical Report No. 60, Antenna Laboratory, University of Illinois, December, 1962.

5. R. L. Bell, C. T. Elfving and R. E. Franks, "Near Field Measurements on a Logarithmically Periodic Antenna," IRE Transactions on Antennas and Propagation, November, 1960; Volume AP-8, pp. 559-567.

6. Raj Mittra, "Theoretical Study of a Class of Logarithmically Periodic Circuits," Technical Report No. 59, Antenna Laboratory, University of Illinois, July, 1962.

7. J. D. Dyson, "Frequency Independent Antennas; Survey of Development," Electronics, April 20, 1962; pp. 39-44. (This article has an extensive bibliography containing over 75 references pertaining to wideband and frequency independent antennas).

8. R. S. Elliott, "A View of Frequency Independent Antennas," The Microwave Journal, December, 1962; pp. 61-68.

9. J. D. Dyson, "The Equiangular Spiral Antenna," IRE Transactions on Antennas and Propagation, April, 1960; Volume AP-7, pp. 181-187.

10. H. Jasik, "Antenna Engineering Handbook," McGraw Hill Book Company, 1961; Chapter 18.

11. B. R. S. Cheo, V. H. Rumsey and W. J. Welch, "A Solution to the Frequency - Independent Problem," IRE Transactions on Antennas and Propagation, November, 1961; Volume AP-9, pp. 527-534.

12. J. D. Dyson, "The Unidirectional Equiangular Antenna," IRE Transactions on Antennas and Propagation, October, 1959; Volume AP-7, pp. 329-334.

13. J. D. Dyson, "New Circularly-Polarized Frequency Independent Antennas With Conical Beam or Omnidirectional Patterns," IRE Transactions on Antennas and Propagation, July, 1961; Volume AP-9, pp. 334-342.

14. R. H. DuHamel and F. R. Ore, "Logarithmically Periodic Antenna Designs," IRE National Convention Record, Part 1, 1958; pp. 139-151.

15. D. E. Isbell, "Log Periodic Dipole Arrays," IRE Transactions on Antennas and Propagation, May, 1960; Volume AP-8, pp. 260-267.

16. P. E. Mayes and R. L. Carrel, "Log Periodic Resonant-V Arrays," Technical Report No. 47, Antenna Laboratory, University of Illinois, July, 1960.

17. P. E. Mayes, "Broadband Backward-Wave Antennas," The Microwave Journal, January, 1963; pp. 61-71.

18. R. H. DuHamel and D. G. Berry, "Logarithmically Periodic Antenna Arrays," Wescon Convention Record, 1958; Part 1, pp. 161-174.

19. H. Jasik, "Antenna Engineering Handbook," McGraw Hill Book Company, 1961; Chapter 16.

20. H. W. Ehrenspeck and H. Poehler, "A New Method of Obtaining Maximum Gain From Yagi Antennas," IRE Transactions on Antennas and Propagation, 1959; Volume AP-7, pp. 479-386.

21. J. Brown and J. O. Spector, "The Radiating Properties of End Fire Arrays," Proceedings of the Institute of Electrical Engineers, Volume 104, Part B, January, 1957; pp. 27-34.

22. J. O. Spector, "An Investigation of Periodic Rod Structures for Yagi Aerials," Proceedings of the Institute of Electrical Engineers, Volume 104, Part B, 1958; pp. 38-44.

23. R. E. Collin, "Analytic Solution for a Leaky Wave Antenna," IRE Transactions on Antennas and Propagation, September, 1962; Volume AP-10, pp. 561-565.

24. R. C. Honey, "A Flush-Mounted Leaky Wave Antenna With Predictable Patterns," IRE Transactions on Antennas and Propagation, October, 1959; Volume AP-7, pp. 320-329.

25. F. Schwering, "On the Range of Validity of Fresnel-Kerchhoff's Approximation Formula," IRE Transactions on Antennas and Propagation, January, 1962; Volume AP-10, pp. 99-100.

26. R. E. Collin, "Field Theory of Guided Waves," McGraw Hill Book Company Incorporated, New York, N. Y., 1960; Chapter 11.

27. E. C. Jordan, "Electromagnetic Waves and Radiating Systems," Prentice Hall, Incorporated, Englewood Cliffs, N. J., 1950; Chapter 10.

28. H. Jasik, "Antenna Engineering Handbook," McGraw Hill Book Company, 1961; Chapter 30.

29. A. Hessel, "On the Influence of Complex Poles on the Radiation Pattern of Leaky-Wave Antennas," IRE Transactions on Antennas and Propagation, September, 1962; Volume AP-10, pp. 646-647.

APPENDIX A

APPENDIX A: THE SADDLE-POINT METHOD OF APPROXIMATE INTEGRATION

The saddle-point method of approximate integration allows integrals of the form given by (33) in Section 3 to be evaluated for large arguments using an assymptotic expansion. The following analysis of this method is a condensed version of that given in Reference (26) and is put in a convenient form to be used in Section 3.

Equation (33), the integral to be solved using this approximate method of integration, is

$$E_y(x,z) = \frac{E_a \gamma_z}{j\pi} \int_C \frac{e^{-\gamma_x'(x-a) - \gamma_z' z}}{\gamma_z^2 - \gamma_z'^2} \, d\gamma_z' \qquad (33)$$

where the path of integration lies along the imaginary axis $-j\infty \le \gamma_z' \le j\infty$ in the complex γ_z plane. This integral could be solved by closing the contour at infinity and using Cauchy's residue theorem. However, the branch points given by $\gamma_x' = j(k_o^2 + \gamma_z'^2)^{1/2} = 0$ which occur at $\gamma_z' = \pm jk_o$ must not be enclosed by the contour. Therefore, the contour must come back in from infinity on one side of the branch line, encircle the branch point, $\gamma_z' = jk_o$, and recede out to infinity along the opposite side of the branch line. This contour is shown in Figure 37, assuming k_o has a small loss term (i.e. k_o is complex), for an arbitrary position of the branch line. Although the orientation of the branch line is arbitrary, it must be chosen carefully if the integral is to vanish along the semi-circle closing the contour at infinity and so a rigorous solution based on this approach may be nearly impossible to obtain.

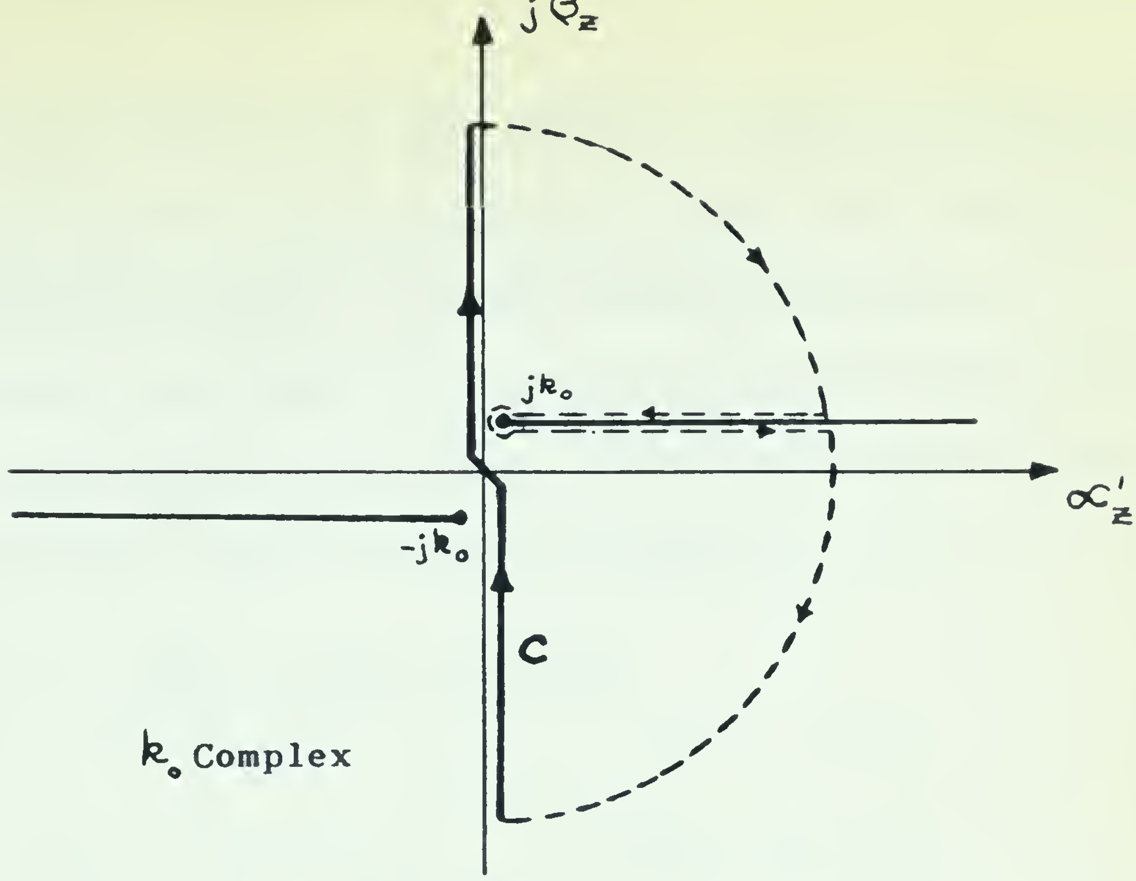

FIGURE 37

CONTOUR C FOR EQUATION 33

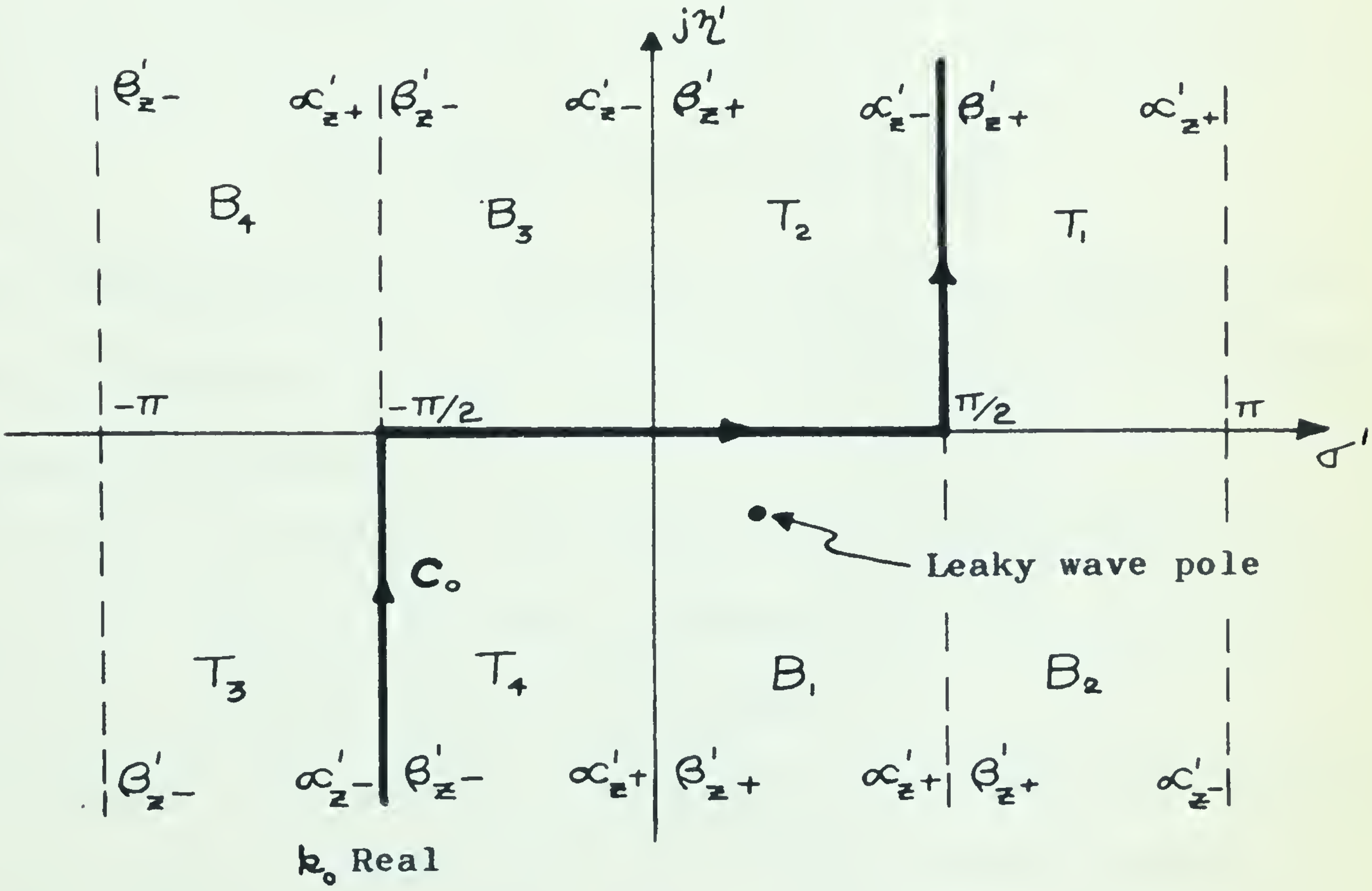

FIGURE 38

MAPPING OF TWO SHEETS OF γ_z' PLANE

ON TO A STRIP OF THE ϕ' PLANE

For large values of $r = [(x-a)^2 + z^2]^{1/2}$, integrals of this type may be solved assymptotically using the saddle-point method (or method of steepest descent) of approximate integration.

Since only one square root is involved (with two corresponding Riemann surfaces) it is possible to eliminate the multivaluedness of the integrand in (33) using the transformation

$$\gamma_z' = j k_o \sin \phi' \tag{34}$$

where

$$\gamma_z' = \alpha_z' + j\beta_z' \qquad \phi' = \sigma' + j\eta' \tag{35}$$

Therefore

$$d\gamma_z' = j k_o \cos \phi' \, d\phi' \tag{53}$$

and

$$(\gamma_z'^2 + k_o^2)^{1/2} = +k_o \cos \phi' \tag{54}$$

since $\cos^2\phi' + \sin^2\phi' = 1$. Equation 34 represents a mapping of the complex γ_z' plane into a strip on the complex ϕ' plane. The two sheets of the Riemann surface map into a connected strip of width 2π along the σ' axis. From (34) and (35) the result

$$\alpha_z' = -k_o \cos \sigma' \sinh \eta' \tag{55}$$

$$\beta_z' = k_o \sin \sigma' \cosh \eta' \tag{56}$$

is obtained. This mapping is illustrated in Figure 38. The quadrants in which β_z' and α_z' are positive or negative are found from (55) and (56) and are specified in the Figure. The proper (top) Riemann surface is the one for which the integral (33) converges on the

infinite semicircle in the γ_z' plane and is given by $Im(j\gamma_x')$ $= Im(\gamma_z'^2 + k_o^2)^{1/2} < 0$ (For the improper, or bottom, Riemann surface, given by $Im(j\gamma_x') > 0$, the integral does not converge at infinity.) Therefore, from (54) the corresponding proper part of the ϕ' plane is determined by the condition that $\sin\sigma' \sinh\eta' > 0$. The The four quadrants of the top and bottom sheets of the γ_z' plane map into the regions designated T_i and B_i (i = 1 , 2 , 3 , 4) respectively, in the Figure. The positive sign in (54) was chosen so that the quadrants T_1 , T_2 and T_3 , T_4 would map into adjacent strips. There are no branch lines in the ϕ' plane since (34) maps both sheets of the Riemann surface into a connected strip.

As a further convenience, the rectangular coordinates, x, z, are changed to the cylindrical coordinates, r , θ , where θ is measured from the x axis.

$$x - a = r \cos\theta \tag{57}$$

$$z = r \sin\theta \tag{58}$$

Using Equations (34), (53), (54), (57) and (58) the integral (33) becomes

$$E_y(r,\theta) = \frac{E_a \gamma_z k_o}{\pi} \int_{C_o} \frac{e^{-jk_o r \cos(\phi' - \theta)} \cos\phi'}{k_o^2 \sin^2\phi' + \gamma_z^2} \, d\phi' \tag{36}$$

where C_o, the contour of integration is shown in Figure 38. This integral may be put in the form

$$I = \int_{C_o} R(\phi) \, e^{f(\phi)} \, d\phi' \tag{59}$$

where

$$R(\phi) = \frac{E_a \gamma_z k_o}{\pi} \cdot \frac{\cos\phi'}{k_o^2 \sin^2\phi' + \gamma_z^2} \tag{60}$$

and

$$f(\phi') = -jk_o r \cos(\phi' - \theta) \tag{61}$$

Since there are no branch lines in the ϕ' plane the contour of integration may be deformed into any other convenient contour without changing the integral (59) provided no poles of $R(\phi')$ are swept across.

In the integrand for (36)

$$f(\phi) = -jk_o r \cos(\phi' - \theta) \tag{61}$$

and the derivative of $f(\phi)$ with respect to ϕ' ,

$$\frac{df}{d\phi'} = jk_o r \sin(\phi' - \theta) \tag{62}$$

is equal to zero at $\phi' = \theta$ (or $\sigma' = \theta$, $\eta' = 0$). Since a complex function cannot have a maximum or a minimum, these stationary points are saddle points. In the vicinity of the saddle point, a Taylor's expansion gives

$$f(\phi') = f(\theta) + \left.\frac{df}{d\phi'}\right|_{\theta}(\phi' - \theta) + \frac{1}{2}\left.\frac{d^2 f}{d\phi'^2}\right|_{\theta}(\phi' - \theta)^2 + ----$$

$$f(\phi') = -jk_o r + j\frac{k_o r}{2}(\phi' - \theta)^2 + ---- \tag{63}$$

since the first derivative vanishes and the second derivative equals $jk_o r$ at θ . Let ρ and s be the radial and angular coordinates with their origin at θ in the ϕ plane. Therefore,

$$(\phi' - \theta) = (\sigma' - \theta + j\eta') = \rho e^{js} \tag{64}$$

Let

$$f_1 + jf_2 = f(\phi') - f(\theta) \tag{65}$$

Therefore, in the vicinity of the saddle point at $\phi' = \theta$

$$f_1 + j f_2 = \left[-j k_o r + \frac{j k_o r}{2}(\phi' - \theta)^2 + \text{----}\right] - \left[-j k_o r\right]$$

$$f_1 + j f_2 = j \frac{k_o r}{2} \rho^2 e^{j2s} + \text{----}$$

and in the limiting case as $\rho \to 0$

$$f_1 = -\frac{k_o r}{2} \rho^2 \sin 2s \tag{66}$$

$$f_2 = \frac{k_o r}{2} \rho^2 \cos 2s \tag{67}$$

The contours f_1 = constant are orthogonal to the contours f_2 = constant. These contours are sketched in Figure 39. The maximum rate of change of f_1 with ρ occurs for $S = \frac{\pi}{4}$ and $\frac{\pi}{4} + \pi$ and also for $S = \frac{3\pi}{4}$ and $-\frac{\pi}{4}$. Along these paths of steepest descent $f_2 = 0$.

In view of the properties of the functions f_1 and f_2, it is clear that it is desirable to deform the contour C_o in (59) into a steepest descent contour (i.e. along $f_2 = 0$) passing through the saddle point, $\phi' = \theta$, at an angle $S = \frac{\pi}{4}$ since, along this path f_1 is negative and hence $e^{f(\phi')}$ will decrease rapidly away from the saddle point. Therefore, the major contribution to the integral comes from a small region $0 < \rho < \rho_1$, along the steepest descent contour. For a general value of ϕ', (61) and (65) give

$$f_1 = -k_o r \sin(\sigma' - \theta) \sinh \eta' \tag{68}$$

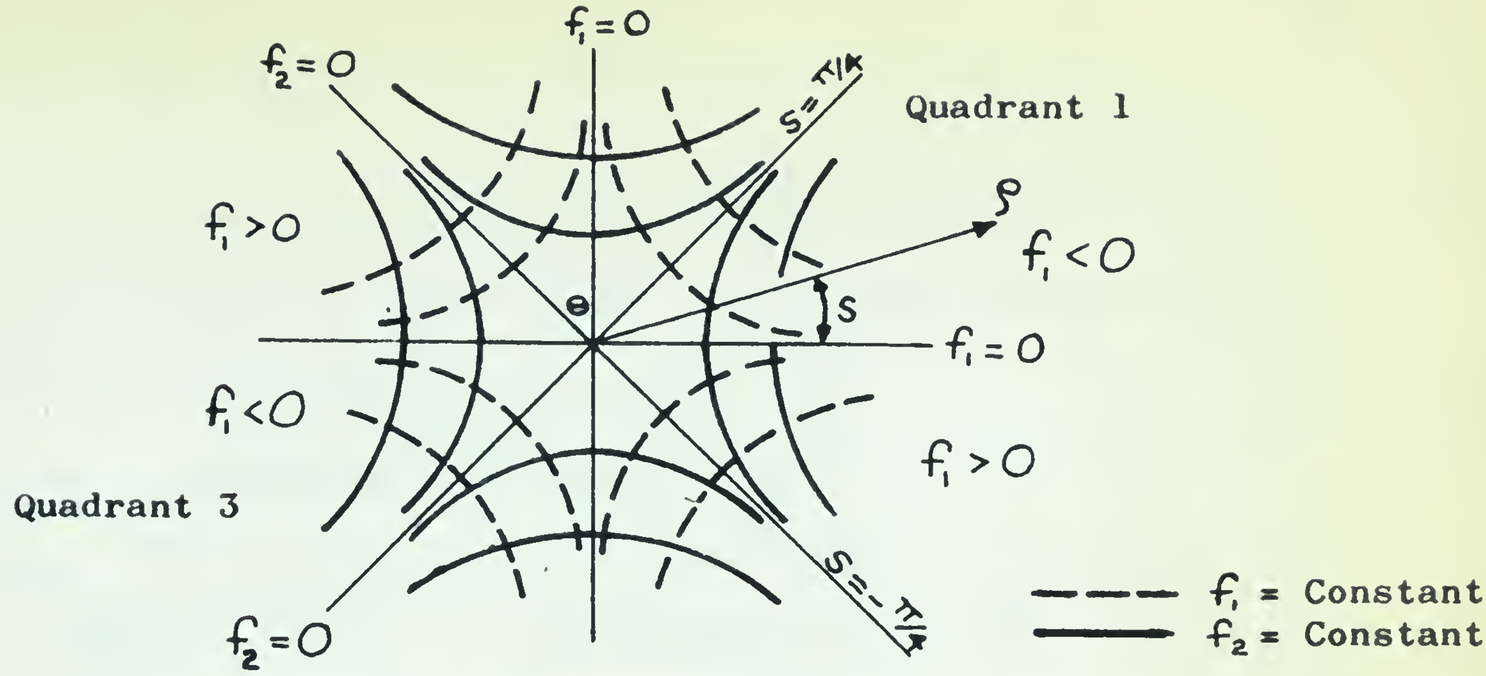

FIGURE 39

CONTOURS OF CONSTANT f_1 AND f_2

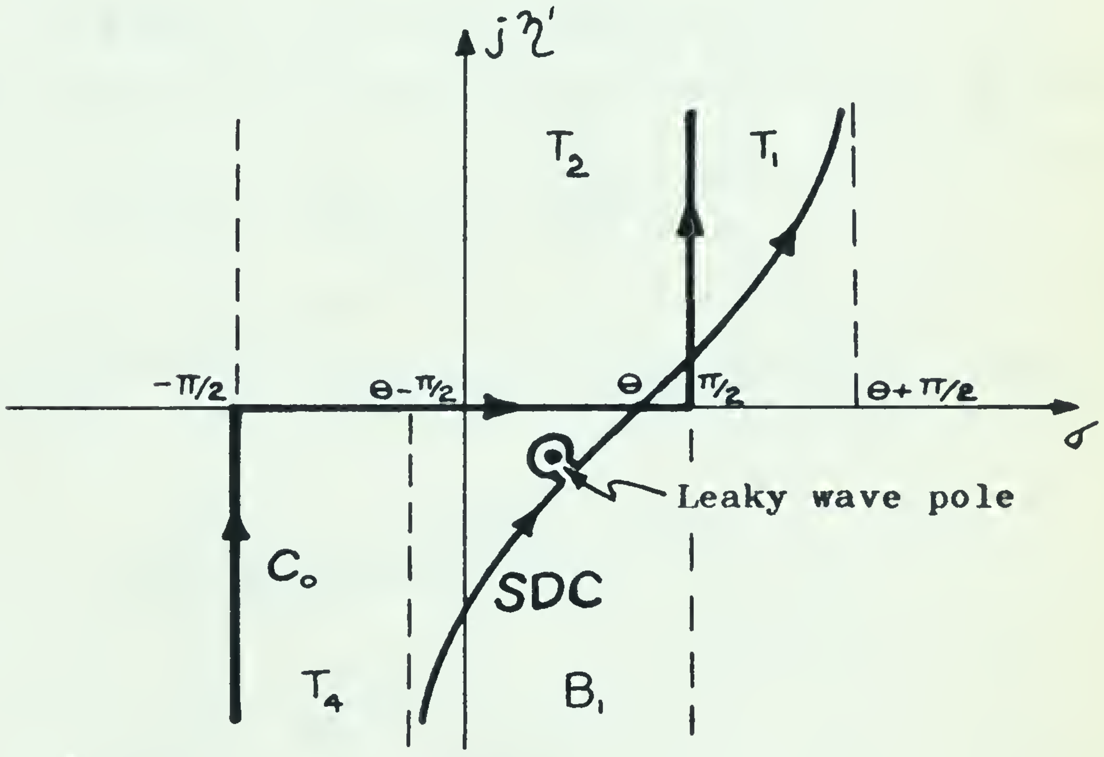

FIGURE 40

DEFORMATION OF CONTOUR C_o INTO

STEEPEST DESCENT CONTOUR SDC

$$f_2 = k_0 r \left[1 - \cos(\sigma' - \theta) \cosh \eta' \right] \tag{69}$$

The steepest descent is given by $f_2 = 0$ and hence the steepest descent contour is given by

$$\cos(\sigma' - \theta) \cosh \eta' = 1 \tag{70}$$

This contour is illustrated as the contour SDC in Figure 40. Any poles of $R(\phi')$ encountered while deforming C_0 into SDC must not be swept over. The contour passes through the saddle point at an angle $\frac{\pi}{4}$ in accordance with (67) which is valid near the saddle point.

In the vicinity of the saddle point, (63) and (64) give

$$f(\phi') \approx -jk_0 r + j\frac{k_0 r}{2} \rho^2 e^{2js}$$

which becomes, along the steepest descent contour $s = \frac{\pi}{4}$ and $\frac{\pi}{4} + \pi$

$$f(\phi') \approx -jk_0 r - \frac{k_0 r}{2} \rho^2 \tag{71}$$

Along this path $\phi' = \theta + \rho e^{j\pi/4}$ in the first quadrant ($s = \frac{\pi}{4}$) and $\phi' = \theta + \rho e^{j(\pi + \pi/4)}$ in the third quadrant ($s = \pi + \pi/4$).

Therefore,

$$\phi' - \theta = \rho e^{j\pi/4} \tag{72}$$

and

$$d\phi' = e^{j\pi/4} d\rho \tag{73}$$

in the first quadrant and

$$\phi' - \theta = -\rho e^{j\pi/4} \tag{74}$$

and

$$d\phi' = -e^{j\pi/4}\, d\rho \tag{75}$$

in the third quadrant. Therefore, the integral, (59),

$$I = \int_{C_0} R(\phi')\, e^{f(\phi')}\, d\phi' \tag{59}$$

becomes

$$I = \int_{SDC} R(\phi')\, e^{f(\phi')}\, d\phi' - j2\pi \sum_{p} F(\phi'_p)\, e^{f(\phi'_p)} \tag{76}$$

where $F(\phi'_p)$ is the residue of $R(\phi')$ at a pole, ϕ'_p, which the contour encounters when it is deformed from C_0 to SDC. The series arises from integrating about the circles surrounding these poles.

If $R(\phi')$ does not have a pole in the vicinity of the saddle point, the integral along the steepest descent contour can be evaluated by expanding $R(\phi')$ in a Taylor series about the saddle point, $\phi' = \theta$. Thus

$$R(\phi') = R(\theta) + \sum_{n=1}^{\infty} R^{n}(\theta)\, \frac{(\phi' - \theta)^n}{n!} \tag{77}$$

where

$$R^{n}(\theta) = \left. \frac{d^n R(\phi')}{d\phi'^n} \right|_{\phi' = \theta}$$

The steepest descent contour integral may be solved by substituting (71), (72), (73), (74), (75) and (77) in the steepest descent contour integral part of (76). Making the above substitutions gives

$$I_{SDC} = \sum_{n=0}^{\infty}\left\{\int_{\rho_1}^{0}\left[R^{n}(\theta)\frac{(-\rho e^{j\pi/4})^{n}}{n!}\right]\left[e^{-jk_0 h - \frac{k_0 h}{2}\rho^2}\right]\left[-e^{j\pi/4}\,d\rho\right]\right.$$

$$\left. + \int_{0}^{\rho_1}\left[R^{n}(\theta)\frac{(\rho e^{j\pi/4})^{n}}{n!}\right]\left[e^{-jk_0 h - \frac{k_0 h}{2}\rho^2}\right]\left[e^{j\pi/4}\,d\rho\right]\right\}$$

$$I_{SDC} = e^{-j(k_0 h - \pi/4)} \sum_{n=0}^{\infty} \frac{R^{n}(\theta)}{n!} e^{j\frac{n\pi}{4}}\left[1+(-1)^{n}\right]\int_{0}^{\rho_1}\rho^{n} e^{-\frac{k_0 h \rho}{2}}\,d\rho \tag{78}$$

The integral over ρ does not change much if ρ_1 is extended to infinity. The result is

$$\int_{0}^{\infty}\rho^{n} e^{-\frac{k_0 h}{2}\rho^2}\,d\rho = \frac{\Gamma\left(\frac{n+1}{2}\right)}{2\left(\frac{k_0 h}{2}\right)^{\frac{n+1}{2}}} \qquad n > -1 \tag{79}$$

where Γ is the gamma function. Therefore,

$$I_{SDC} = e^{-j(k_0 h - \pi/4)} \sum_{n=0,2\cdots} \frac{R^{n}(\theta)}{n!} e^{j\frac{n\pi}{4}}\left(\frac{2}{k_0 h}\right)^{\frac{n+1}{2}}\Gamma\left(\frac{n+1}{2}\right) \tag{80}$$

and the total solution of (76), and hence (59), is

$$I = e^{-j(k_0 h - \pi/4)} \sum_{n=0,2\cdots} \frac{R^{n}(\theta)}{n!} e^{j\frac{n\pi}{4}}\left(\frac{2}{k_0 h}\right)^{\frac{n+1}{2}}\Gamma\left(\frac{n+1}{2}\right)$$

$$-j2\pi \sum_{p} F(\phi'_p)\, e^{-jk_0 h \cos(\phi'_p - \theta)} \tag{81}$$

where $F(\phi_p)$ is the residue of $R(\phi)$ at the pole, ϕ'_p, encountered when the contour is deformed from C_0 to SDC and

$$R^{n}(\theta) = \left.\frac{d^{n} R(\phi)}{d\phi'^{n}}\right|_{\phi'=\theta}$$

The saddle point method of approximate integration is valid only if $\frac{k_0 h \rho^2}{2}$ is large for small values of ρ. This means that $k_0 h$ must be very large.

For the far field pattern h approaches infinity and (81)

becomes

$$I = \left(\frac{2\pi}{k_o r}\right)^{1/2} e^{-j(k_o r - \frac{\pi}{4})} R(\theta) \tag{82}$$

since $\Gamma(1/2) = \sqrt{\pi}$. For large r the contribution of the residues at the leaky wave poles of $R(\phi)$ are neglected because they damp out exponentially in any radial direction from the origin within their wedges of contribution.[29]

Therefore, the solution of $E_y(r,\theta)$ in (36) is, using (59),

$$E_y(r,\theta) = E_a \gamma_z k_o \left(\frac{2}{\pi k_o r}\right)^{1/2} e^{-j(k_o r - \pi/4)} f_1(\theta) \tag{37}$$

where the pattern function $f_1(\theta)$ is given by

$$f_1(\theta) = \frac{\cos\theta}{k_o^2 \sin^2\theta + \gamma_z^2} \tag{38}$$

where r and θ are the components of a cylindrical coordinate system in the x,z plane and θ is measured from the x axis.

APPENDIX B

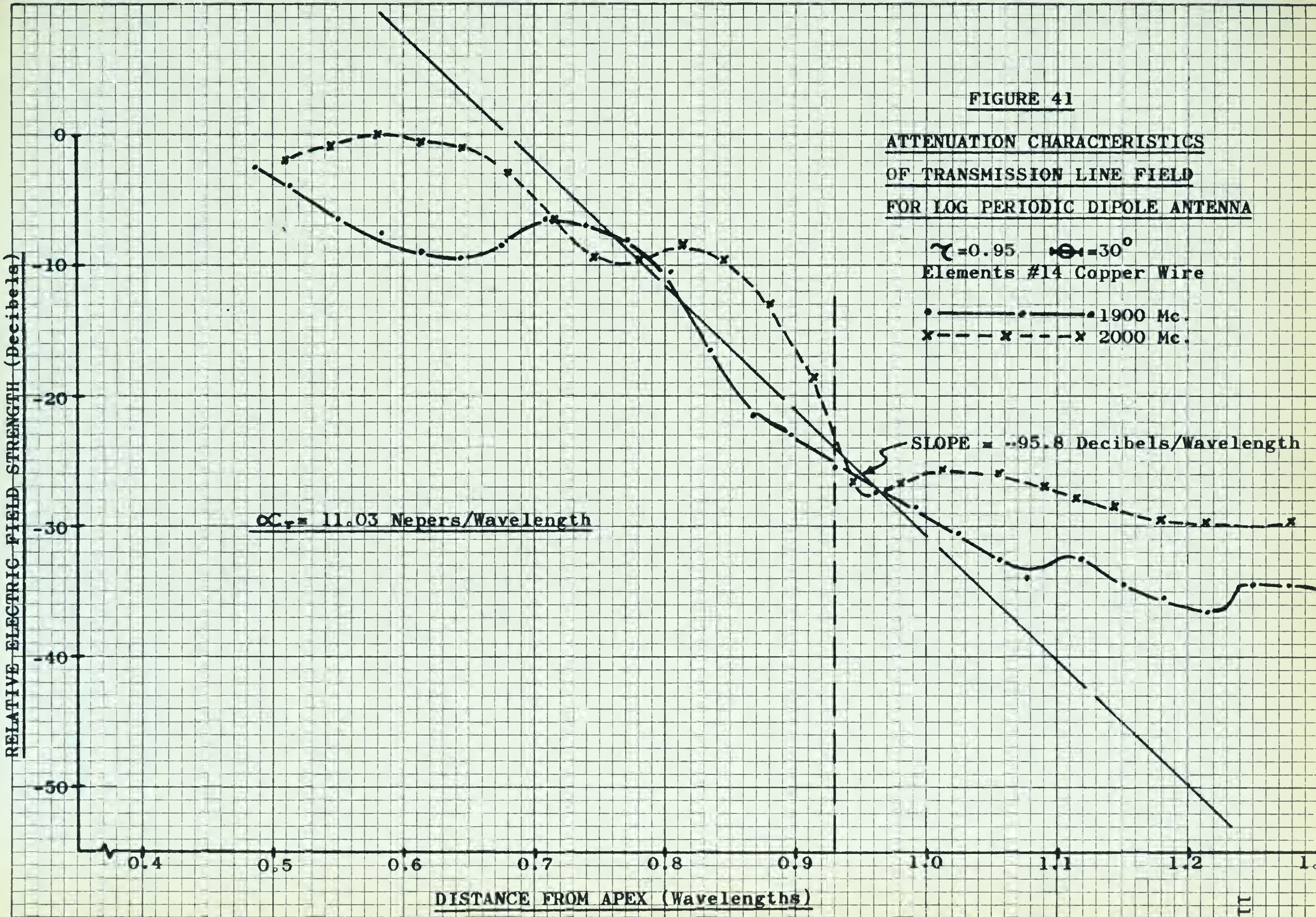
FIGURE 41
ATTENUATION CHARACTERISTICS
OF TRANSMISSION LINE FIELD
FOR LOG PERIODIC DIPOLE ANTENNA
τ=0.95 θ=30°
Elements #14 Copper Wire
1900 Mc.
2000 Mc.
SLOPE = -95.8 Decibels/Wavelength
α_T = 11.03 Nepers/Wavelength
RELATIVE ELECTRIC FIELD STRENGTH (Decibels)
DISTANCE FROM APEX (Wavelengths)
0
-10
-20
-30
-40
-50
0.4
0.5
0.6
0.7
0.8
0.9
1.0
1.1
1.2
1.3

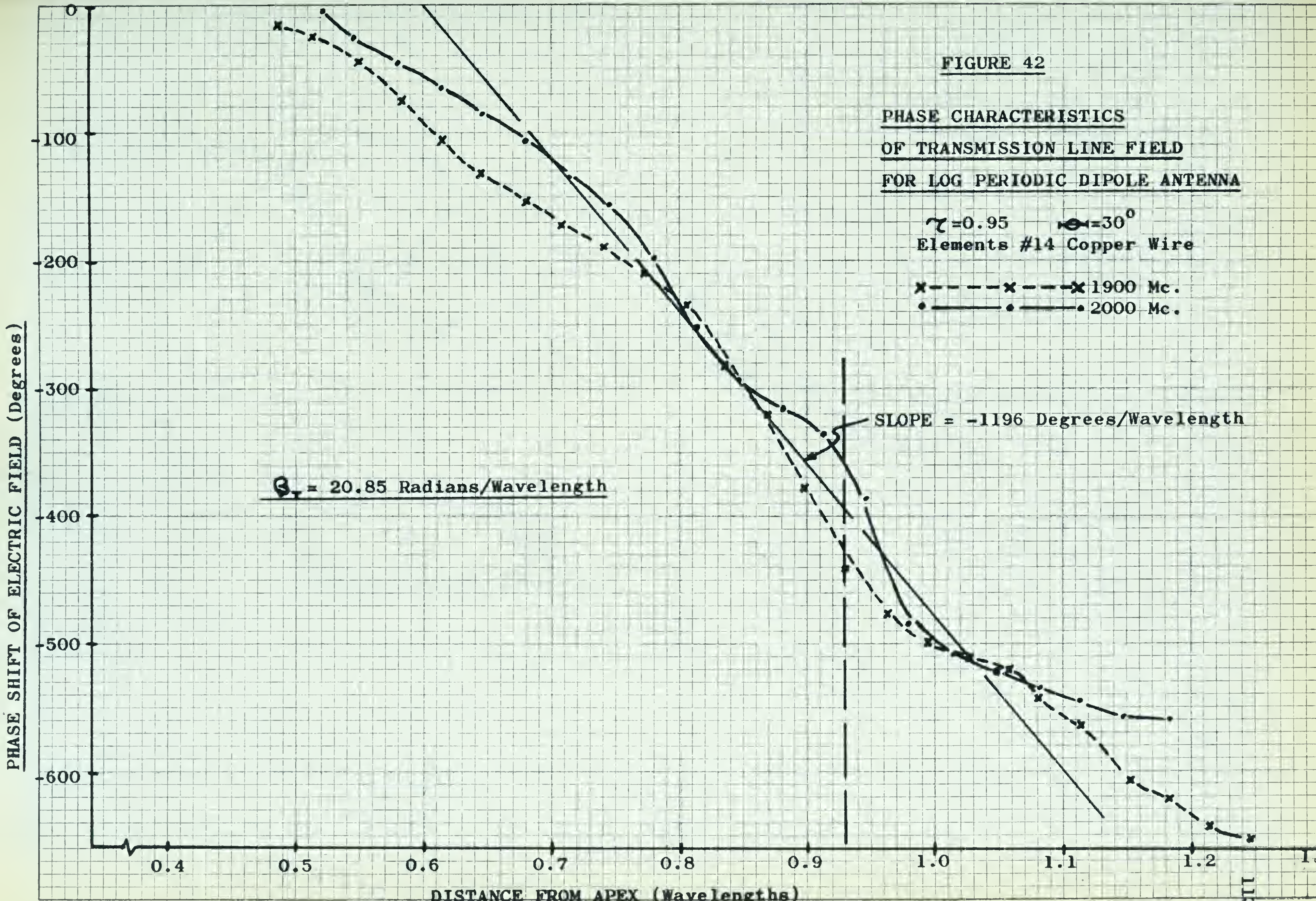
FIGURE 42
PHASE CHARACTERISTICS
OF TRANSMISSION LINE FIELD
FOR LOG PERIODIC DIPOLE ANTENNA
τ=0.95 α=30°
Elements #14 Copper Wire
1900 Mc.
2000 Mc.
SLOPE = -1196 Degrees/Wavelength
β = 20.85 Radians/Wavelength
0
-100
-200
-300
-400
-500
-600
PHASE SHIFT OF ELECTRIC FIELD (Degrees)
0.4
0.5
0.6
0.7
0.8
0.9
1.0
1.1
1.2
1.3
DISTANCE FROM APEX (Wavelengths)

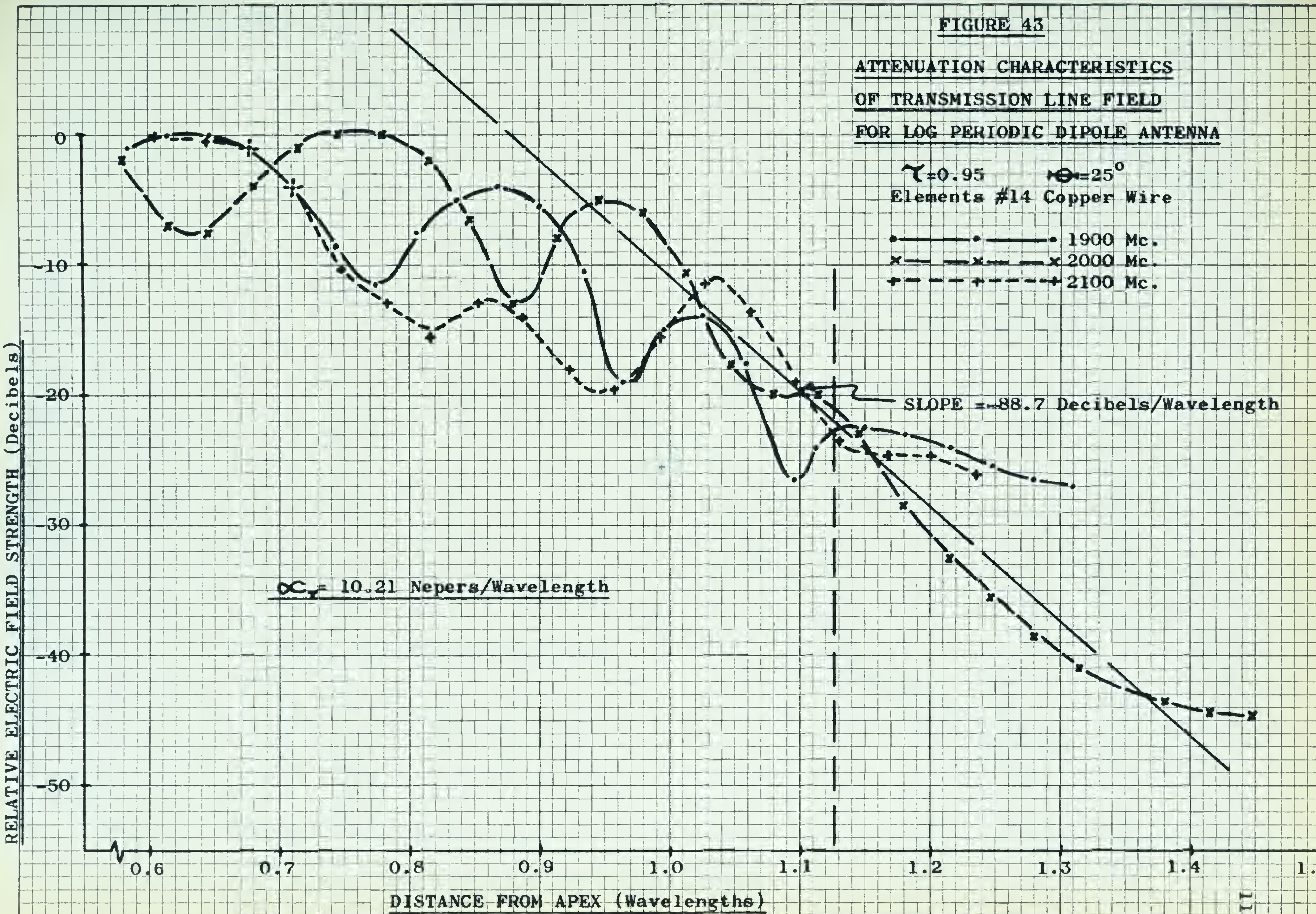
FIGURE 43
ATTENUATION CHARACTERISTICS
OF TRANSMISSION LINE FIELD
FOR LOG PERIODIC DIPOLE ANTENNA
τ=0.95 Θ=25°
Elements #14 Copper Wire
1900 Mc.
2000 Mc.
2100 Mc.
SLOPE = -88.7 Decibels/Wavelength
α_T = 10.21 Nepers/Wavelength
0
-10
-20
-30
-40
-50
RELATIVE ELECTRIC FIELD STRENGTH (Decibels)
0.6
0.7
0.8
0.9
1.0
1.1
1.2
1.3
1.4
1.5
DISTANCE FROM APEX (Wavelengths)

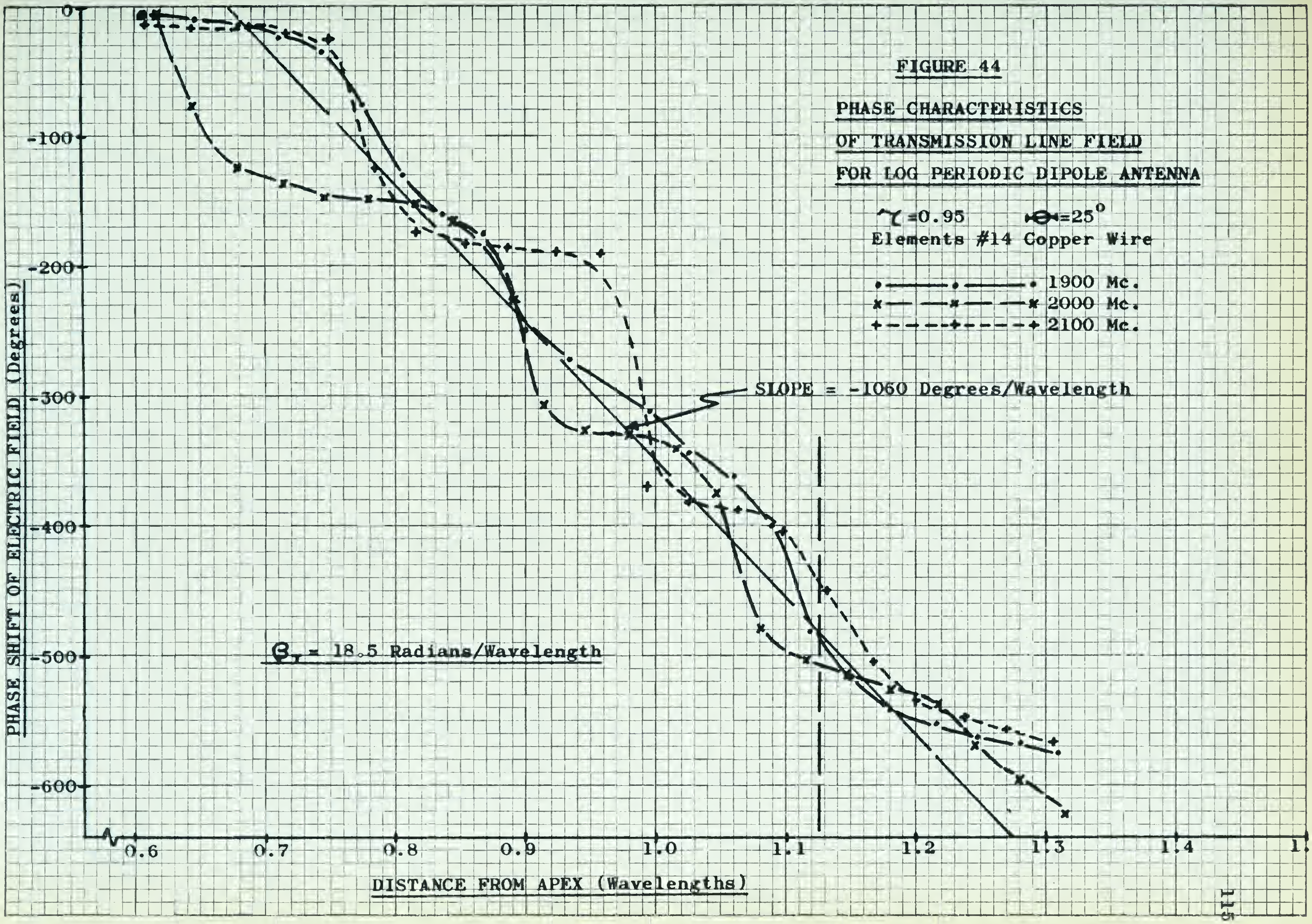
FIGURE 44
PHASE CHARACTERISTICS
OF TRANSMISSION LINE FIELD
FOR LOG PERIODIC DIPOLE ANTENNA
τ = 0.95
θ = 25°
Elements #14 Copper Wire
1900 Mc.
2000 Mc.
2100 Mc.
SLOPE = -1060 Degrees/Wavelength
β_r = 18.5 Radians/Wavelength
PHASE SHIFT OF ELECTRIC FIELD (Degrees)
DISTANCE FROM APEX (Wavelengths)
0
-100
-200
-300
-400
-500
-600
0.6
0.7
0.8
0.9
1.0
1.1
1.2
1.3
1.4
1.5

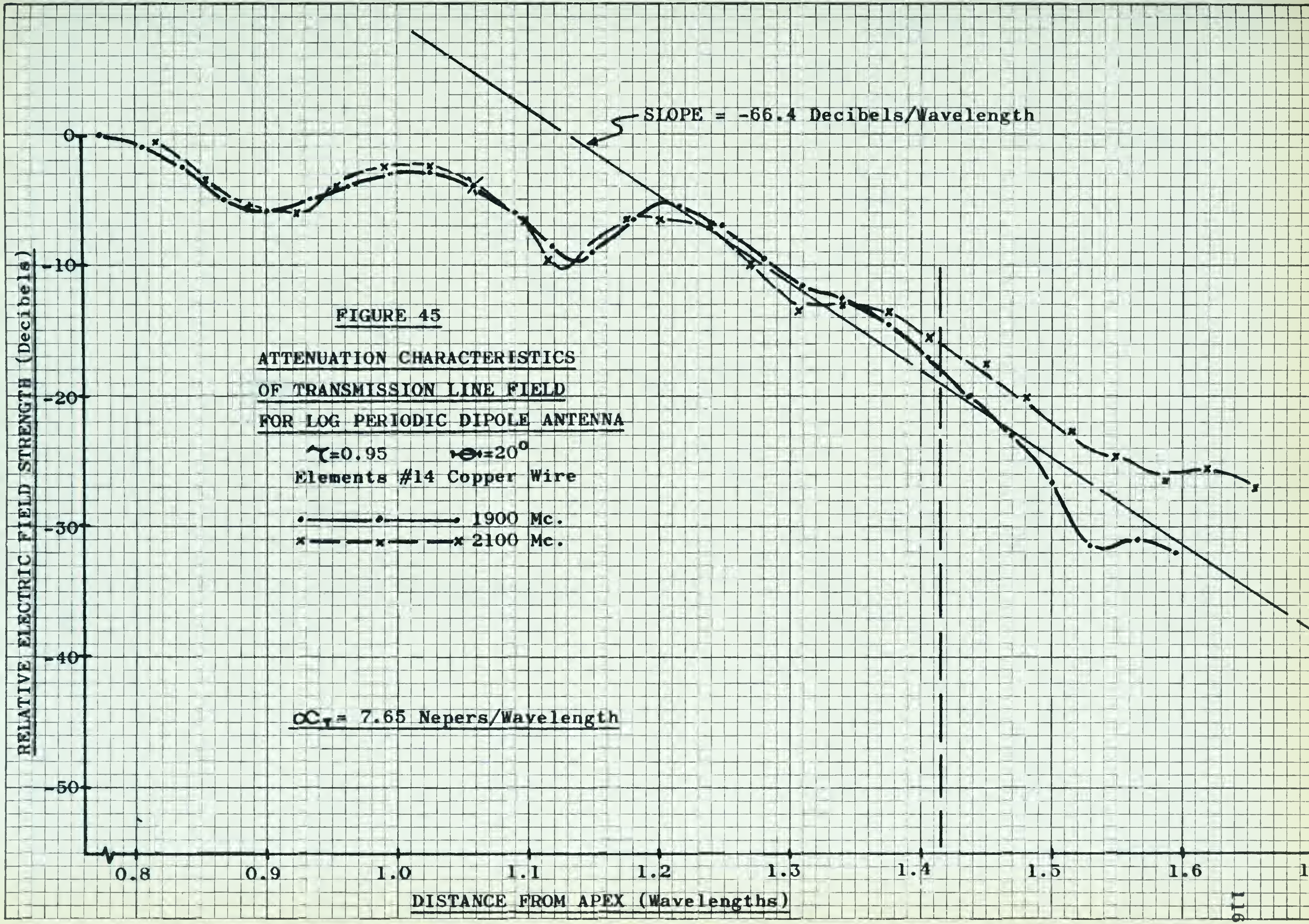

FIGURE 45

ATTENUATION CHARACTERISTICS OF TRANSMISSION LINE FIELD FOR LOG PERIODIC DIPOLE ANTENNA

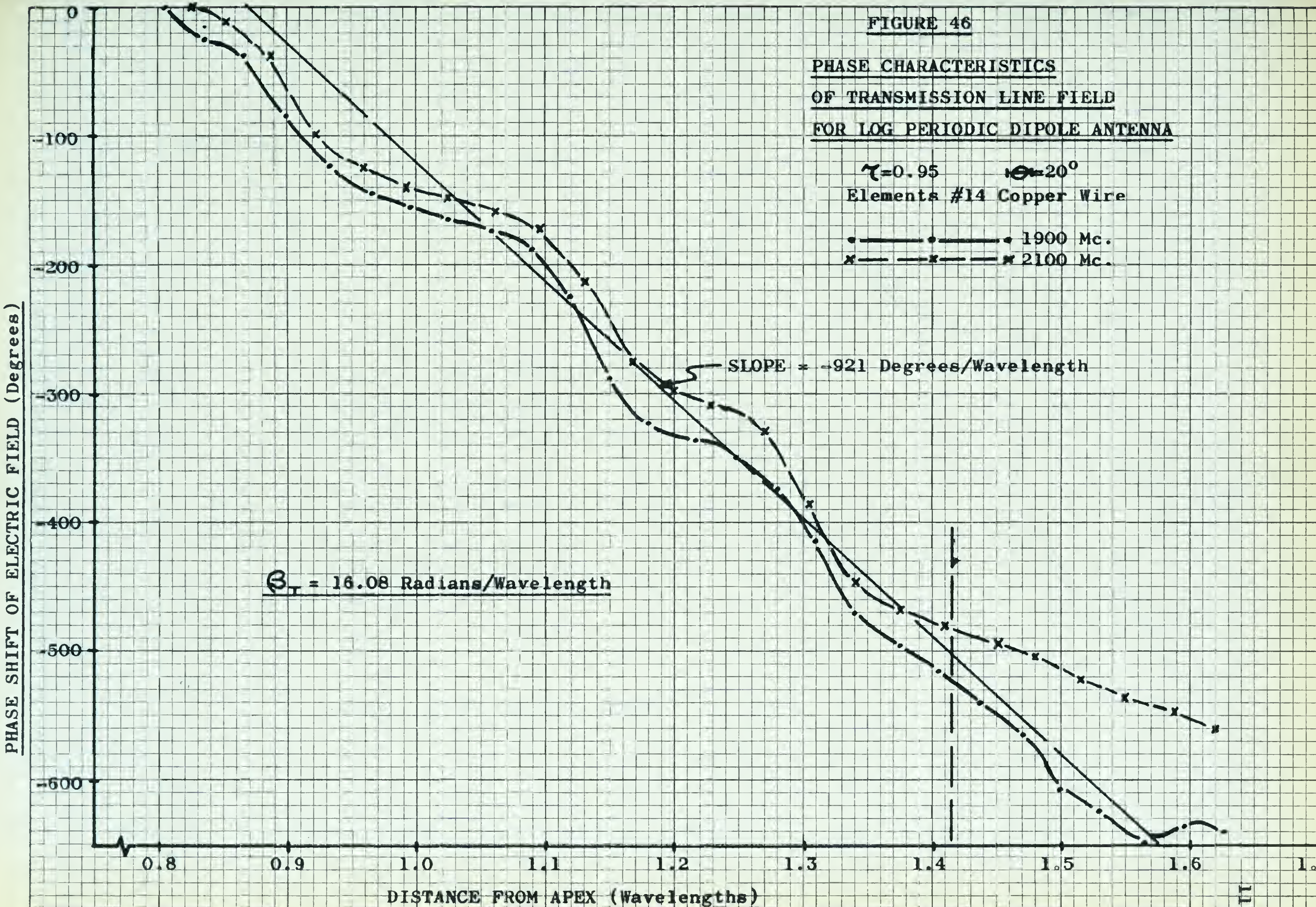

FIGURE 46

PHASE CHARACTERISTICS
OF TRANSMISSION LINE FIELD
FOR LOG PERIODIC DIPOLE ANTENNA

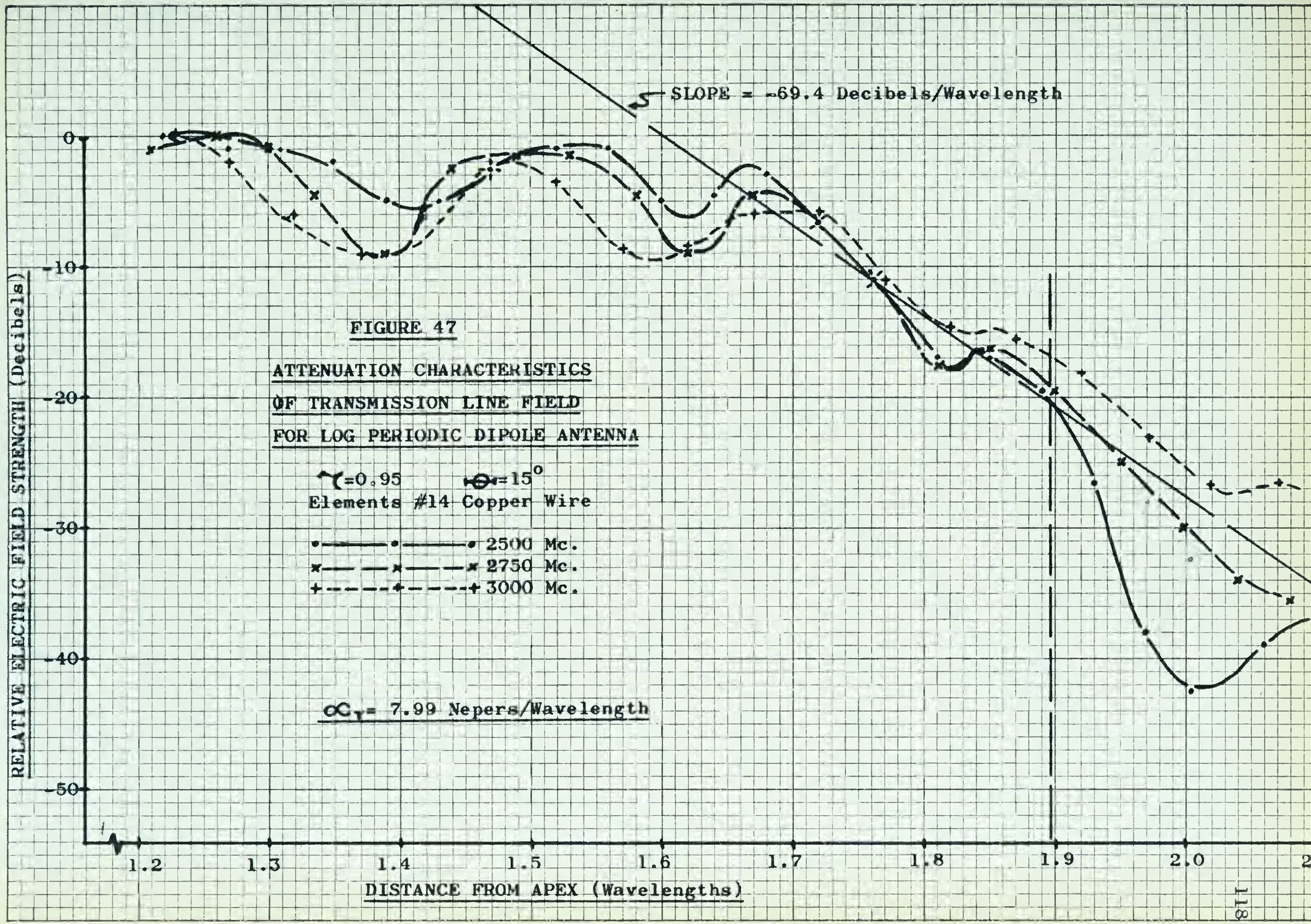

FIGURE 47

ATTENUATION CHARACTERISTICS OF TRANSMISSION LINE FIELD FOR LOG PERIODIC DIPOLE ANTENNA

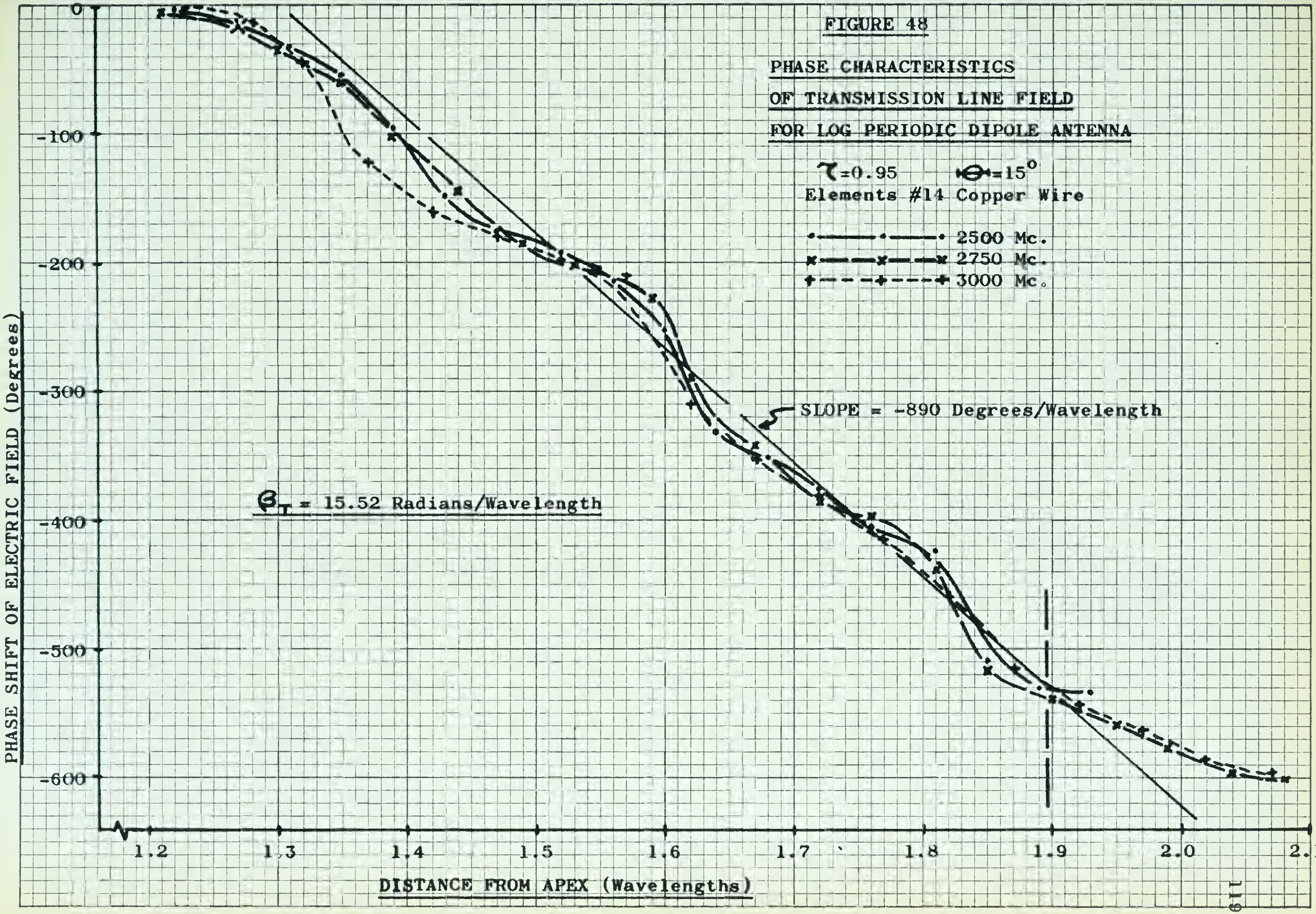
FIGURE 48
PHASE CHARACTERISTICS
OF TRANSMISSION LINE FIELD
FOR LOG PERIODIC DIPOLE ANTENNA
τ=0.95
Θ=15°
Elements #14 Copper Wire
2500 Mc.
2750 Mc.
3000 Mc.
SLOPE = -890 Degrees/Wavelength
β_T = 15.52 Radians/Wavelength
PHASE SHIFT OF ELECTRIC FIELD (Degrees)
DISTANCE FROM APEX (Wavelengths)
0
-100
-200
-300
-400
-500
-600
1.2
1.3
1.4
1.5
1.6
1.7
1.8
1.9
2.0
2.1

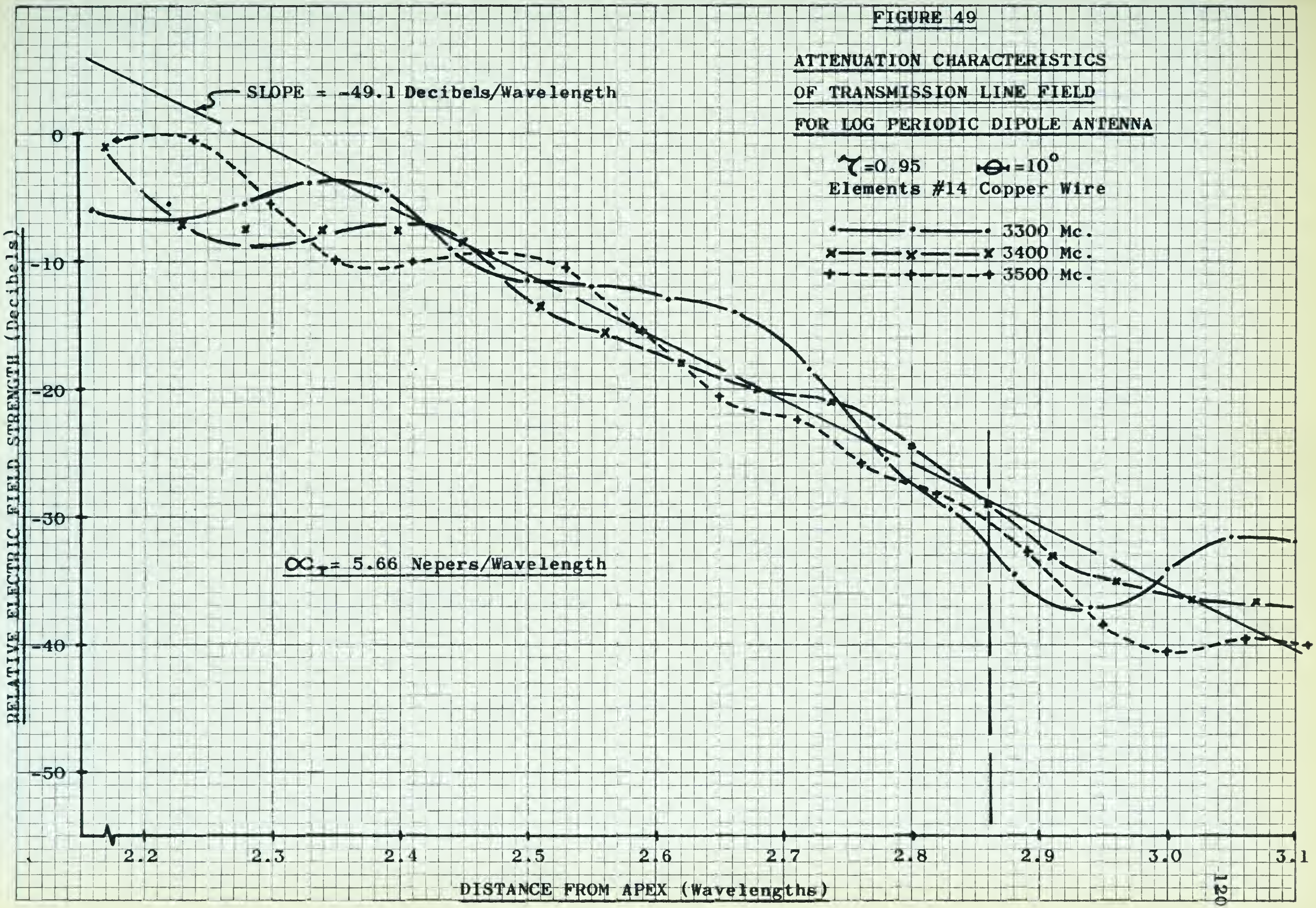

FIGURE 49
ATTENUATION CHARACTERISTICS
OF TRANSMISSION LINE FIELD
FOR LOG PERIODIC DIPOLE ANTENNA
τ=0.95 Φ=10°
Elements #14 Copper Wire
3300 Mc.
3400 Mc.
3500 Mc.
SLOPE = -49.1 Decibels/Wavelength
α_T = 5.66 Nepers/Wavelength
RELATIVE ELECTRIC FIELD STRENGTH (Decibels)
0
-10
-20
-30
-40
-50
2.2
2.3
2.4
2.5
2.6
2.7
2.8
2.9
3.0
3.1
DISTANCE FROM APEX (Wavelengths)

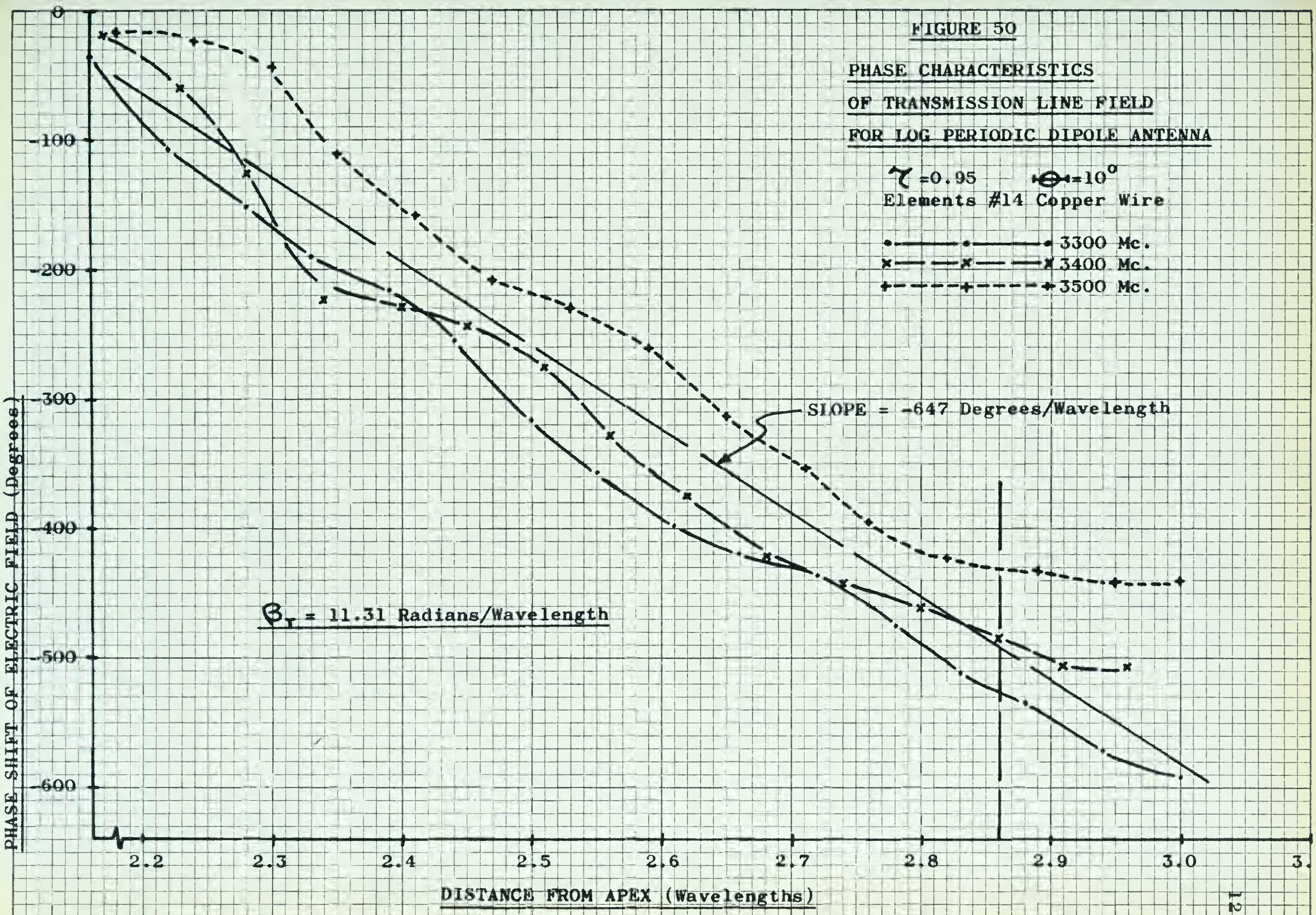
FIGURE 50
PHASE CHARACTERISTICS
OF TRANSMISSION LINE FIELD
FOR LOG PERIODIC DIPOLE ANTENNA
τ =0.95 Θ=10°
Elements #14 Copper Wire
3300 Mc.
3400 Mc.
3500 Mc.
SLOPE = -647 Degrees/Wavelength
β_r = 11.31 Radians/Wavelength
PHASE SHIFT OF ELECTRIC FIELD (Degrees)
DISTANCE FROM APEX (Wavelengths)
0
-100
-200
-300
-400
-500
-600
2.2
2.3
2.4
2.5
2.6
2.7
2.8
2.9
3.0
3.1

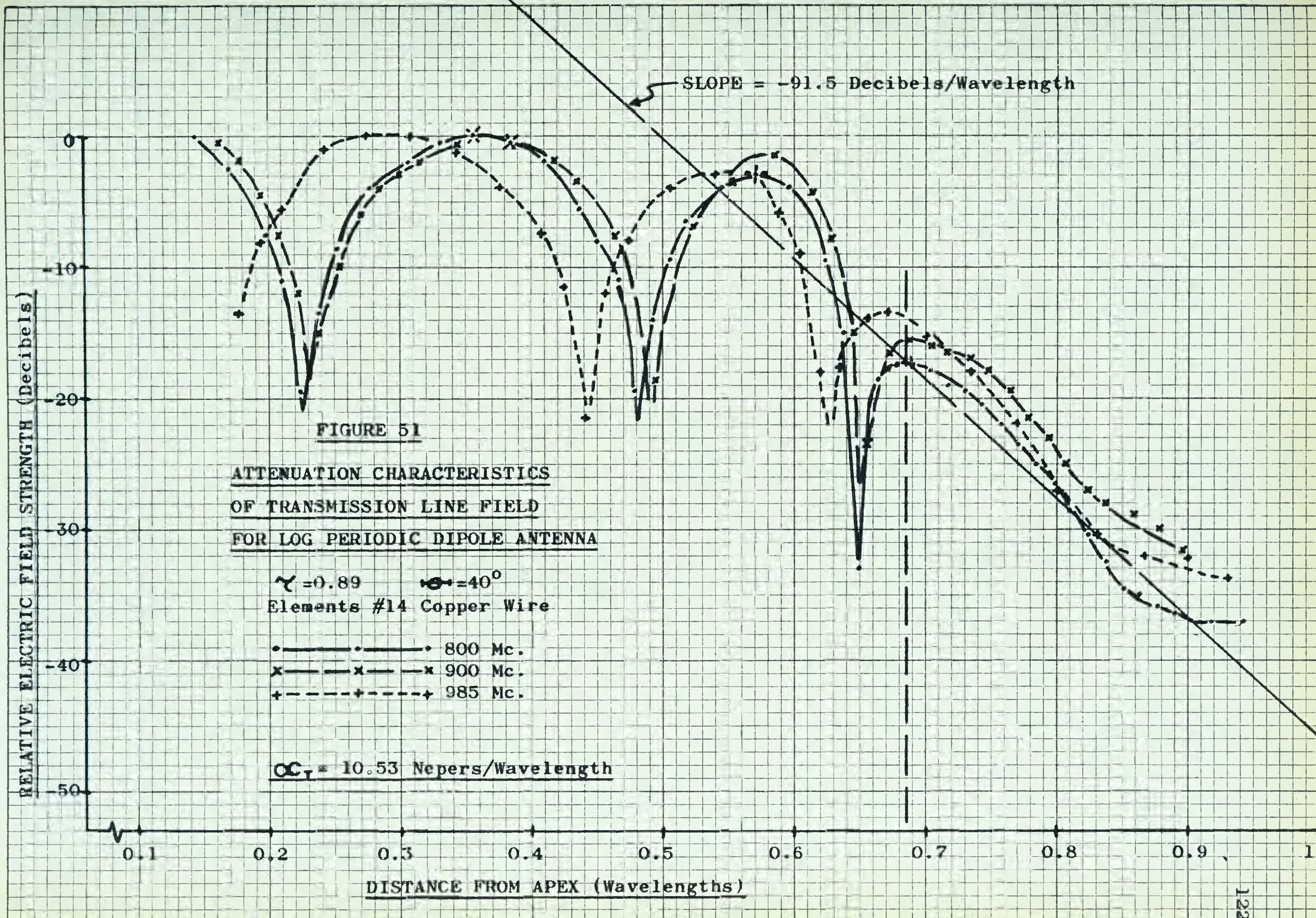

FIGURE 51

ATTENUATION CHARACTERISTICS OF TRANSMISSION LINE FIELD FOR LOG PERIODIC DIPOLE ANTENNA

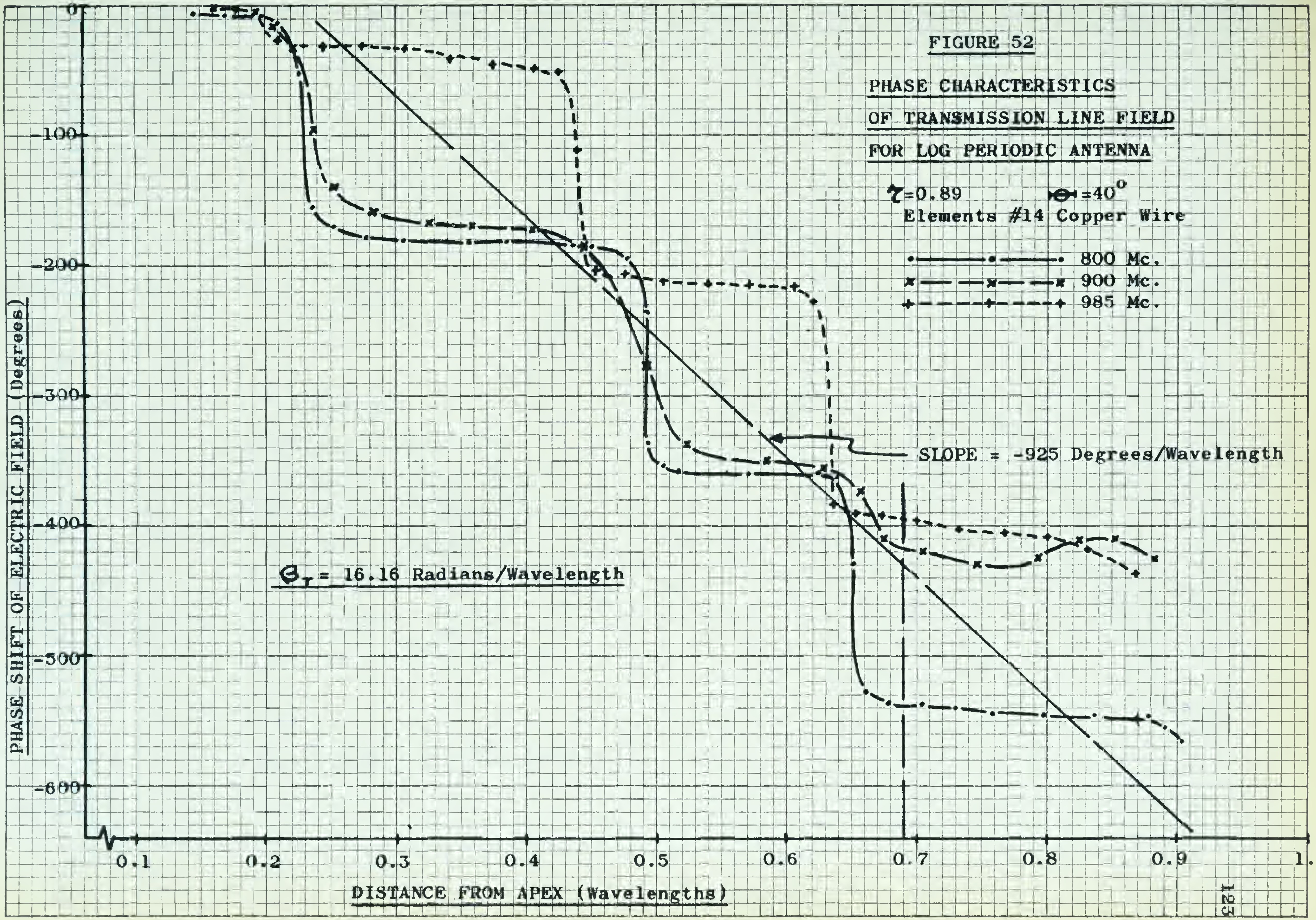

FIGURE 52
PHASE CHARACTERISTICS
OF TRANSMISSION LINE FIELD
FOR LOG PERIODIC ANTENNA
τ=0.89
Θ=40°
Elements #14 Copper Wire
800 Mc.
900 Mc.
985 Mc.
SLOPE = -925 Degrees/Wavelength
β_T = 16.16 Radians/Wavelength
PHASE SHIFT OF ELECTRIC FIELD (Degrees)
0
-100
-200
-300
-400
-500
-600
0.1
0.2
0.3
0.4
0.5
0.6
0.7
0.8
0.9
1.0
DISTANCE FROM APEX (Wavelengths)

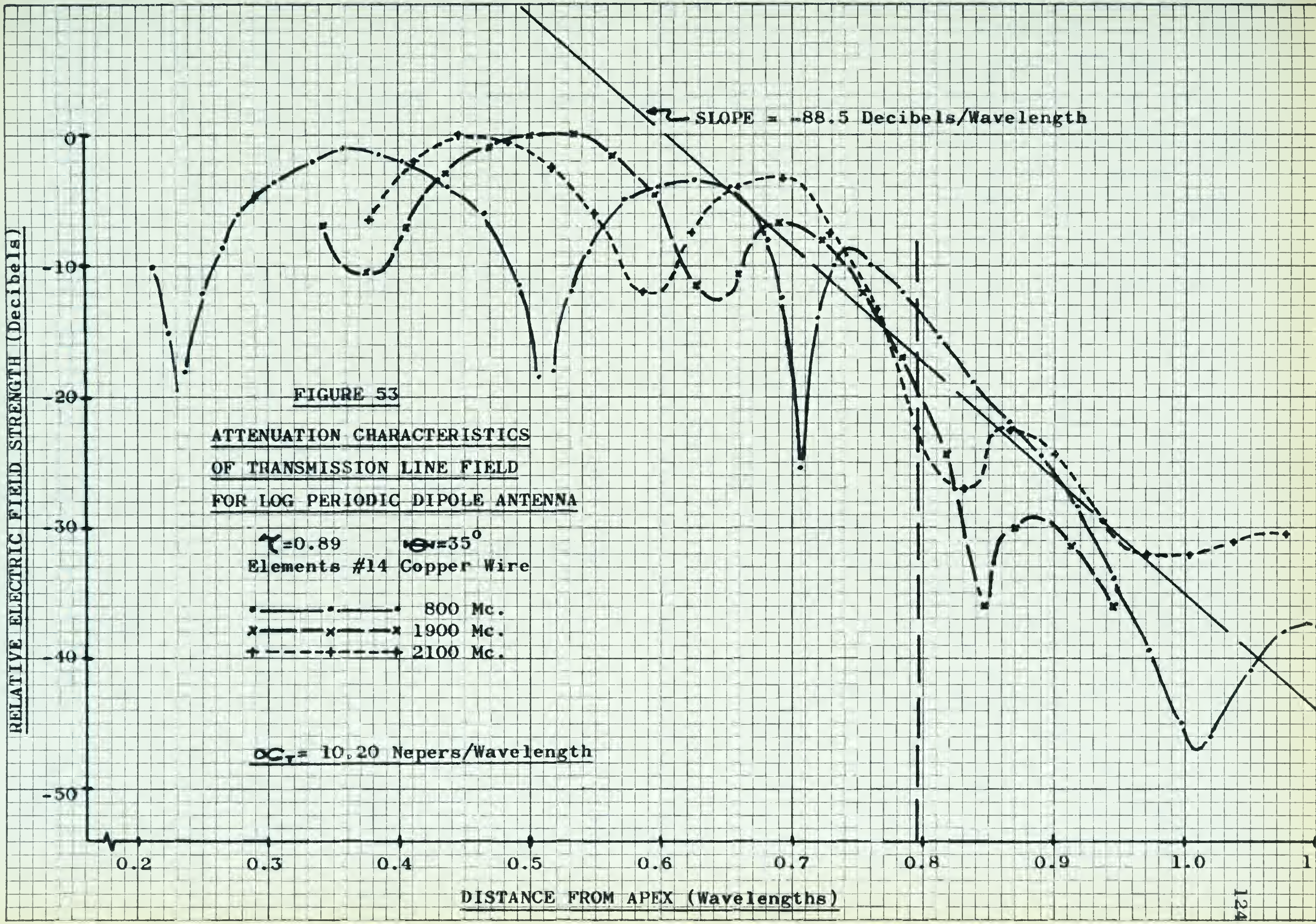

FIGURE 53

ATTENUATION CHARACTERISTICS OF TRANSMISSION LINE FIELD FOR LOG PERIODIC DIPOLE ANTENNA

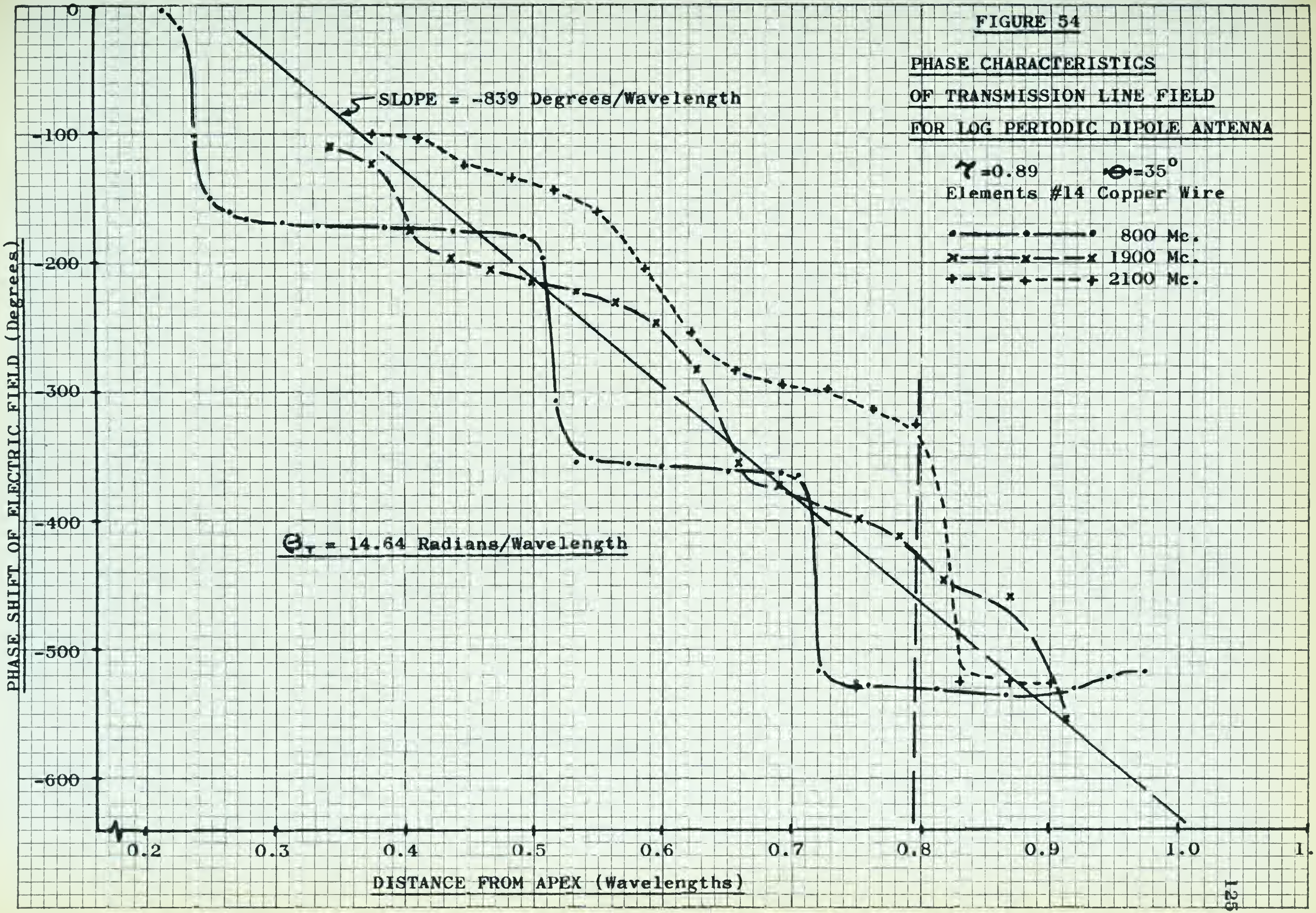
FIGURE 54
PHASE CHARACTERISTICS
OF TRANSMISSION LINE FIELD
FOR LOG PERIODIC DIPOLE ANTENNA
τ =0.89
Θ=35°
Elements #14 Copper Wire
800 Mc.
1900 Mc.
2100 Mc.
SLOPE = -839 Degrees/Wavelength
Θ_τ = 14.64 Radians/Wavelength
0
-100
-200
-300
-400
-500
-600
0.2
0.3
0.4
0.5
0.6
0.7
0.8
0.9
1.0
1.1
DISTANCE FROM APEX (Wavelengths)
PHASE SHIFT OF ELECTRIC FIELD (Degrees)

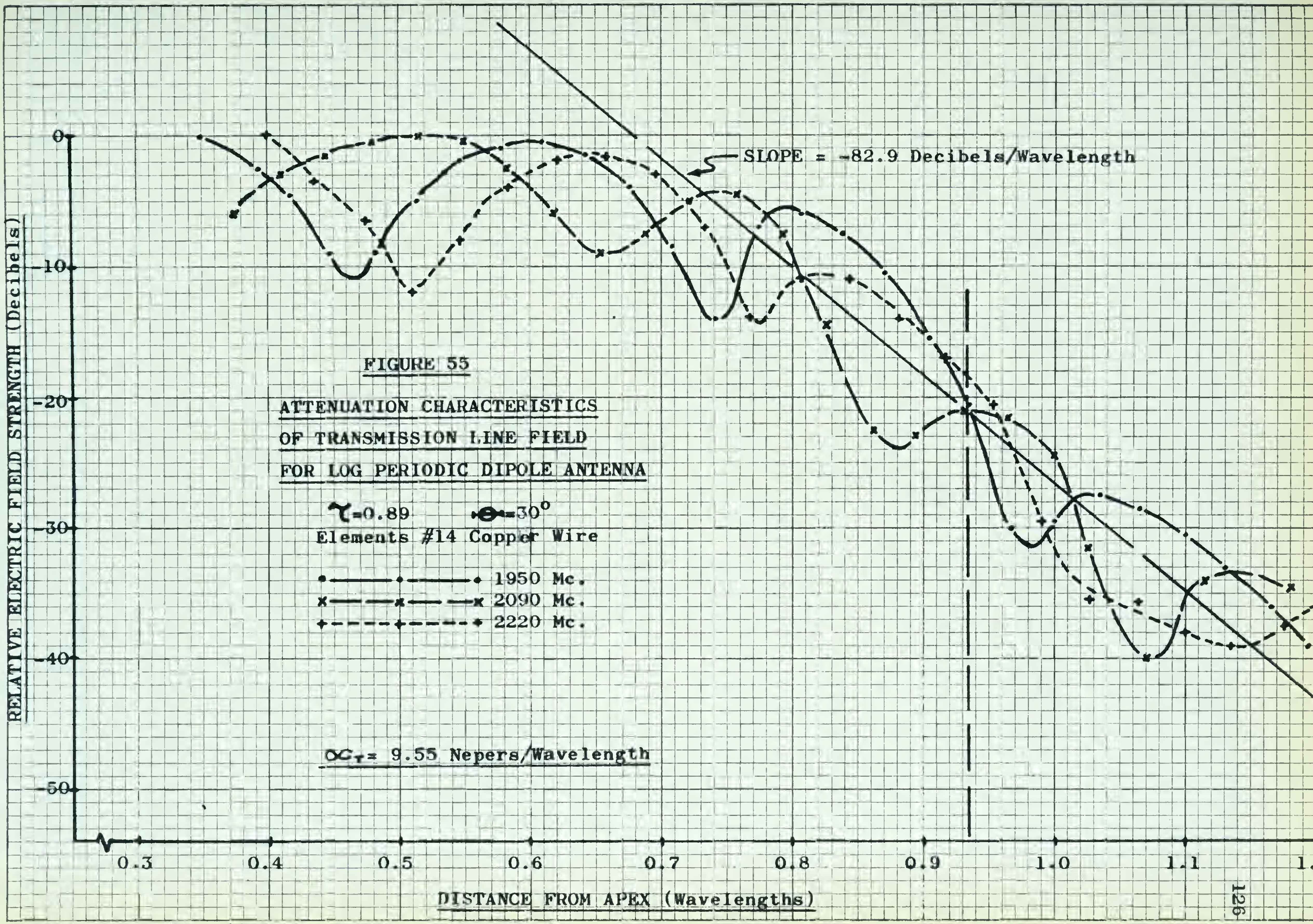

FIGURE 55

ATTENUATION CHARACTERISTICS OF TRANSMISSION LINE FIELD FOR LOG PERIODIC DIPOLE ANTENNA

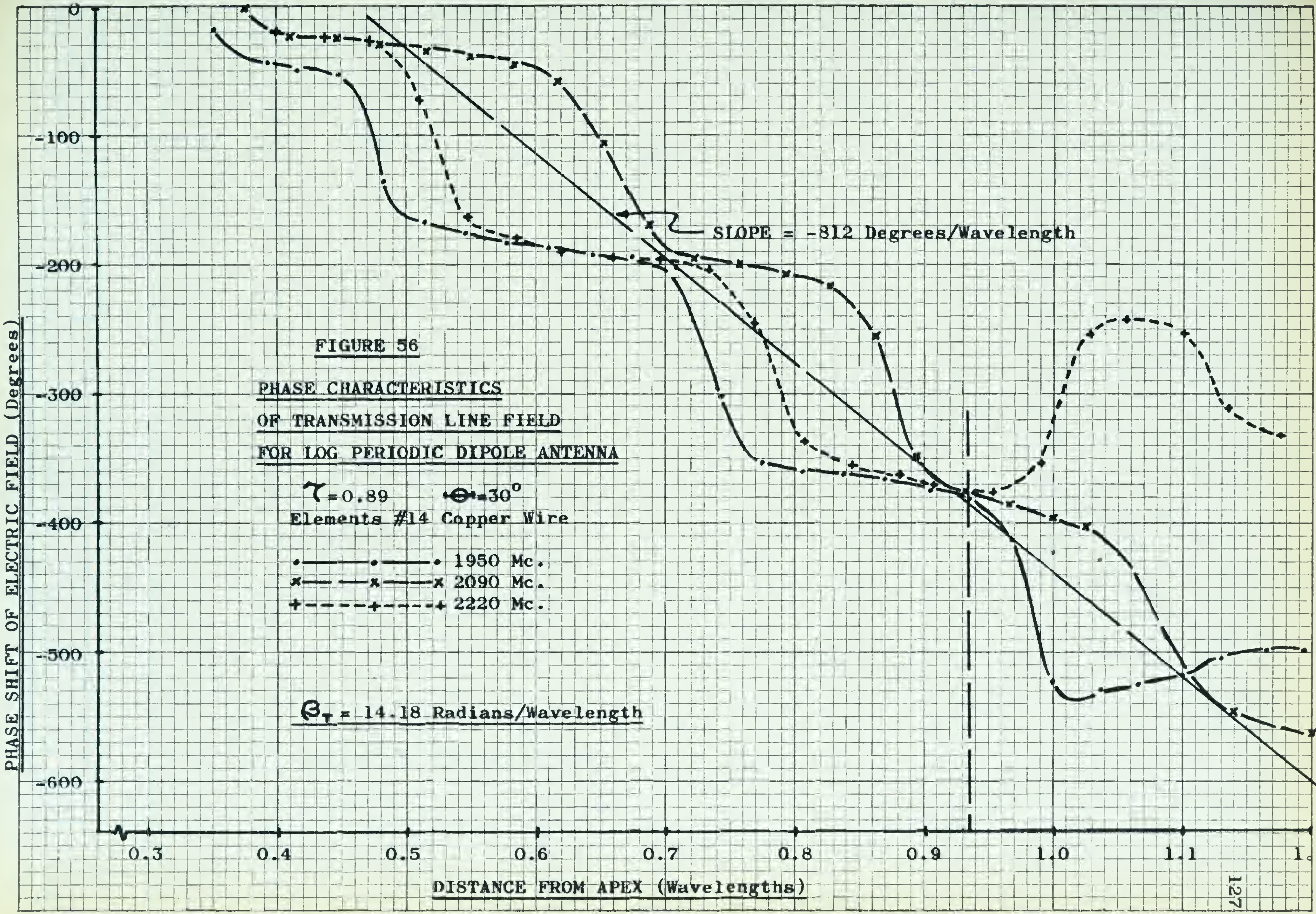
FIGURE 56
PHASE CHARACTERISTICS
OF TRANSMISSION LINE FIELD
FOR LOG PERIODIC DIPOLE ANTENNA
τ = 0.89   Θ = 30°
Elements #14 Copper Wire
1950 Mc.
2090 Mc.
2220 Mc.
SLOPE = -812 Degrees/Wavelength
β_T = 14.18 Radians/Wavelength
PHASE SHIFT OF ELECTRIC FIELD (Degrees)
0
-100
-200
-300
-400
-500
-600
DISTANCE FROM APEX (Wavelengths)
0.3
0.4
0.5
0.6
0.7
0.8
0.9
1.0
1.1
1.2

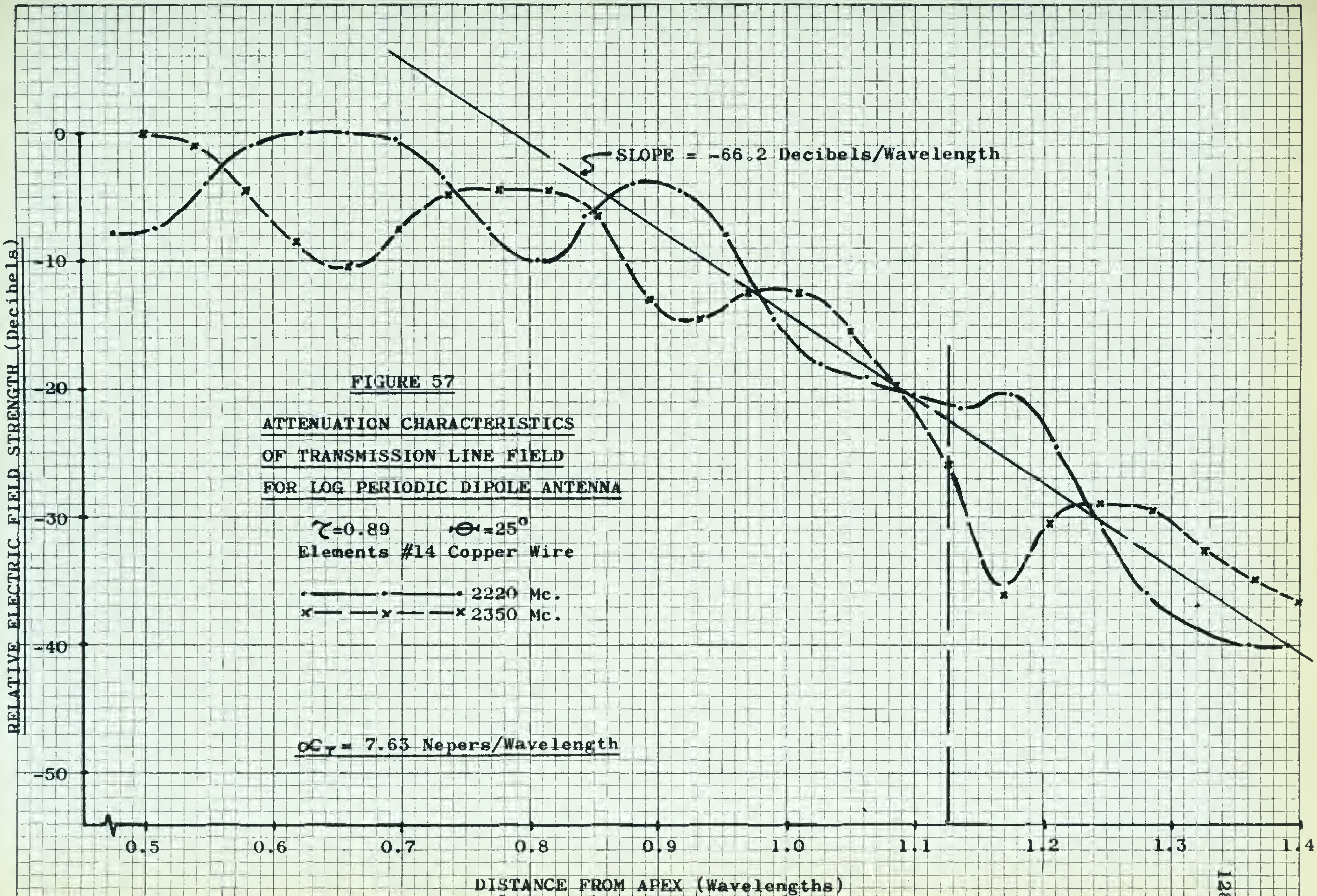

FIGURE 57

ATTENUATION CHARACTERISTICS OF TRANSMISSION LINE FIELD FOR LOG PERIODIC DIPOLE ANTENNA

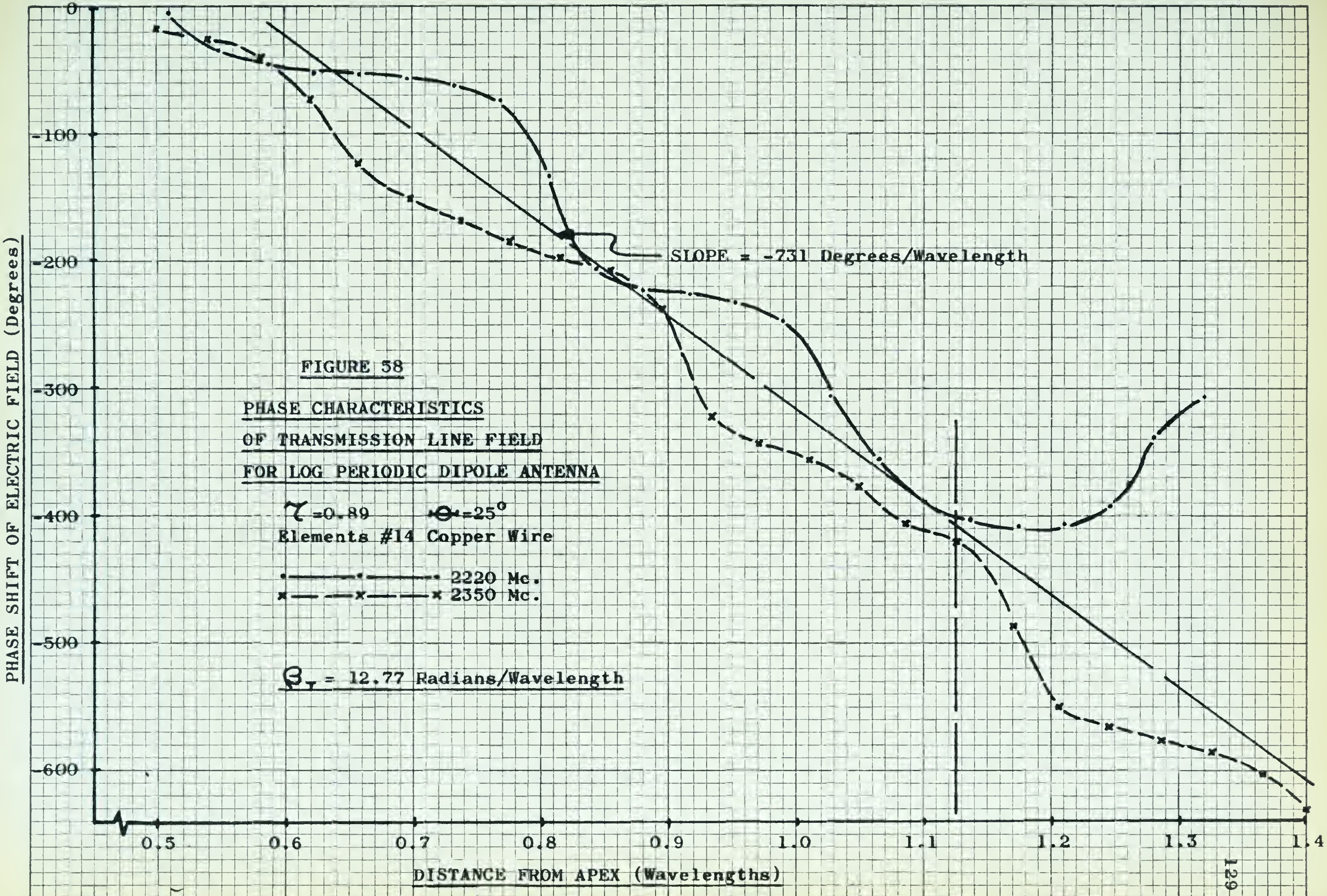
SLOPE = -731 Degrees/Wavelength
FIGURE 58
PHASE CHARACTERISTICS
OF TRANSMISSION LINE FIELD
FOR LOG PERIODIC DIPOLE ANTENNA
τ = 0.89 σ = 25°
Elements #14 Copper Wire
2220 Mc.
2350 Mc.
β_T = 12.77 Radians/Wavelength
0
-100
-200
-300
-400
-500
-600
0.5
0.6
0.7
0.8
0.9
1.0
1.1
1.2
1.3
1.4
PHASE SHIFT OF ELECTRIC FIELD (Degrees)
DISTANCE FROM APEX (Wavelengths)

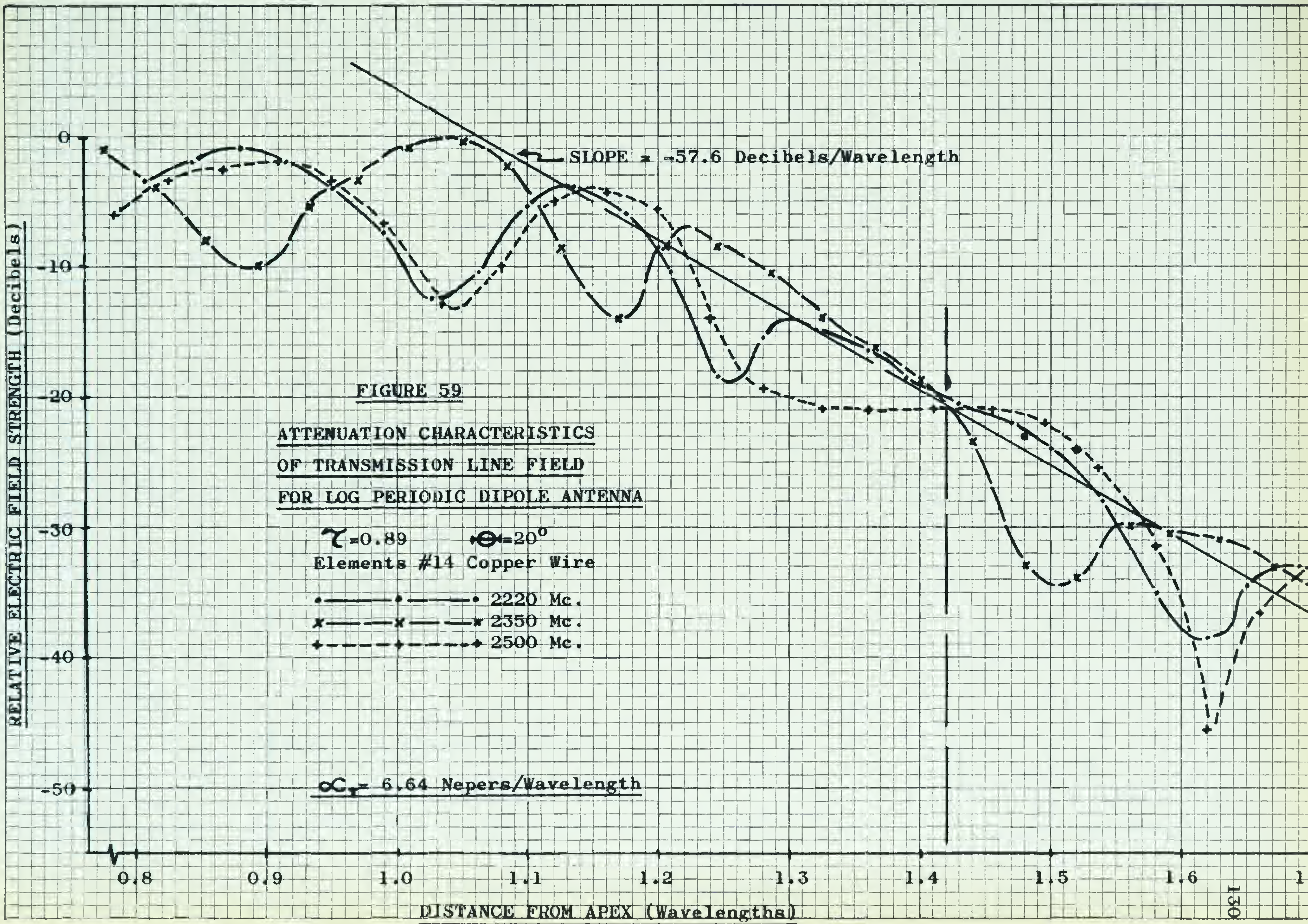

FIGURE 59

ATTENUATION CHARACTERISTICS OF TRANSMISSION LINE FIELD FOR LOG PERIODIC DIPOLE ANTENNA

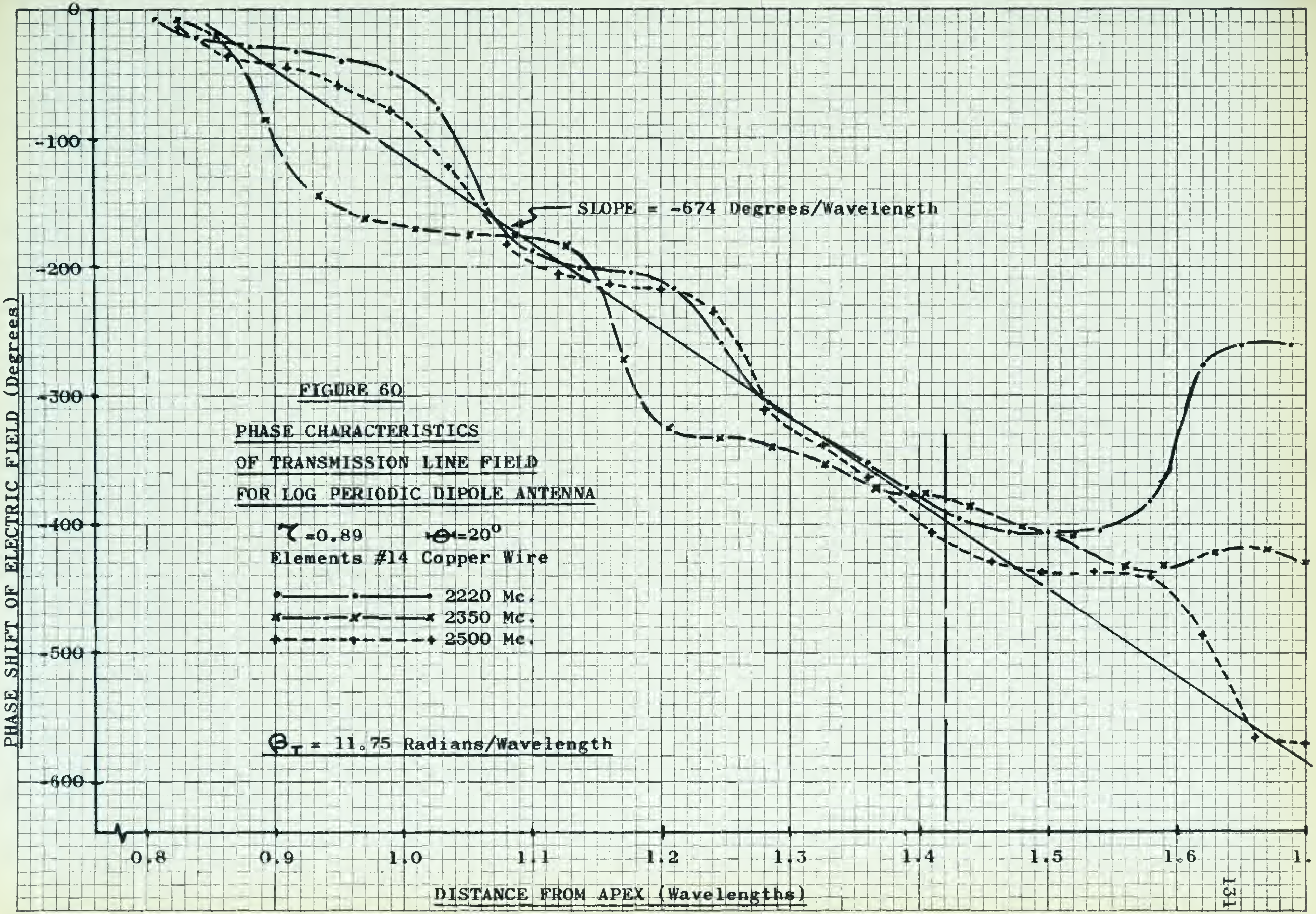
SLOPE = -674 Degrees/Wavelength
FIGURE 60
PHASE CHARACTERISTICS
OF TRANSMISSION LINE FIELD
FOR LOG PERIODIC DIPOLE ANTENNA
τ =0.89 Θ=20°
Elements #14 Copper Wire
2220 Mc.
2350 Mc.
2500 Mc.
Θ_T = 11.75 Radians/Wavelength
0
-100
-200
-300
-400
-500
-600
PHASE SHIFT OF ELECTRIC FIELD (Degrees)
0.8
0.9
1.0
1.1
1.2
1.3
1.4
1.5
1.6
1.7
DISTANCE FROM APEX (Wavelengths)

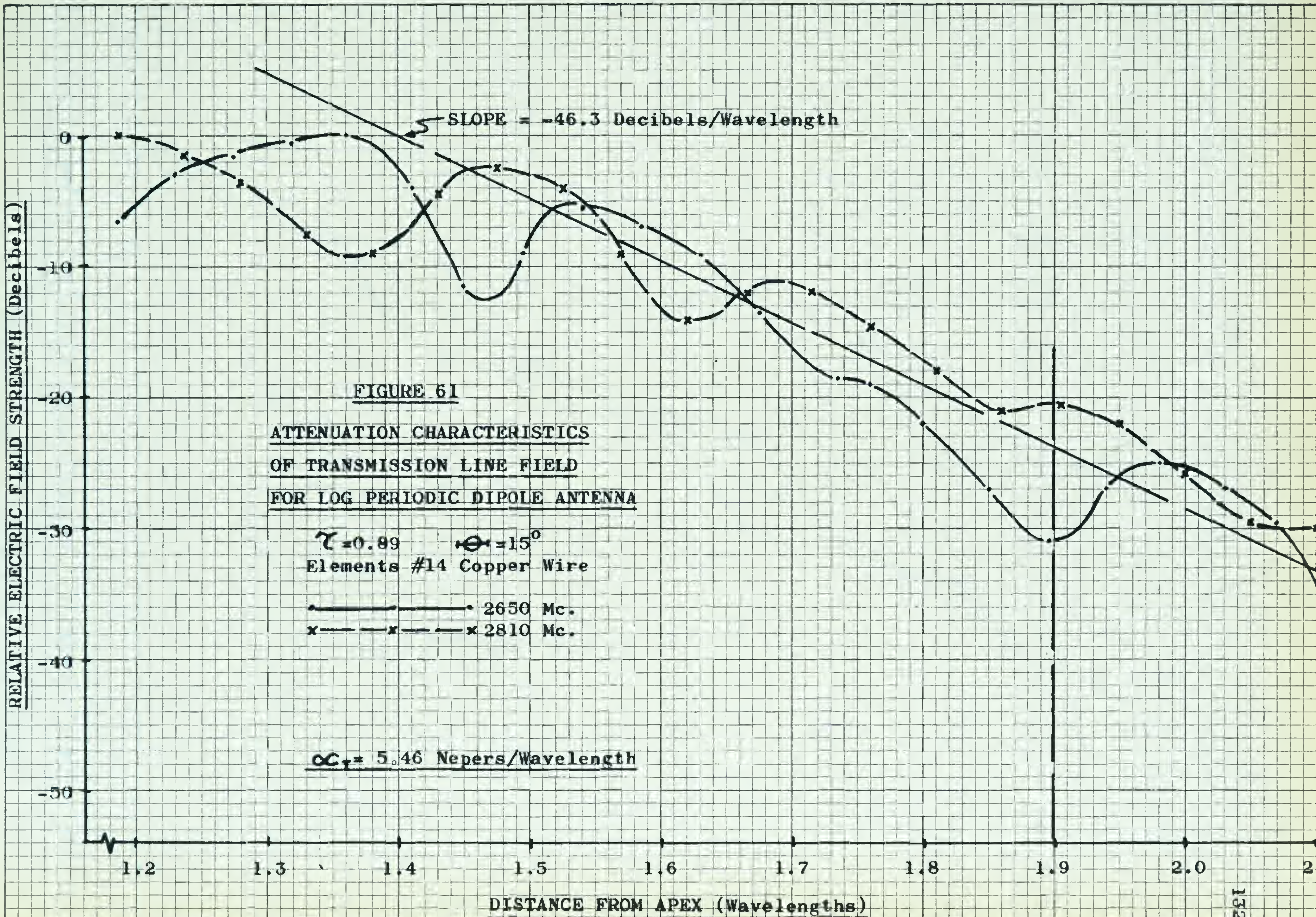

FIGURE 61

ATTENUATION CHARACTERISTICS OF TRANSMISSION LINE FIELD FOR LOG PERIODIC DIPOLE ANTENNA

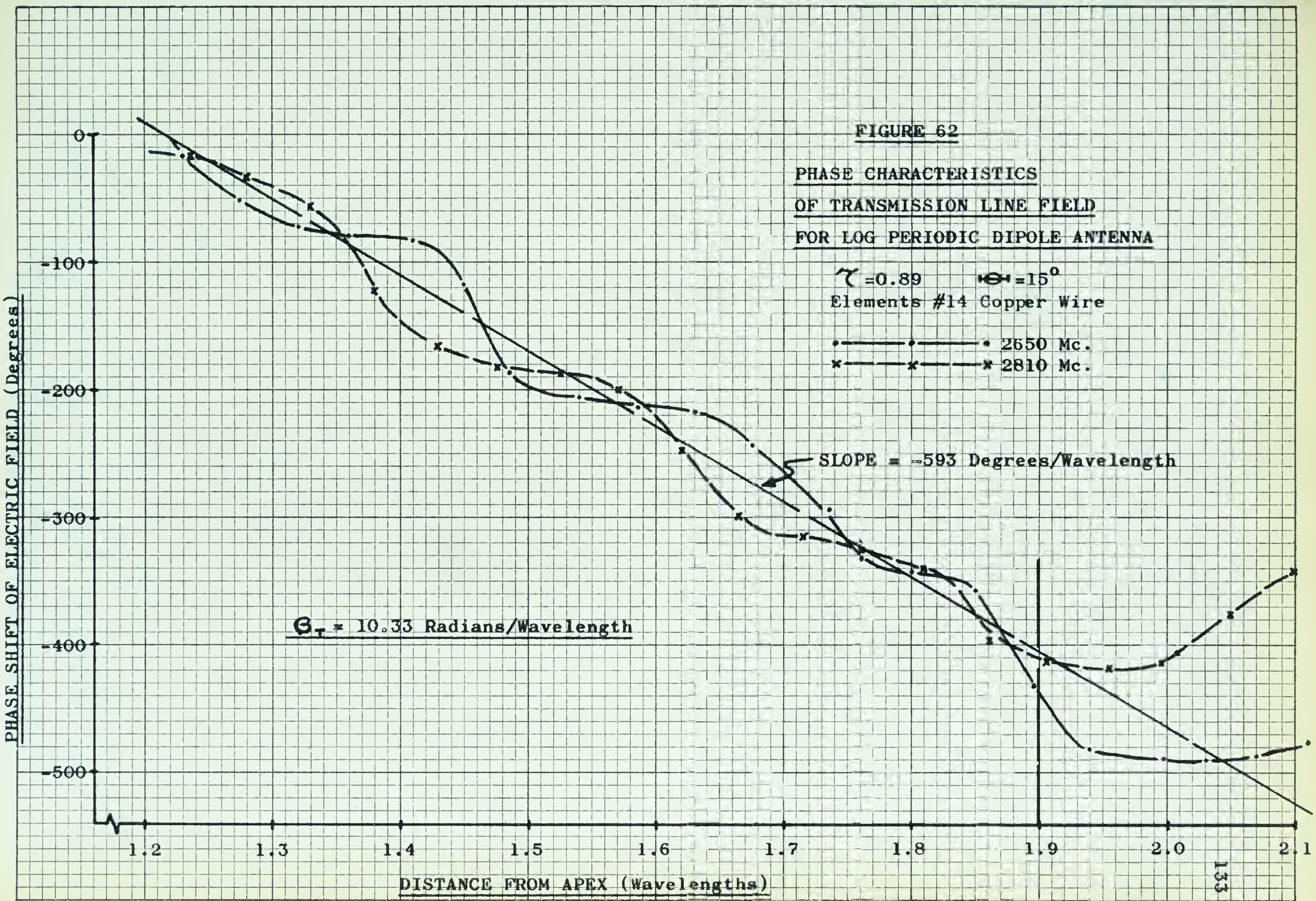
FIGURE 62
PHASE CHARACTERISTICS
OF TRANSMISSION LINE FIELD
FOR LOG PERIODIC DIPOLE ANTENNA
τ =0.89 Θ =15°
Elements #14 Copper Wire
2650 Mc.
2810 Mc.
SLOPE = -593 Degrees/Wavelength
Θ_T = 10.33 Radians/Wavelength
PHASE SHIFT OF ELECTRIC FIELD (Degrees)
0
-100
-200
-300
-400
-500
DISTANCE FROM APEX (Wavelengths)
1.2
1.3
1.4
1.5
1.6
1.7
1.8
1.9
2.0
2.1

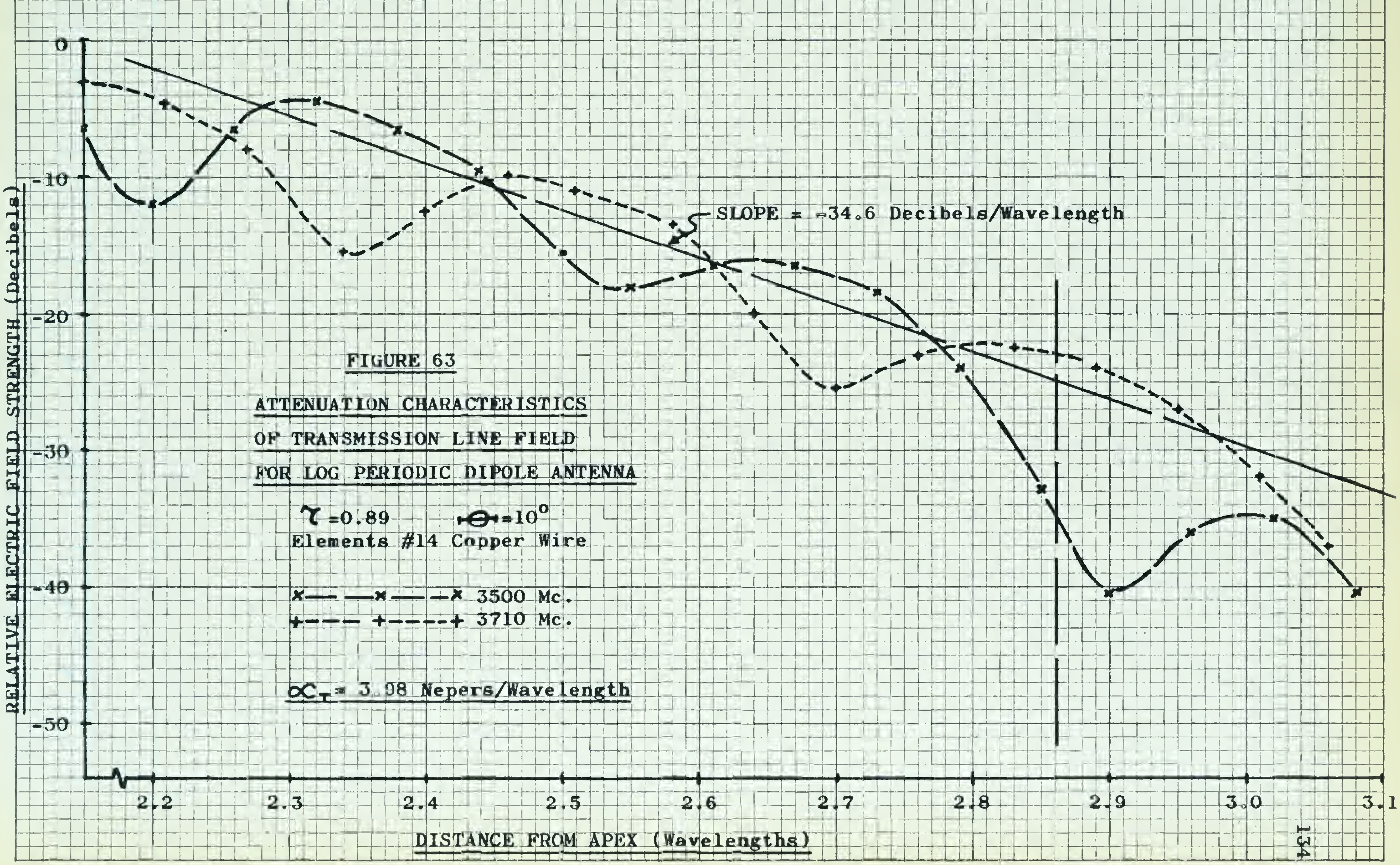
FIGURE 63
ATTENUATION CHARACTERISTICS
OF TRANSMISSION LINE FIELD
FOR LOG PERIODIC DIPOLE ANTENNA
$\tau = 0.89$ $\Theta = 10^{\circ}$
Elements #14 Copper Wire
3500 Mc.
3710 Mc.
α_T = 3.98 Nepers/Wavelength
SLOPE = -34.6 Decibels/Wavelength
RELATIVE ELECTRIC FIELD STRENGTH (Decibels)
0
-10
-20
-30
-40
-50
DISTANCE FROM APEX (Wavelengths)
2.2
2.3
2.4
2.5
2.6
2.7
2.8
2.9
3.0
3.1

FIGURE 64

PHASE CHARACTERISTICS OF TRANSMISSION LINE FIELD FOR LOG PERIODIC DIPOLE ANTENNA

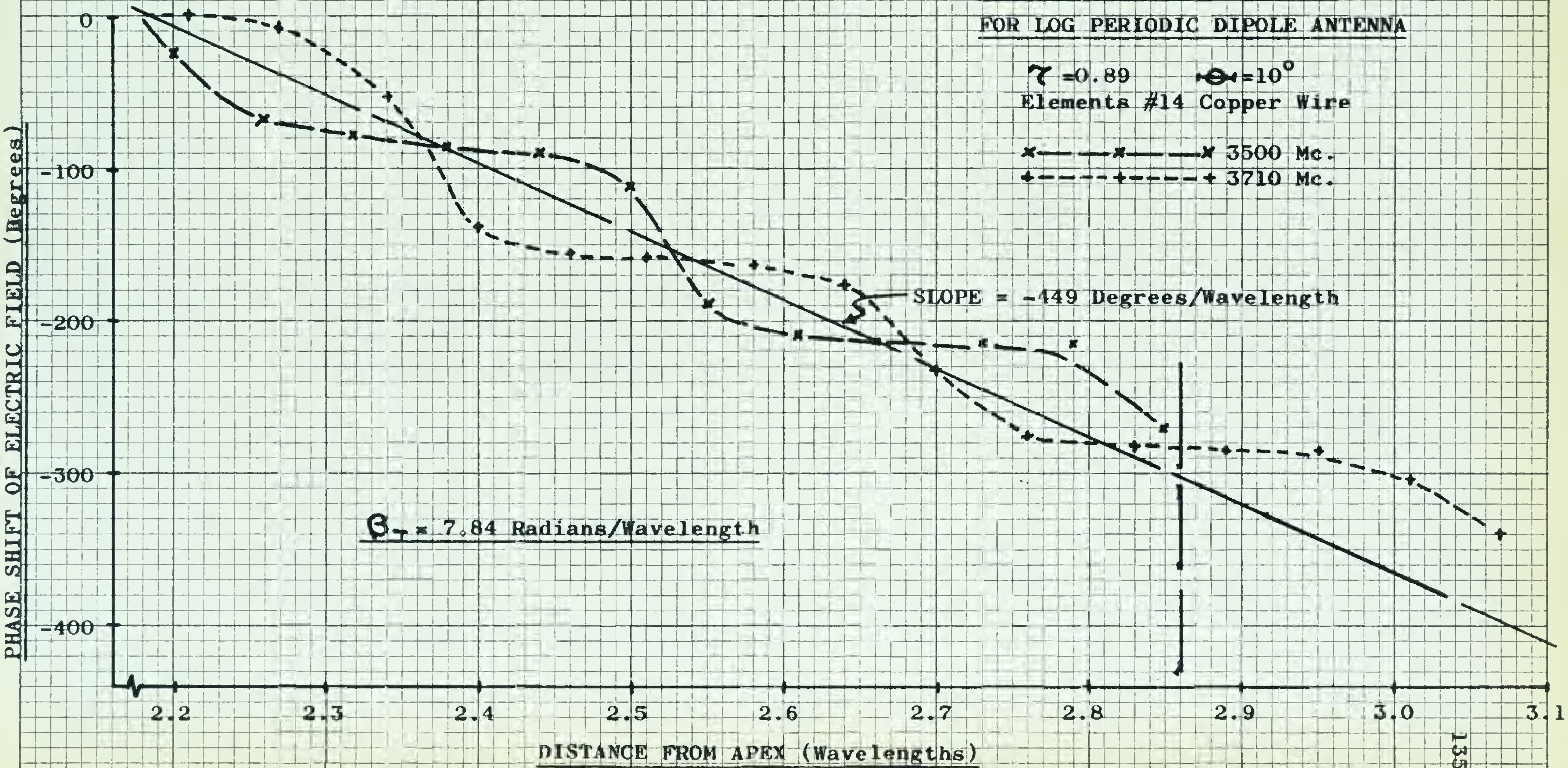

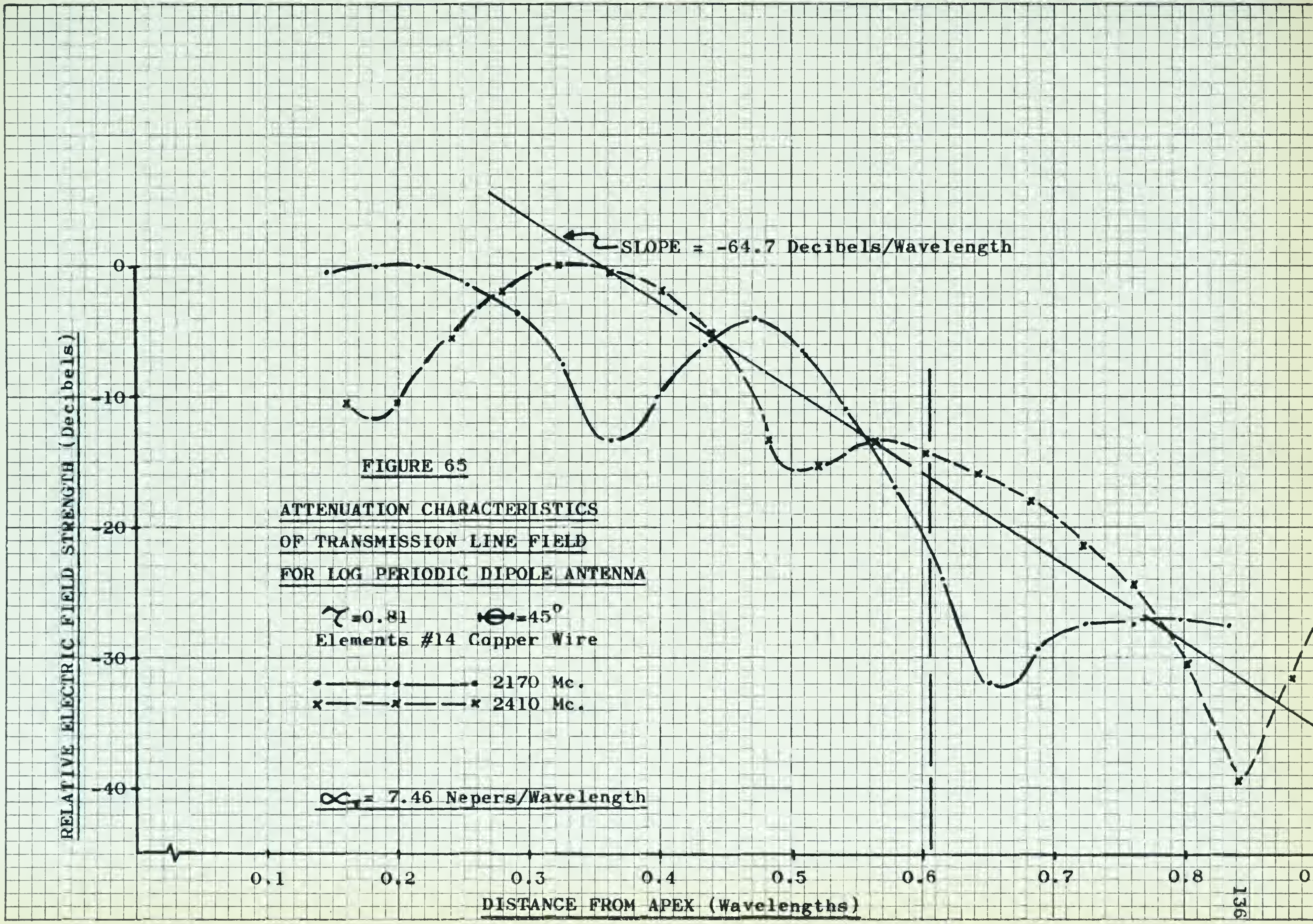

FIGURE 65

ATTENUATION CHARACTERISTICS OF TRANSMISSION LINE FIELD FOR LOG PERIODIC DIPOLE ANTENNA

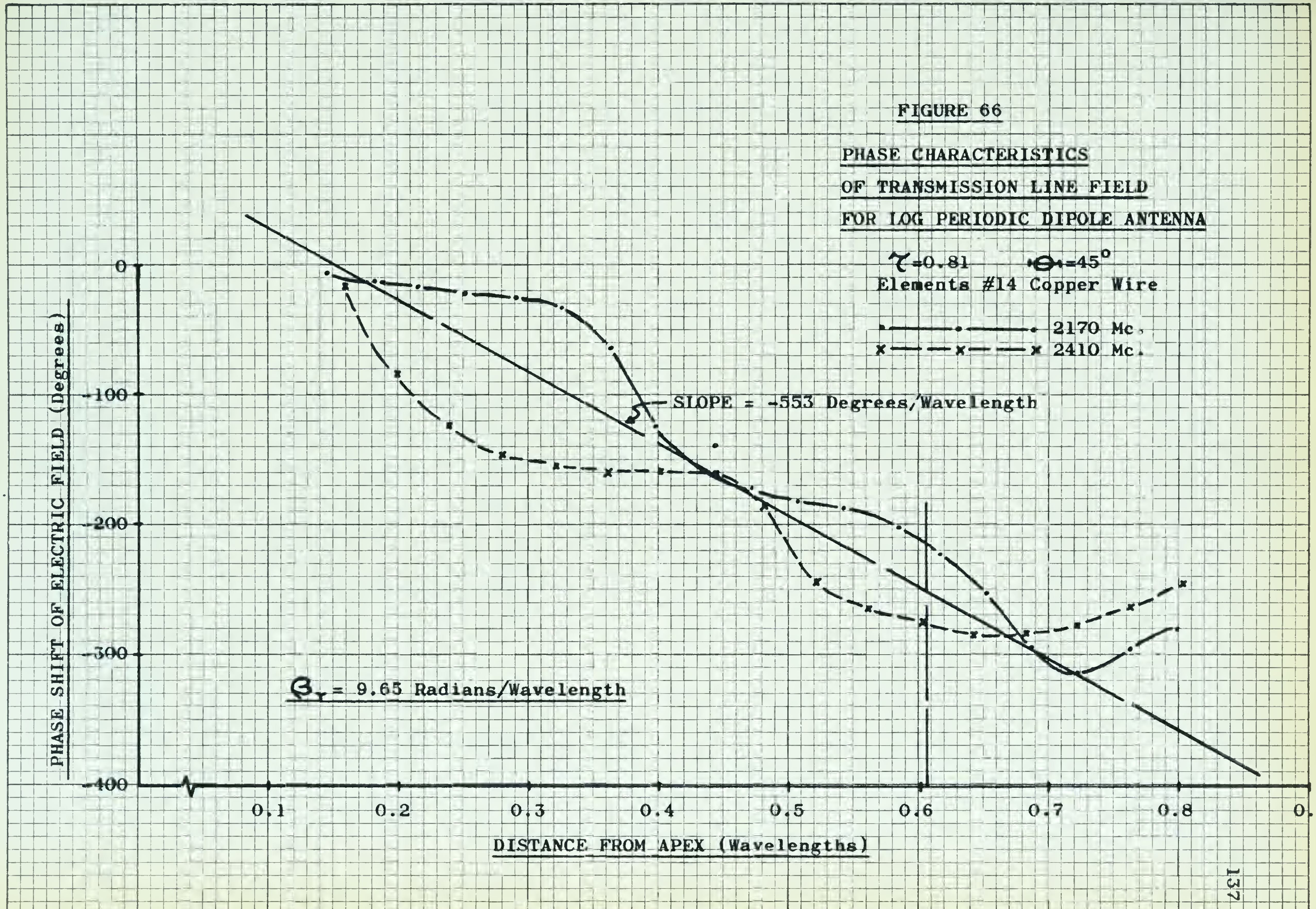

FIGURE 66

PHASE CHARACTERISTICS OF TRANSMISSION LINE FIELD FOR LOG PERIODIC DIPOLE ANTENNA

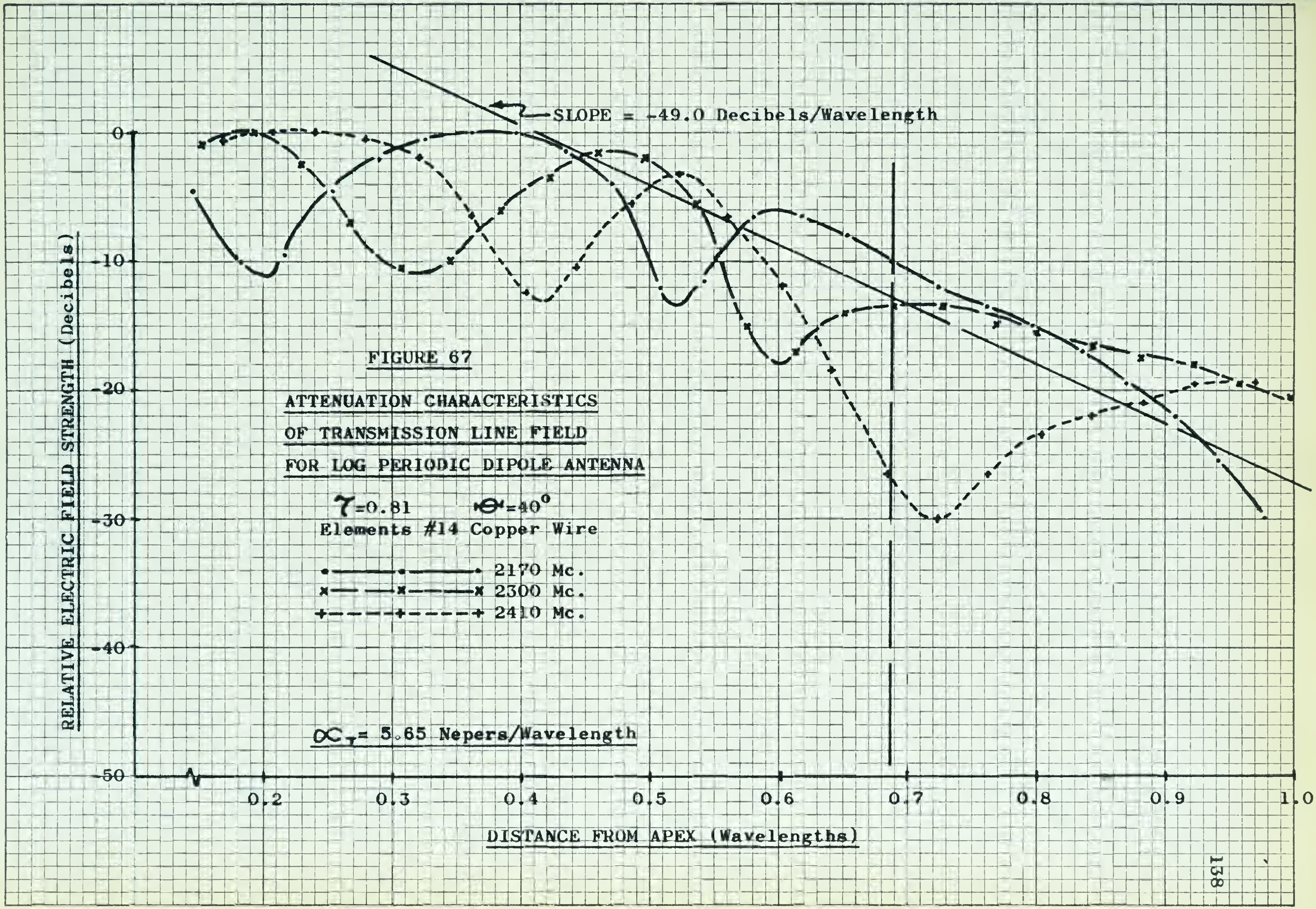

FIGURE 67

ATTENUATION CHARACTERISTICS OF TRANSMISSION LINE FIELD FOR LOG PERIODIC DIPOLE ANTENNA

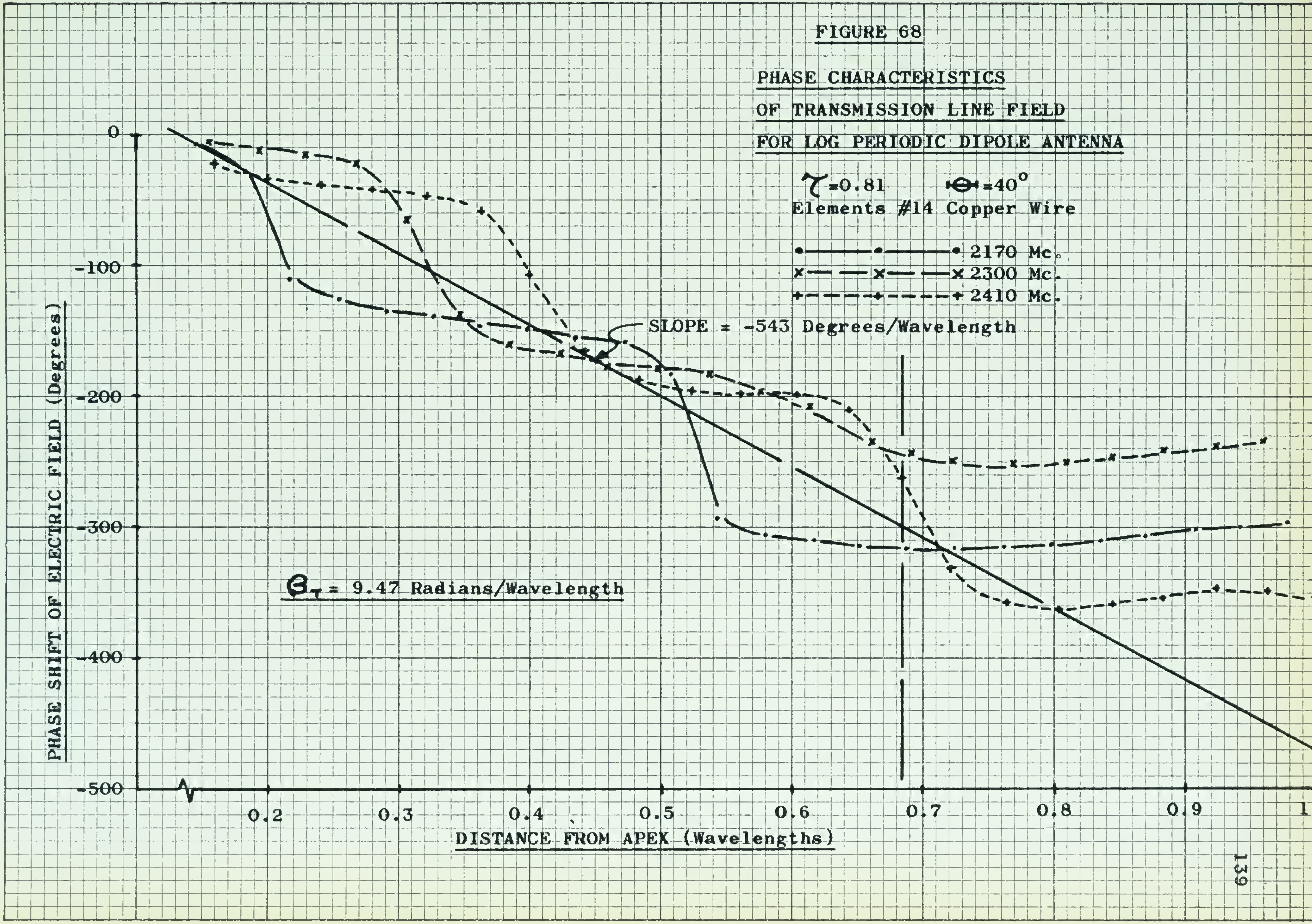
FIGURE 68
PHASE CHARACTERISTICS
OF TRANSMISSION LINE FIELD
FOR LOG PERIODIC DIPOLE ANTENNA
τ=0.81 Θ=40°
Elements #14 Copper Wire
2170 Mc.
2300 Mc.
2410 Mc.
SLOPE = -543 Degrees/Wavelength
β = 9.47 Radians/Wavelength
PHASE SHIFT OF ELECTRIC FIELD (Degrees)
DISTANCE FROM APEX (Wavelengths)
0
-100
-200
-300
-400
-500
0.2
0.3
0.4
0.5
0.6
0.7
0.8
0.9
1.0

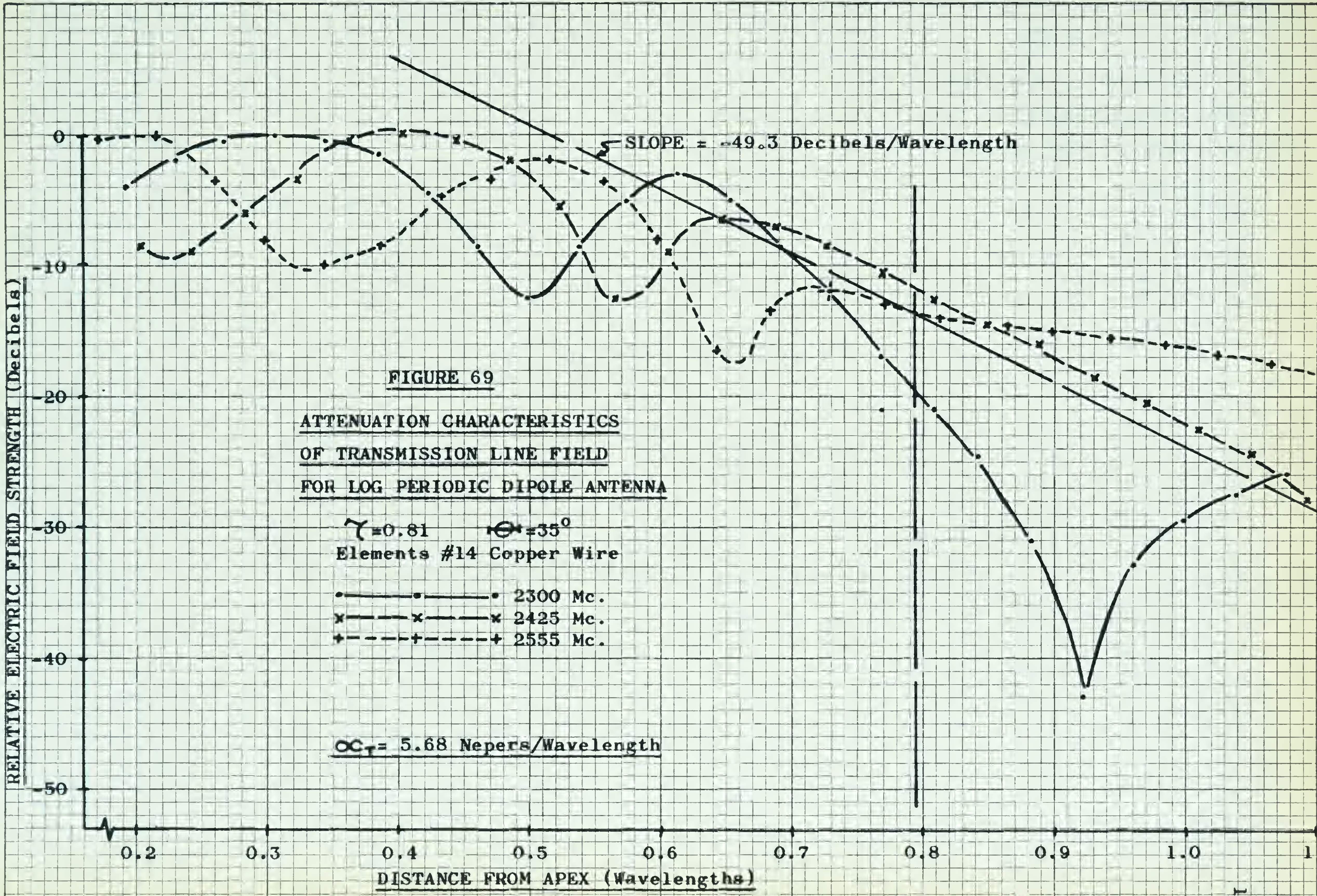
FIGURE 69
ATTENUATION CHARACTERISTICS
OF TRANSMISSION LINE FIELD
FOR LOG PERIODIC DIPOLE ANTENNA
τ=0.81 Θ=35°
Elements #14 Copper Wire
2300 Mc.
2425 Mc.
2555 Mc.
α_T = 5.68 Nepers/Wavelength
SLOPE = -49.3 Decibels/Wavelength
RELATIVE ELECTRIC FIELD STRENGTH (Decibels)
DISTANCE FROM APEX (Wavelengths)
0
-10
-20
-30
-40
-50
0.2
0.3
0.4
0.5
0.6
0.7
0.8
0.9
1.0
1.1

FIGURE 70

PHASE CHARACTERISTICS
OF TRANSMISSION LINE FIELD
FOR LOG PERIODIC DIPOLE ANTENNA

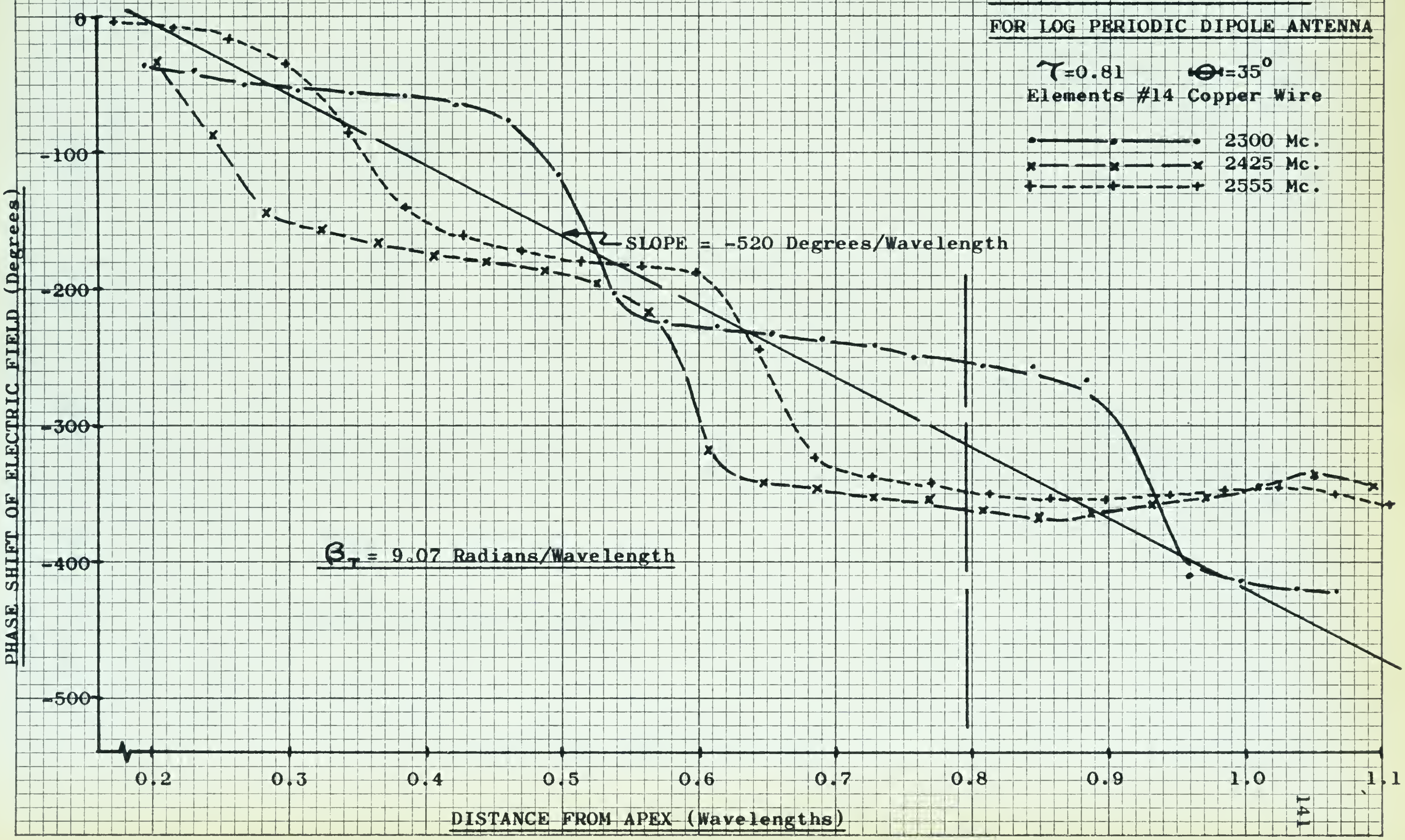

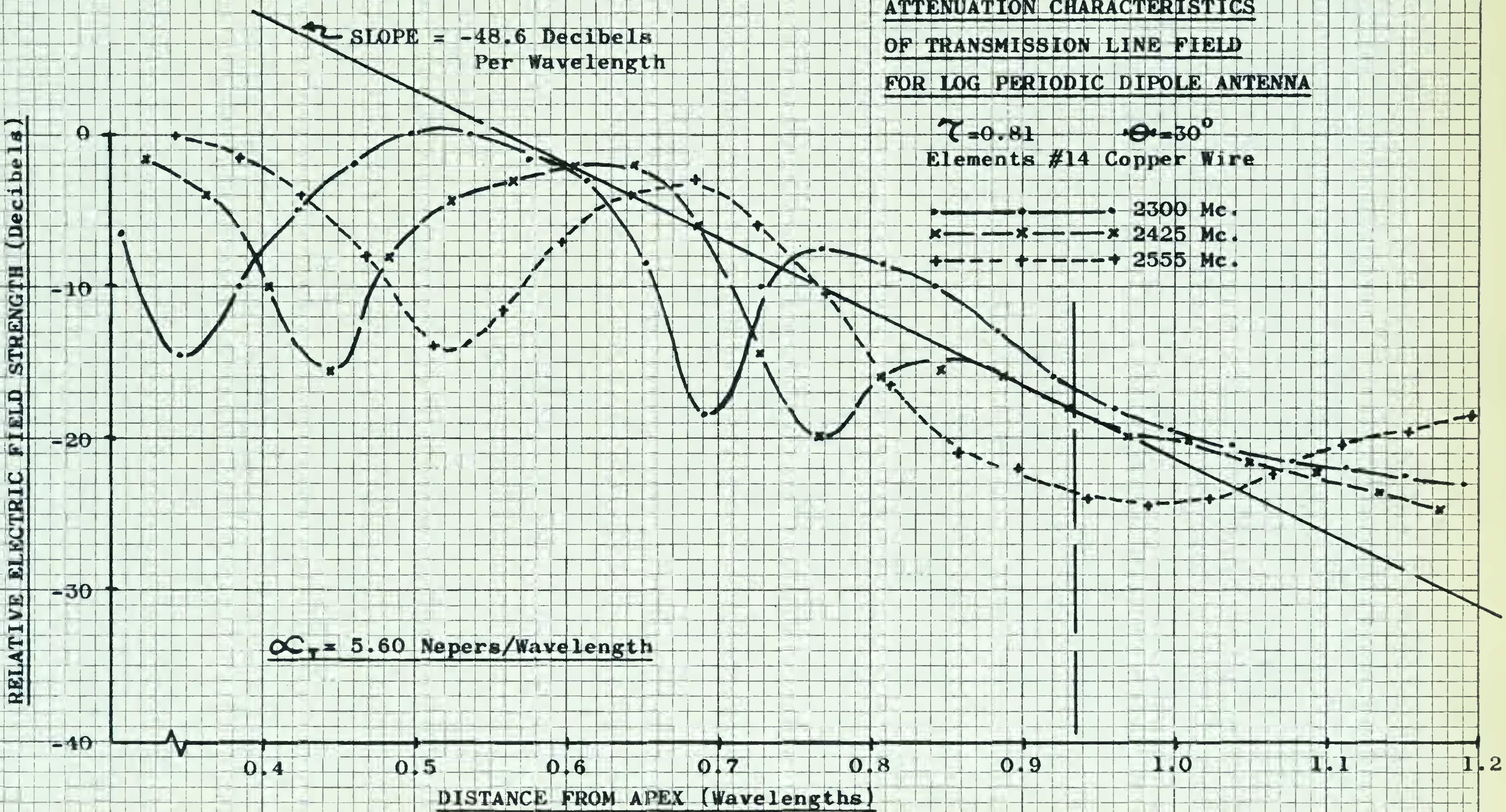

FIGURE 71

ATTENUATION CHARACTERISTICS
OF TRANSMISSION LINE FIELD
FOR LOG PERIODIC DIPOLE ANTENNA

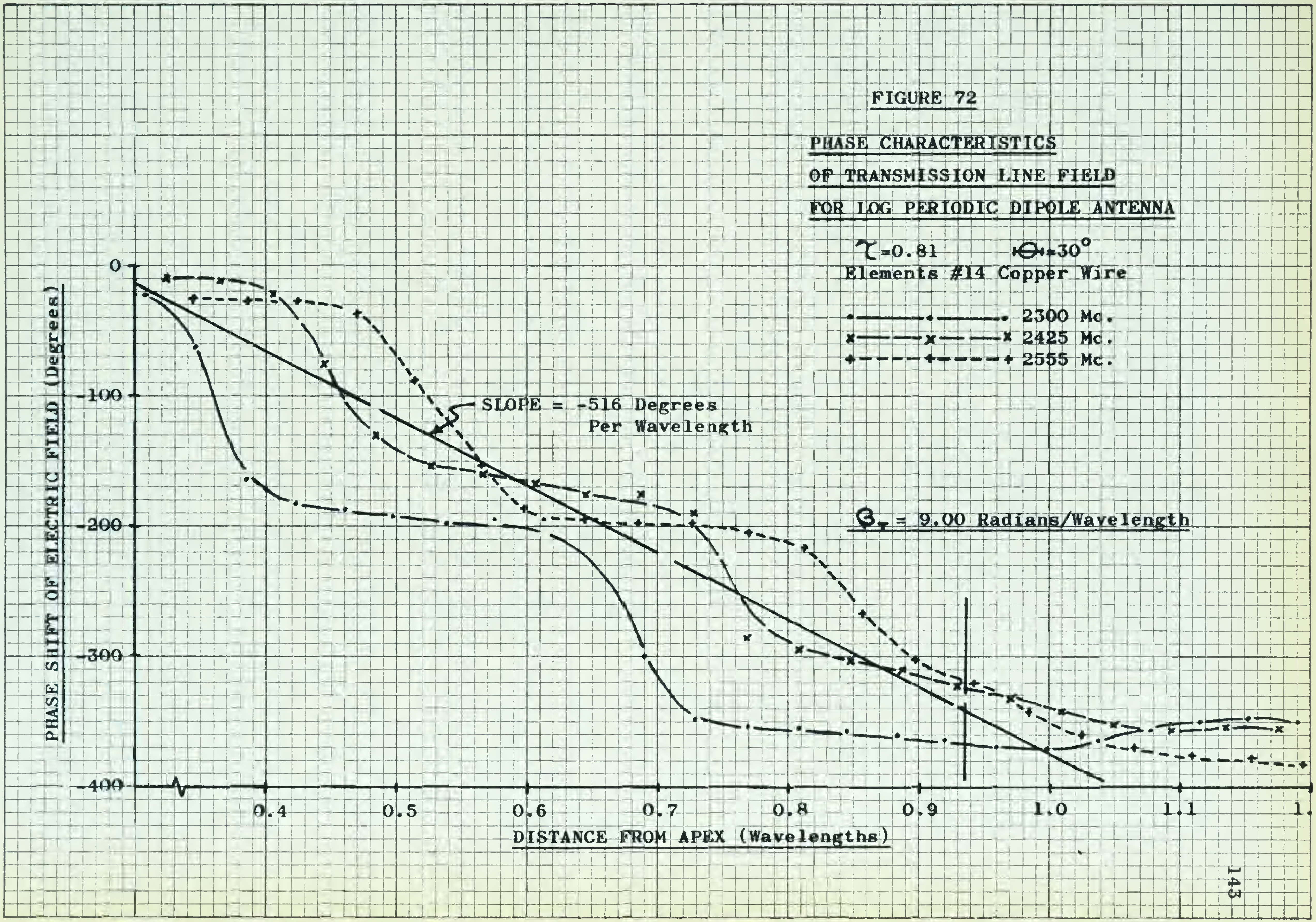

FIGURE 72

PHASE CHARACTERISTICS OF TRANSMISSION LINE FIELD FOR LOG PERIODIC DIPOLE ANTENNA

FIGURE 73

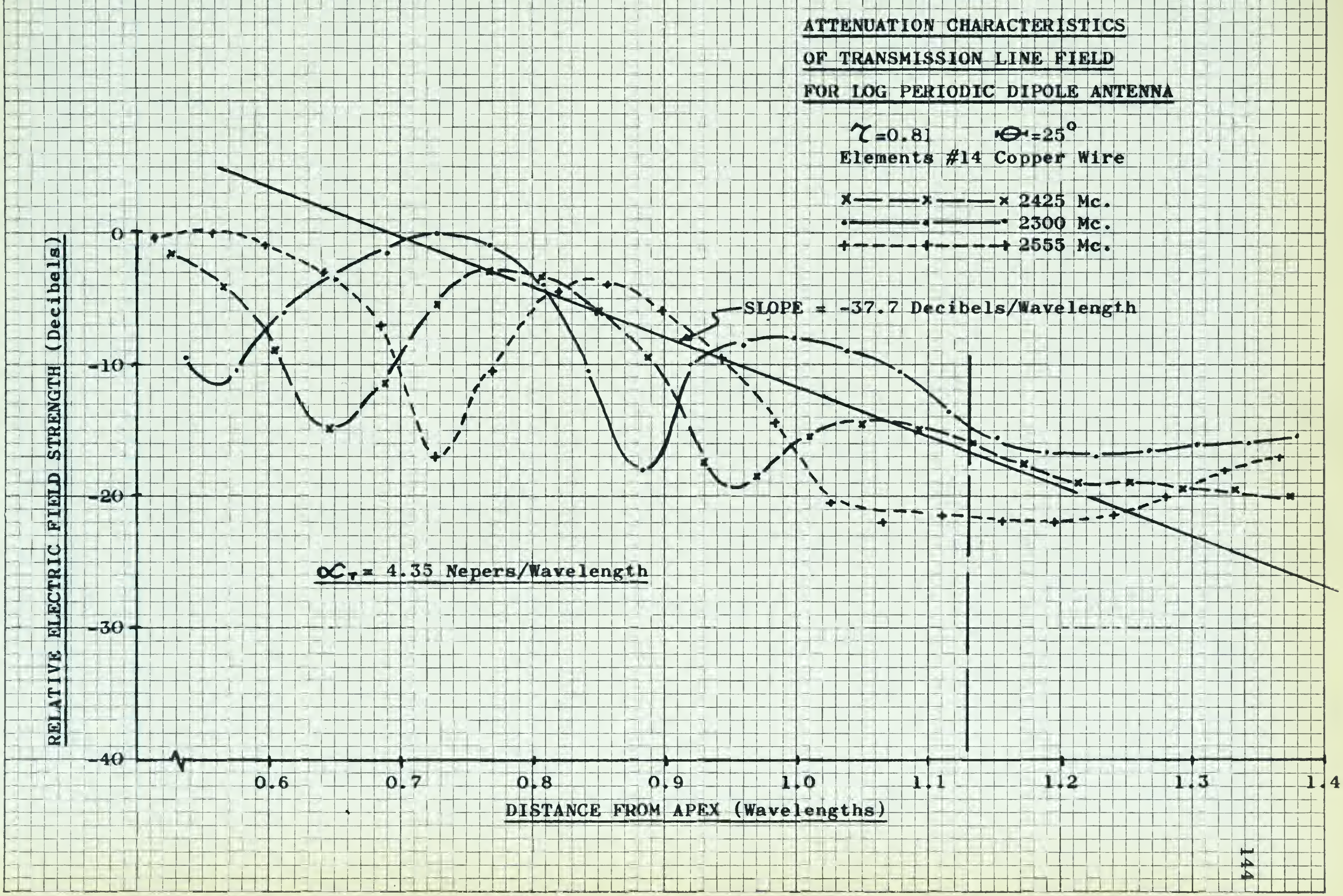
ATTENUATION CHARACTERISTICS
OF TRANSMISSION LINE FIELD
FOR LOG PERIODIC DIPOLE ANTENNA
τ=0.81 Θ=25°
Elements #14 Copper Wire
2425 Mc.
2300 Mc.
2555 Mc.
SLOPE = -37.7 Decibels/Wavelength
α_T = 4.35 Nepers/Wavelength
RELATIVE ELECTRIC FIELD STRENGTH (Decibels)
0
-10
-20
-30
-40
DISTANCE FROM APEX (Wavelengths)
0.6
0.7
0.8
0.9
1.0
1.1
1.2
1.3
1.4

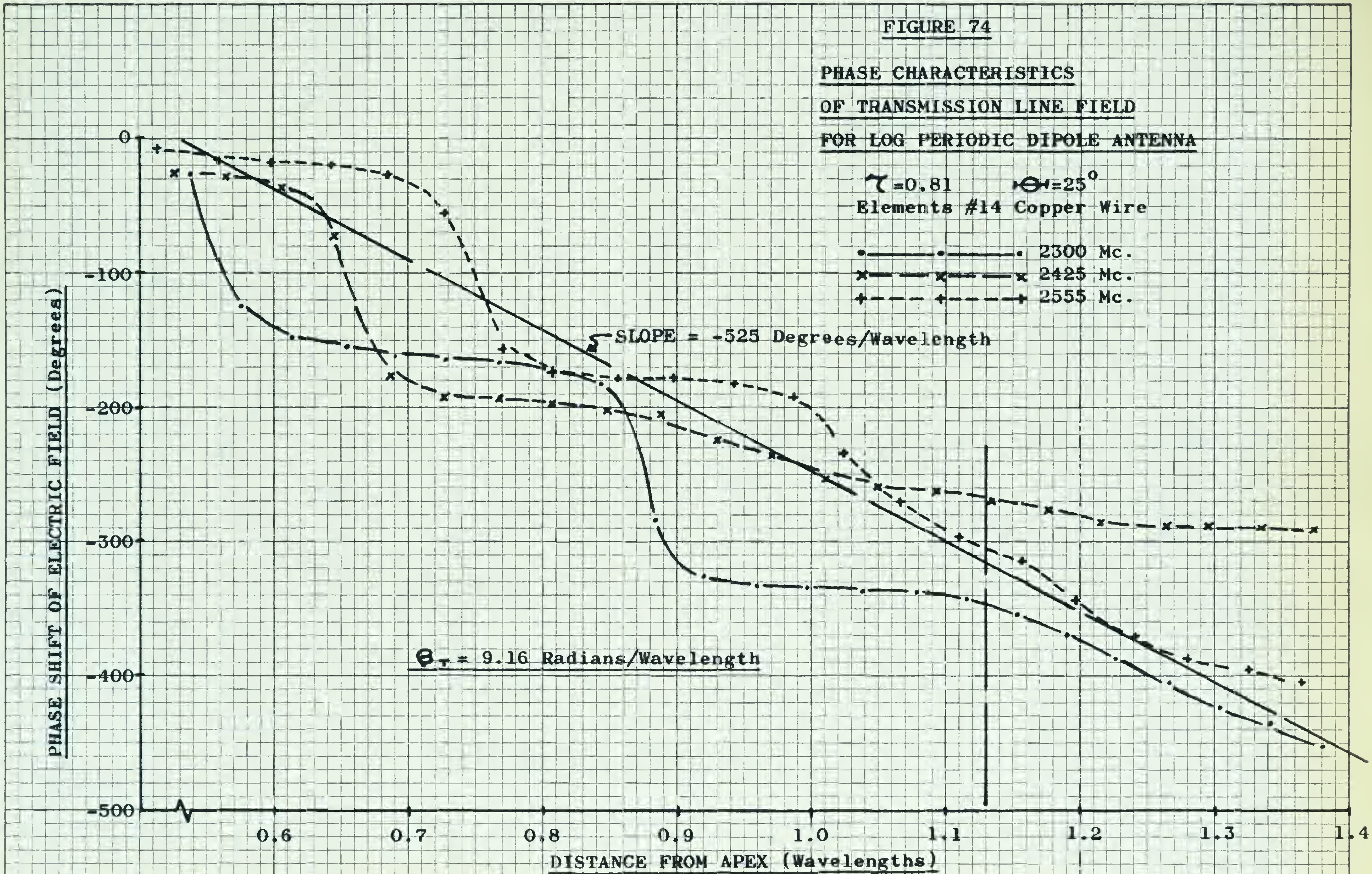
FIGURE 74
PHASE CHARACTERISTICS
OF TRANSMISSION LINE FIELD
FOR LOG PERIODIC DIPOLE ANTENNA
τ=0.81 θ=25°
Elements #14 Copper Wire
2300 Mc.
2425 Mc.
2555 Mc.
SLOPE = -525 Degrees/Wavelength
β_T = 9.16 Radians/Wavelength
PHASE SHIFT OF ELECTRIC FIELD (Degrees)
0
-100
-200
-300
-400
-500
0.6
0.7
0.8
0.9
1.0
1.1
1.2
1.3
1.4
DISTANCE FROM APEX (Wavelengths)

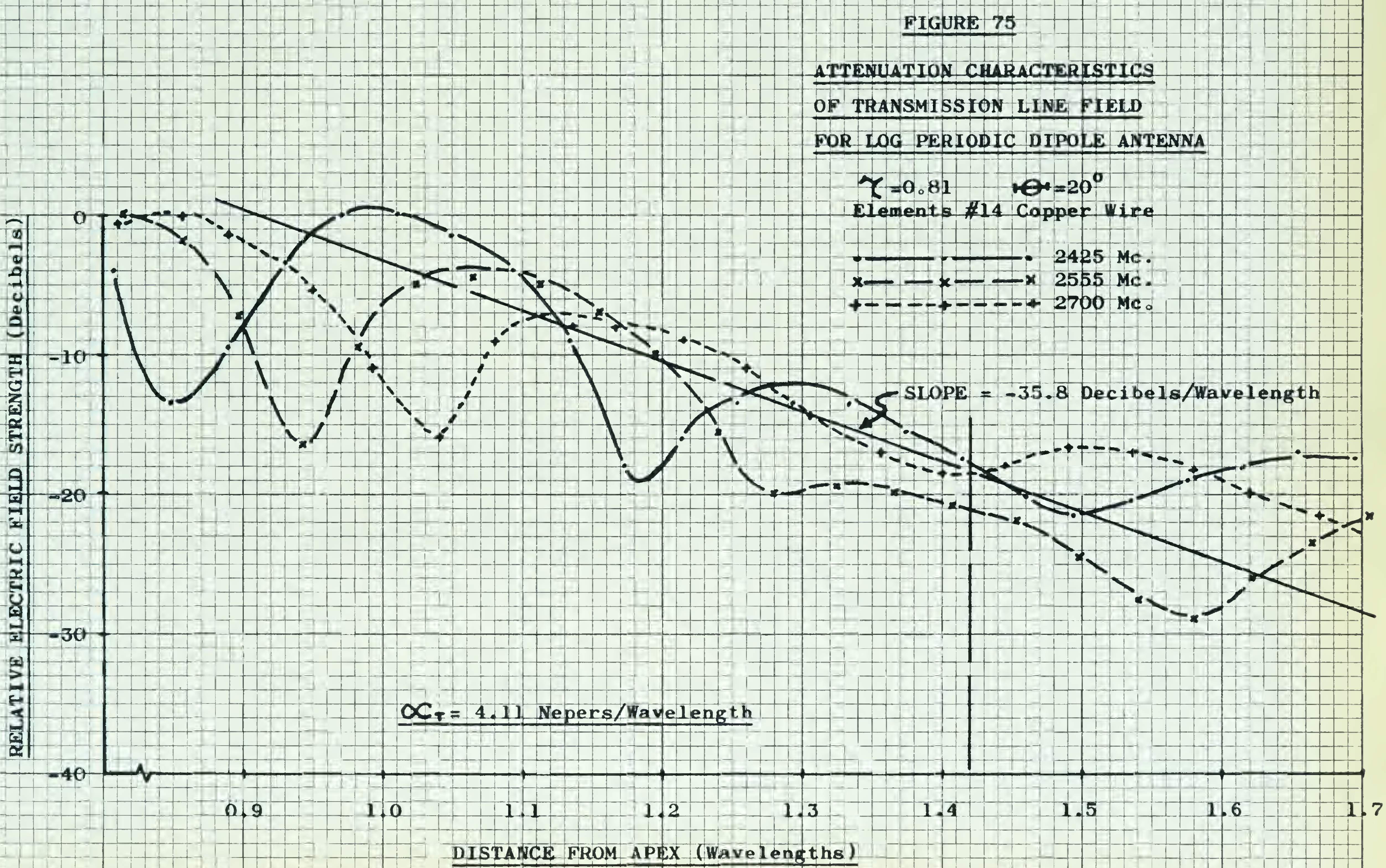
FIGURE 75
ATTENUATION CHARACTERISTICS
OF TRANSMISSION LINE FIELD
FOR LOG PERIODIC DIPOLE ANTENNA
τ = 0.81 θ = 20°
Elements #14 Copper Wire
2425 Mc.
2555 Mc.
2700 Mc.
SLOPE = -35.8 Decibels/Wavelength
α_T = 4.11 Nepers/Wavelength
RELATIVE ELECTRIC FIELD STRENGTH (Decibels)
0
-10
-20
-30
-40
0.9
1.0
1.1
1.2
1.3
1.4
1.5
1.6
1.7
DISTANCE FROM APEX (Wavelengths)

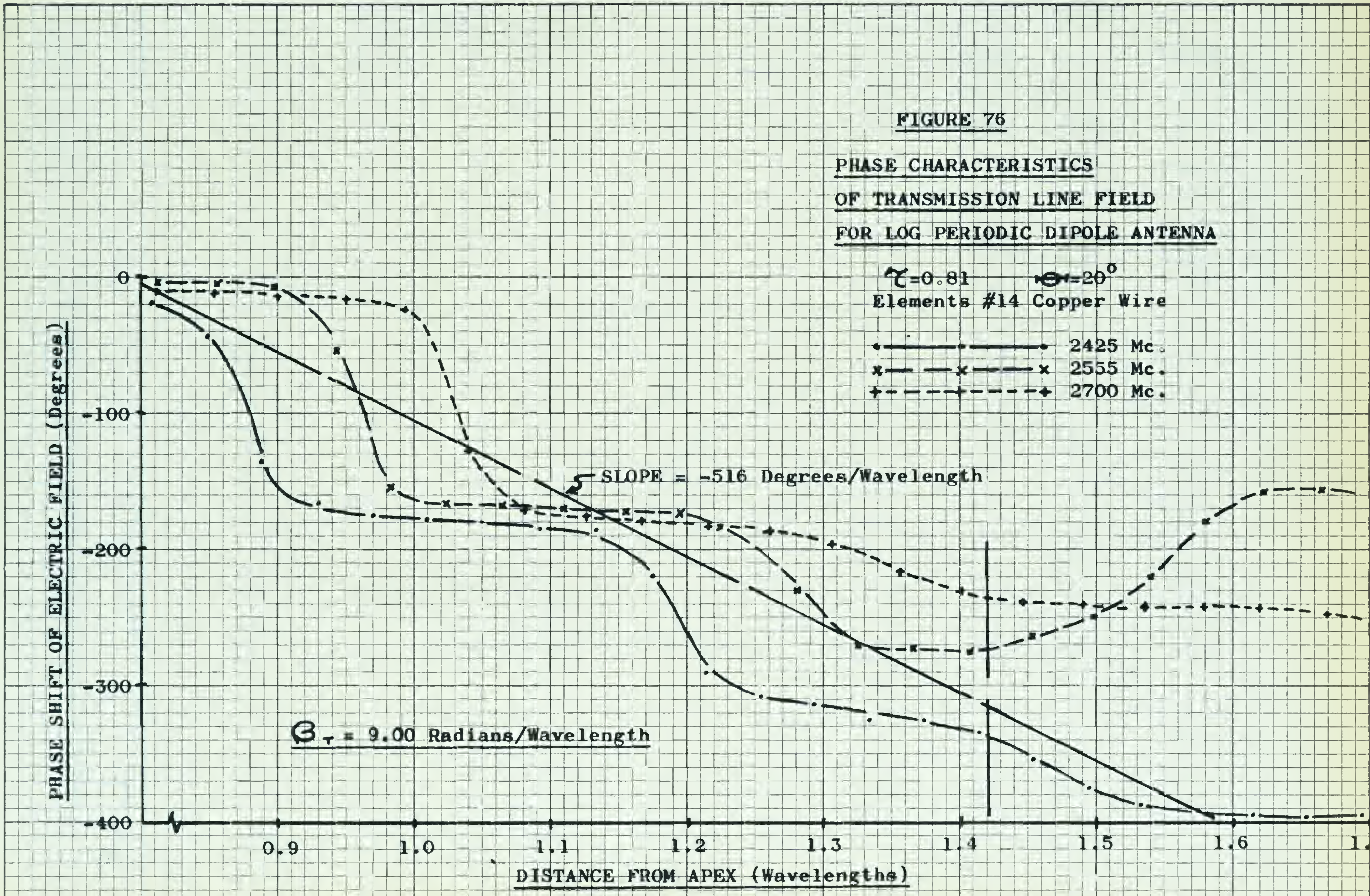
FIGURE 76
PHASE CHARACTERISTICS
OF TRANSMISSION LINE FIELD
FOR LOG PERIODIC DIPOLE ANTENNA
τ=0.81 σ=20°
Elements #14 Copper Wire
2425 Mc.
2555 Mc.
2700 Mc.
SLOPE = -516 Degrees/Wavelength
β = 9.00 Radians/Wavelength
PHASE SHIFT OF ELECTRIC FIELD (Degrees)
DISTANCE FROM APEX (Wavelengths)
0
-100
-200
-300
-400
0.9
1.0
1.1
1.2
1.3
1.4
1.5
1.6
1.7

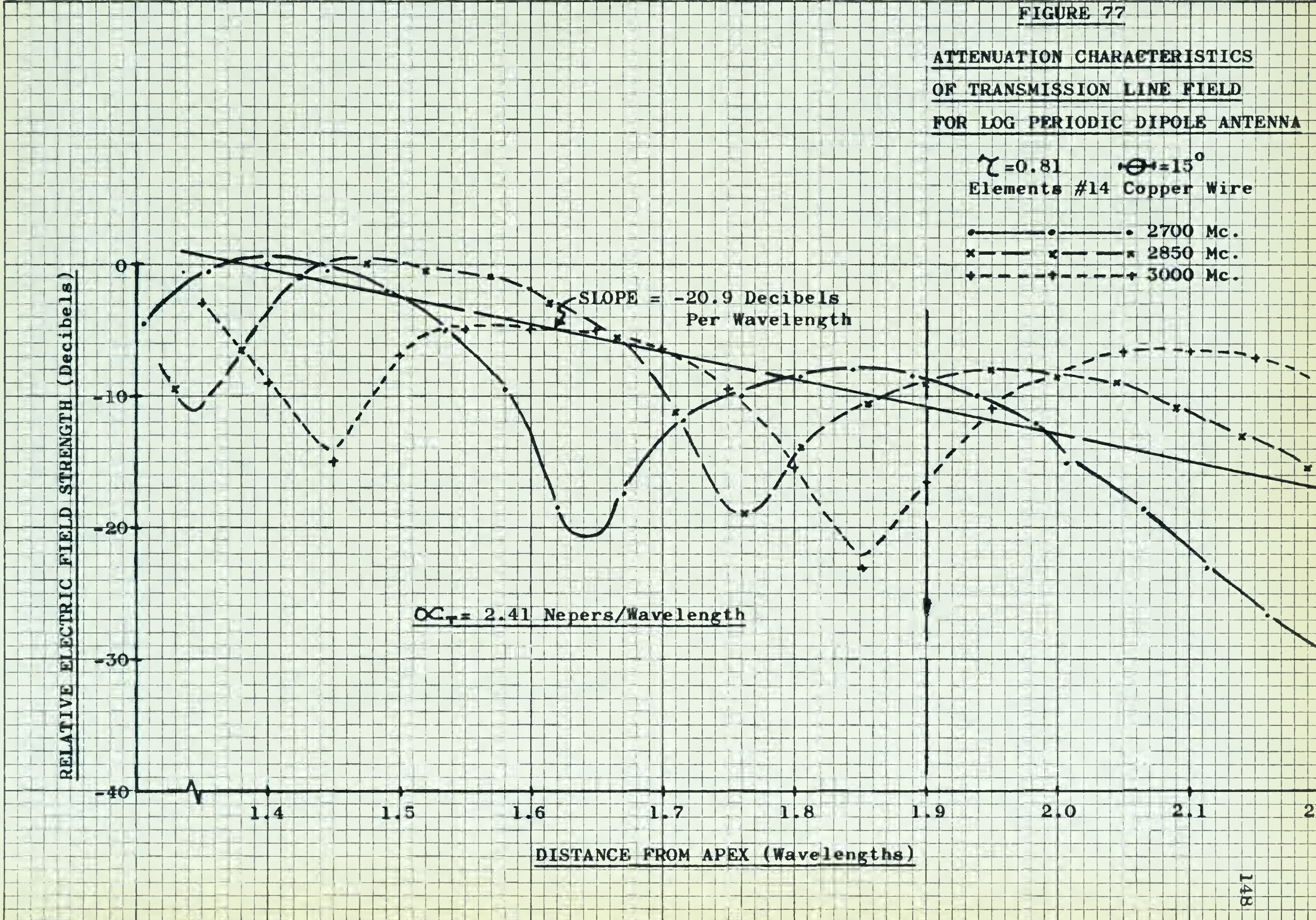

FIGURE 77

ATTENUATION CHARACTERISTICS OF TRANSMISSION LINE FIELD FOR LOG PERIODIC DIPOLE ANTENNA

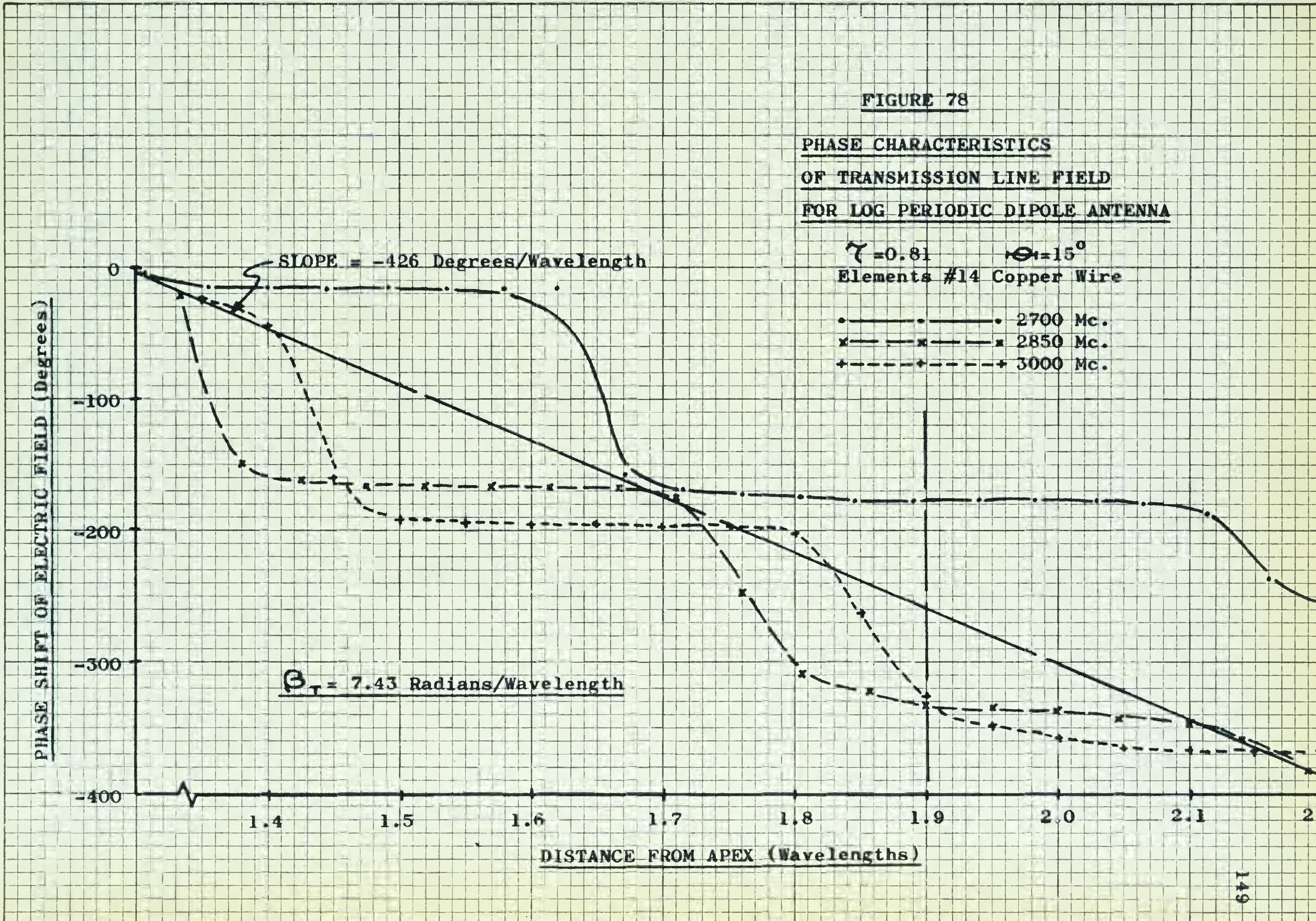
FIGURE 78
PHASE CHARACTERISTICS
OF TRANSMISSION LINE FIELD
FOR LOG PERIODIC DIPOLE ANTENNA
τ =0.81   Θ =15°
Elements #14 Copper Wire
2700 Mc.
2850 Mc.
3000 Mc.
SLOPE = -426 Degrees/Wavelength
β_T = 7.43 Radians/Wavelength
0
-100
-200
-300
-400
1.4
1.5
1.6
1.7
1.8
1.9
2.0
2.1
2.2
DISTANCE FROM APEX (Wavelengths)
PHASE SHIFT OF ELECTRIC FIELD (Degrees)